MECHANISM OF INTERFERON-GAMMA ACTION IN CONTROL OF *TRYPANOSOMA CRUZI* INFECTION

by

KARA L. CUMMINGS

(Under the Direction of Rick L. Tarleton)

ABSTRACT

Immune control of *Trypanosoma cruzi*, the causative agent of Chagas disease, requires the cytokine interferon-γ. The mechanism by which interferon-γ acts in control of infection is investigated here. Among the effector functions induced by interferon-γ is production of the microbicidal agent nitric oxide (NO) and other proteins that guide effector cells to sites of infection. While there is evidence to support a role for NO in control of *T. cruzi* infection, this study demonstrates that NO is not absolutely required for survival in *T. cruzi* infection. The increased production of certain cytokines by infected NO-deficient mice may compensate for the lack of NO and therefore contribute to the control of *T. cruzi* infection. Additionally, interferon-γ mediates recruitment of effector cells to infection sites by induction of chemokine ligands and chemokine receptors. In the absence of IFN-γ such recruitment is significantly delayed. Nitric oxide production and chemokine and chemokine receptor expression are part of a network of IFN-γ inducible responses that collectively contribute to the control *T. cruzi* infection.

INDEX WORDS: *Trypanosoma cruzi*, Interferon-γ, Nitric oxide, Chemokines, Chemokine Receptors

MECHANISM OF INTERFERON-GAMMA ACTION IN CONTROL OF *TRYPANOSOMA CRUZI* INFECTION

by

KARA L. CUMMINGS

B.S., Auburn University, 1997

A Dissertation Submitted to the Graduate Faculty of The University of Georgia in Partial Fulfillment of the Requirements for the Degree

DOCTOR OF PHILOSOPHY

ATHENS, GEORGIA

2003

MECHANISM OF INTERFERON-GAMMA ACTION IN CONTROL OF *TRYPANOSOMA CRUZI* INFECTION

by

KARA L. CUMMINGS

Major Professor: Rick L. Tarleton

Committee: Daniel Colley
Lilianna Jaso-Friedmann
Julie Moore
David Peterson

Electronic Version Approved:

Maureen Grasso
Dean of the Graduate School
The University of Georgia
December 2003

DEDICATION

This work is dedicated to my family, Joseph M. Cummings, Margaret B. Cummings, Crista A. Cummings-Bizier and Michael Bizier. Each family member supported and encouraged me in their own way during the process of earning my doctoral degree and I deeply appreciate it.

ACKNOWLEDGEMENTS

I would like to acknowledge the help and moral support of several individuals. I thank Mark and Nancy Heiges; Mark for all the knowledge he passed on to me and answering the really stupid questions I asked, Nancy and Mark for hosting *Buffy* nights to which I owe a great deal of my current sanity. I thank Diana Martin not only for willingly discussing my results with me but for her boundless friendship and her amazing snickerdoodles. My thanks go to Bolyn Hubby Fralish and Tami Rosario McBreyer for their friendship and for dragging me to the gym on a regular basis. Additionally, thanks go to Woo (Rebecca Woo, M.D.) for befriending me when I first came to Athens and including me in her family of friends. Thanks go to Marian Thomas, for the weekly *Buffy* discussions and all her help with the paperwork that is involved in being a graduate student. Todd Minning has my eternal thanks for always having the answers and for having wickedly funny e-mails. Also, my thanks go to Courtney Boehlke and Tammy Andros for being there when I needed to bitch for a minute or three (okay, maybe an hour or three). To Becky Bundy go my thanks for movie nights with her and John as well as sharing the *Lord of the Rings* experience with such enthusiasm. Also, to the late comers to the lab, thank you to Brent Weatherly for the limitless nicknames (Blondie, Greenbean, KC, Blueberry, K-Rock, etc.) and Drew Etheridge for making me laugh so much my final year. These individuals were all a part of making my graduate experience an enjoyable and memorable time. Thank you.

TABLE OF CONTENTS

Page

LIST OF TABLES

Page

LIST OF FIGURES

Page

CHAPTER 1

INTRODUCTION AND LITERATURE REVIEW

In Latin America, 16-18 million people are infected with the protozoan parasite *Trypanosoma cruzi* and 100 million more are at risk of becoming infected (1-4). Infection usually occurs when blood feeding reduviid bugs deposit feces containing the metacyclic trypomastigote stage of *T. cruzi* on the mammalian host, near the bite site. Once *T. cruzi* traverses the skin of the vertebrate host, trypomastigotes invade various cell types, where they convert to the replicative intracellular amastigote stage. The amastigotes replicate, convert to trypomastigotes, rupture the infected cell, and invade other cells, continuing the cycle of infection. The acute phase of infection is characterized by systemic parasitemia. In humans the chronic phase is generally asymptomatic for many years before development of disease. Approximately 30% of individuals with chronic infections will develop symptoms of Chagas disease, which include severe cardiac and/or gastrointestinal pathology. Of those infected, 50,000 die each year of congestive heart failure.

Transmission and prevention

Transmission of *T. cruzi* occurs in several ways; 1) *T. cruzi*-infested feces coming in contact with the mucosa or open wound of vertebrate hosts after blood feeding and defecation by an infected insect vector, 2) blood transfusion or organ transplant, 3) infected mothers passing the infection to the baby during pregnancy or delivery, and 4) orally by consuming infected materials, including breast milk. To prevent vector-borne transmission of *T. cruzi* in Latin America several regional programs were initiated to treat houses with insecticides and seal

cracks in walls where the insect dwells (4, 5). In an effort to decrease transmission through blood transfusion and organ transplantation, donor screening programs were established in Latin America (6). In the United States the potential for transmission of *T. cruzi* increases as immigration of individuals from endemic regions occurs (7, 8). Several cases of transmission of *T. cruzi* through blood transfusion have occurred in the U.S. as well as through organ transplant (9-11). Additionally, there are reports of vector-borne transmission in the U.S (12). While there is no cure for *T. cruzi* infection, treatment of infected individuals early in the acute phase with nifurtimox or benznidazole limits disease development but the toxicity of the drugs, especially in adults, prevents wide usage (reviewed in (13, 14)). Additionally, vaccine candidates are actively being examined for potential therapeutic purposes (15-18).

Tropism

A number of studies have documented the restriction of *T. cruzi* to particular tissues during the chronic phase of the infection in murine models (19-21). During the acute phase of infection, *T. cruzi* invades many different tissues, including the lungs, gastrointestinal tract, thymus, lymph nodes, spleen, heart, kidneys, skin and the eyes (22). During the chronic phase, parasite localization is dependent on parasite and host strain genetics. For instance, C57Bl/6J mice infected with the Brazil strain of *T. cruzi* have parasite persistence in skeletal muscle, while parasites localize to cardiac muscle in C3H mice chronically infected with the Sylvio X10/4 clone.

Immunity to T. cruzi

Control of *T. cruzi* infection requires the activation of multiple immune effector mechanisms. Control of the extracellular stage of *T. cruzi*, the trypomastigotes, is probably mediated primarily by antibodies. Injection of anti-*T. cruzi* antibodies in *T. cruzi* infected mice

results in rapid clearance of parasites (23, 24). Additionally, mice lacking antibody-producing B cells fail to control infection (25). While the humoral response is necessary for control of trypomastigotes a cell-mediated response involving $CD4^+$ T cells or $CD8^+$ T cells against the intracellular amastigotes is also required. Mice lacking in either $CD4^+$ T cells or $CD8^+$ T cells are highly susceptible to infection and exhibit increased blood and tissue parasite levels as compared to wild-type mice (26-31). In mice deficient in both $CD4^+$ T cells and $CD8^+$ T cells susceptibility to infection is even greater than that seen in single knockouts (28).

While both major T cell types are necessary for control of *T. cruzi* infection, they likely have different immune functions. $CD4^+$ T cells, known as T helper cells (Th), are further classified as Th1 or Th2 cells. The primary function of T helper cells is activation of cell types including B cells, cytolytic cells ($CD8^+$ T cells), and macrophages. This activation is through cytokine production; Th1 cells produce type 1 cytokines such as interferon-gamma (IFN-γ) and Th2 cells produce the type 2 cytokines interleukin-4 (IL-4), IL-5, and IL-13. The importance of Th1 and Th2 responses during *T. cruzi* infection has been studied using a number of approaches. Stat4 is a transcriptional regulator responsible for transduction of IL-12 signals from cell surface receptors to the nucleus, enhancing the expansion of Th1 cells. Mice lacking Stat4 fail to generate Th1 cells, thus producing dramatically less IFN-γ, and are highly susceptible to *T. cruzi* infection (32). Alternatively, Stat6 transduces IL-4 signals from cell surface receptors to the nucleus, driving Th2 expansion. Mice lacking Stat6 are largely unable to generate Th2 response, produce normal levels of IFN-γ, and are similar to WT mice in their resistance to *T. cruzi* infection (32). These results highlight the importance of Th1 responses in control of *T. cruzi* infection. Alternatively, $CD8^+$ T cells mediate immune control through induction of cell lysis by Fas/FasL interaction, by perforin/granzyme B secretion or by cytokine production, specifically

IFN-γ. In *T. cruzi* infection $CD8^+$ T cells are the predominant lymphocyte population found in sites of parasite persistence (31). It is known that several *T. cruzi* proteins are targets for $CD8^+$ T cells (33-35) and these molecules can elicit protective responses when delivered as vaccines (18, 34, 36).

Interferon-gamma

IFN-gamma is a cytokine secreted by natural killer (NK) cells, $CD8^+$ T cells and Th1 $CD4^+$ T cells, and regulates over 200 genes involved in the immune response (reviewed in (37))(38, 39). In terms of its effect on $CD4^+$ T cells, IFN-γ stimulates the secretion of IL-2, which binds receptors on naïve $CD4^+$ T cells and promotes the differentiation or expansion of Th1 cells (40-43). IFN-γ also promotes Th1 cell differentiation by inducing the transcription factor T-bet (44). Additionally IFN-γ enhances MHC class II expression on antigen presenting cells, increasing the chance of interaction with $CD4^+$ T cells (45-47). IFN-γ affects responses by $CD8^+$ T cells through its effects on antigen presentation cells, including 1) stimulation of LMP-2 and LMP-7 proteins which enhance antigen processing in proteasomes , 2) induction of the transporter associated with antigen processing (TAP) which transports peptide to the ER, and 3) stimulation of the production of MHC class I molecules which are loaded with peptide in the ER and transported to the cell surface where interaction with $CD8^+$ T cells occurs (48-53). Once T cells are activated they must traffic to sites of infection and IFN-γ supports this movement by promoting lymphocyte recruitment, adhesion to endothelial cells and extravasation, by IFN-γ-inducible chemokines released at sites of infection (54-64). Additionally, IFN-γ acts on B cells, resulting in switching of IgG to subclasses which bind receptors on macrophages and activate complement components, thus enhancing opsinization of microbes (65, 66). Finally, secretion of

IFN-γ by both T cells and NK cells stimulates production of reactive oxygen intermediates and nitric oxide which destroys microbes (67-71).

Regulation of downstream genes by IFN-γ is mediated through the JAK/STAT signaling pathway and involves the translocation of gamma-interferon activation factor (GAF), also known as STAT-1, to the nucleus and its binding at gamma activated sites (GAS) in the promoters of primary response genes, leading to induced gene transcription. Among the primary response genes activated by IFN-γ binding are transcription factors such as interferon regulatory factor (IRF), which regulates the expression of secondary response genes through binding to promoters with interferon-stimulated response elements (ISRE) motifs.

IFN-γ is critical for the control of *T. cruzi* in mammals. Susceptibility to *T. cruzi* infection is significantly increased in mice treated with anti-IFN-γ antibodies as well as mice lacking IFN-γ (72-78). Additionally, infected mice respond to IFN-γ administration with enhanced parasite clearance and increased survival as compared to non-treated infected mice (79, 80). IFN-γ is apparent as early as day 6 post infection in mouse spleens and expression persists in the spleen through the chronic phase of the infection (81). The specific mechanism(s) by which IFN-γ contributes to control of *T. cruzi* infection are not known. This work evaluates the production and role of IFN-γ-inducible nitric oxide and chemokines during the course of murine infection with *T. cruzi*.

Nitric oxide

It is proposed that IFN-γ-inducible nitric oxide is a major component of the IFN-γ induced protective response against *T. cruzi*. Nitric oxide (NO) is a small, reactive, diffusible gas that is catalyzed by the enzyme nitric oxide synthase (NOS) which exists in three isoforms, NOS1, NOS2, NOS3 (82, 83). Of the three isoforms only NOS2, also known as inducible nitric

oxide synthase, iNOS, is regulated by microbial products (LPS) and cytokines (IFN-γ, TNF-α, etc.). Induction of iNOS expression by IFN-γ is through both GAF and IRF-1 which bind putative transcription factor recognition boxes, GAS and ISRE respectively, contained in the promoter region of the iNOS gene. Both GAS and IRF-1 are required for maximal expression of iNOS (67, 84). IFN-γ induces not only the enzyme which catalyzes nitric oxide production, NOS, but also the production of arginine, the substrate for NOS (69) and elevates the production of the NOS reaction-limiting cofactor tetrahydrobiopterin (85).

With respect to *T. cruzi* infection, the NO-inducing effect of IFN-γ has been extensively studied. While primarily studied as a product of macrophages in the case of *T. cruzi* infection, a wide variety of cells, including myocytes and fibroblasts produce iNOS in response to pathogens and cytokines (83, 86-90). Induction of iNOS expression by cytokine treatment of *T. cruzi*-infected macrophages results in a dramatic reduction in the ability of amastigotes to survive and replicate in these cells (91). This regulation of parasite growth is reversed by the inclusion of inhibitors of iNOS production in the culture, supporting the role of NO, rather than other cytokine-induced activities, in the control of *T. cruzi* infection in vitro (91, 92). In vivo studies have also suggested a critical role for NO production in control of *T. cruzi* infection. Mice administered iNOS inhibitors N-monomethyl-L-arginine (L-NMMA) or Nomega-nitro-L-arginine (NOARG) exhibit increased parasite levels and greater mortality as compared to untreated mice (89).

Although in vivo and in vitro studies provide strong evidence of an ability of NO to limit the growth of *T. cruzi* this conclusion rests primarily on the use of chemical inhibitors of iNOS, the absolute specificity of which for iNOS has not been proven. An alternate approach to the study of the role of iNOS in vivo would be the infection of mice in which the iNOS gene has

been deleted or inactivated. Three iNOS knockout mouse strains have been generated by insertional deletion of all or part of the mouse iNOS gene (93-95). Wei et al constructed a strain that later was determined to have delayed production of the functional protein (95). In the $Nos2^{tm1Lau}$ strain the calmodulin binding domain of the iNOS gene, which is required for enzymatic activity, is replaced by the neomycin resistance gene and has a disrupted reading frame resulting in an inactive iNOS protein (93). The iNOS deficient mice strain Nos2 N5 lacks the promoter and the first four exons of the iNOS gene (94). In this work, the importance of IFN-γ-inducible iNOS in control of *T. cruzi* infection was examined using mice deficient in iNOS.

Chemokines

The predominant immune effector cell population in infected tissue during both the acute and chronic phases of *T. cruzi* infection is $CD8^+$ T lymphocytes (31, 96) and several studies have reported the requirement for $CD8^+$ T lymphocytes in the control of *T. cruzi* infection in vivo (27, 28, 30, 97). It is believed that activated $CD8^+$ T cells traffic to sites of infection, recognize parasite peptides presented in association with MHC class I molecules on the infected cells surface, and interact with infected cells to control or prevent parasite replication (33, 34, 98). The importance of $CD8^+$ T cells in control of *T. cruzi* infection has led us to focus on genes upregulated by IFN-γ that affect $CD8^+$ T cell recruitment to infected tissues.

Induction of chemokine expression is among the many activities of IFN-γ. Chemokines are a large family of secreted proteins that attract various cell types, including but not limited to neutrophils, dendritic cells, and T cells to specific anatomical sites. In addition to cell recruitment, chemokines are involved in angiogenesis, cell development (dendritic cells, B and T cells), inflammation, and cell compartmentalization in lymphoid organs. Chemokine gradients

guide naïve T cells, by receptor and ligand interaction, to secondary lymphoid tissue where they become activated and then to sites of infection where the activated T cells exhibit effector functions (99, 100).

Immune responses against intracellular pathogens generally require recruitment of effector T cells to sites of infection. IFN-γ upregulates the expression of several chemokines which are known to attract T lymphocytes. The IFN-γ-inducible chemokine, IP-10 (interferon-induced protein of 10 kDa), is essential for recruiting both $CD4^+$ and $CD8^+$ T cells to organs infected with *Toxoplasma gondii* (101). In addition to IP-10, IFN-γ-induced MIP-1α (macrophage inflammatory protein-1α) and MIG (monokine induced by gamma-interferon) also participate in the recruitment of activated T lymphocytes (64, 102, 103).

Recently, Talvani et al examined chemokine production at sites of *T. cruzi* infection in mice infected with the Columbiana strain of *T. cruzi*, a strain which localizes to cardiac tissue in the chronic phase of infection in C57Bl/6 mice (104). These authors found that IFN-γ-inducible chemokines MIP-1α, IP-10 and MIG were all expressed early in the infection, with continued expression of IP-10 and MIG through the chronic phase of infection. The IFN-γ-inducible chemokines MIP-1α, IP-10 and MIG are known to attract activated $CD8^+$ T lymphocytes (64, 102, 103) and we hypothesized that IFN-γ-inducible chemokines are involved in recruiting T cells to sites of *T. cruzi* localization. While IFN-γ-inducible chemokines have been evaluated, the impact of IFN-γ on chemokine receptor expression during *T. cruzi* infection has not been previously studied and is the focus of one aspect of this work.

Quantification of tissue parasite burden

To accurately evaluate the course of *T. cruzi* infection a sensitive and quantitative method to detect parasites is necessary. Microscopic detection of trypomastigotes in host blood, is able

to quantify circulating parasites during the acute stage of infection but lacks the sensitivity necessary for quantitation of the low numbers of parasite found during the chronic stage. Additionally, detection of trypomastigotes in the blood does not necessarily correlate with tissue parasitism. While detection of *T. cruzi* DNA in host blood and tissue by standard PCR is sensitive, it is not quantitative, preventing the evaluation of experimental treatments. In addition, microscopic evaluation of stained tissue from both the acute and chronic phases of infection is qualitative but not quantitative. To effectively evaluate experimental treatments and parasite persistence in the host, both human and experimental models, quantification of parasite burden in tissue is necessary. During the chronic phase of infection, *T. cruzi* is difficult to detect and even more difficult to quantitate. This creates a problem for evaluating the efficacy of experimental treatments, either preventative or therapeutic. Methods that have been used to detect *T. cruzi* in tissue include haematoxylin and eosin staining, in situ PCR and competitive PCR. Although useful for making a qualitative evaluation for the presence of *T. cruzi*, none of these methods are reliable for quantitative purposes. One goal of this work was to develop a method to quantify the number of parasites present in infected tissues.

Recently, real-time PCR techniques have been described that measure and quantify the PCR products synthesized during amplification (105) and the applicability of real-time PCR for diagnosing and monitoring human cytomegalovirus (HCMV) in patient blood samples (106) and *T. gondii* in fetal tissue sections (107) has been reported. Real-time PCR, unlike traditional PCR, detects the amplified products during each PCR amplification cycle and calculates product quantity from the log-linear phase of amplification.

To distinguish *T. cruzi* specific DNA from the more abundant mouse DNA in tissue, a *T. cruzi* DNA target with a high number of copies per parasite is desirable. Kinetoplast DNA

(kDNA) provides a high copy number target for amplification (108). *T. cruzi* kDNA consists of concatenated minicircles and maxicircles. Each minicircle is constructed of 4 similar repeat sequences within which exist conserved regions of 12, 10 and 8 bases each. The four regions on 10,000 minicircles provide 40,000 PCR template molecules per parasite (109). An additional target for amplification is the 195 base-pair nuclear *T. cruzi* DNA repeat sequence. There are approximately 120,000 copies of this tandomly repeated sequence (110). Primers for both *T. cruzi* DNA targets were optimized and the sensitivity of detection of *T. cruzi* DNA was assessed. The PCR technique for quantification of tissue parasite burden was then used to analyze parasite load in a number of murine models of *T. cruzi* infection.

Control of *T. cruzi* infection requires a competent cell-mediated immune response and the activation of $CD8^+$ T cells and subsequent production of IFN-γ. Effector cells must traffic to sites of infections, and such trafficking may be regulated by IFN-γ-inducible chemokines. Additionally, at the site of infection, IFN-γ-inducible iNOS may be necessary for limiting parasite growth. This work evaluates the importance of iNOS production and the production and localization of chemokine and chemokine receptor expression in murine models of *T. cruzi* infection.

CHAPTER 2

RAPID QUANTITATION OF *TRYPANOSOMA CRUZI* IN HOST TISSUE BY REAL-TIME PCR[1]

[1]Cummings K.L. and R.L. Tarleton. 2003. *Molecular and Biochemical Parasitology*. 129:53-59.
Reprinted here with permission from Elsevier.

Abstract

A real-time PCR technique that allows for accurate and sensitive quantitation of tissue parasite burden in animals infected with the protozoan parasite *Trypanosoma cruzi* was developed. The utility of this method was demonstrated by confirmation of higher parasite load in mice with acute infections in comparison to chronically infected mice, detection of tissue-restricted parasite persistence in different parasite:host strain combinations, and the observation of increased tissue parasite burden with higher infective doses. This method should be a useful tool for monitoring parasite burden in hosts under various treatment regimens.

Introduction

Infection with the protozoan *Trypanosoma cruzi* generally results in an acute phase, wherein parasites are relatively plentiful both in the peripheral blood and in tissues, followed by a chronic stage during which parasites are difficult to detect in either the blood or tissue. A variety of methods that have been used to detect *T. cruzi* in tissues, including haematoxylin and eosin staining, in situ PCR and competitive PCR. Although useful for making a qualitative evaluation for the presence of *T. cruzi*, none of these methods are reliable for quantitative purposes. Competitive quantitative PCR is generally considered to be at best semi-quantitative since the calculation of amplified product is limited to the plateau phase of the amplification reaction. Alternatively, real-time PCR acquires data at each cycle of the PCR reaction, allowing for calculation of product amount from the log-linear region of the amplification curve. In this study, we evaluate real-time PCR as a method to quantify the amount of *T. cruzi* in tissue samples from infected mice.

During the acute phase of *T. cruzi* infection, parasites are distributed throughout most tissues of the body (22, 96, 111). However, in both animal models and in humans as the chronic

phase progresses, parasite distribution appears to become more restricted to particular anatomical sites (e.g. heart, skeletal muscle, or gut (19, 21, 112-115). The ability of hosts to survive the acute phase of infection and to progress to the chronic phase, and as well, the distribution of parasites among tissues during the chronic phase is dependent on both host and parasite genetics. For example, C3H/HeSnJ mice chronically infected with the Sylvio X10/4 clone of *T. cruzi* exhibit parasite persistence in the heart but not the skeletal muscle (20, 21). This same mouse strain is highly susceptible to the Brazil strain of *T. cruzi* and rarely survives the acute stage of infection. In contrast, C57Bl/6J mice infected with the Brazil strain develop chronic infections with parasite persistence in the skeletal muscle but not the heart (21, 31). C57Bl/6J mice infected with the Sylvio X10/4 clone rarely survive the acute stage of the infection (20).

In order to determine the accuracy of the observations reviewed above and to test the ability of real-time PCR to quantify parasite levels in tissues of mice infected with *T. cruzi*, we developed protocols for the real-time PCR quantification of *T. cruzi* in tissues of infected mice.

Materials And Methods

Mice and Parasites.

C57BL/6J mice were obtained from The Jackson Laboratory (Bar Harbor, Maine) and C3H/HeSnJ and BALB/cJ were bred in our facilities from stock obtained from The Jackson Laboratory. Mice were infected by i.p. injection with 1,000 blood-form trypomastigotes (BFTs) of the Brazil strain of *Trypanosoma cruzi* (C57BL/6J, BALB/cJ females), or with 10^6 culture form trypomastigotes of the Sylvio X10/4 strain (C3H/HeSnJ males), which leads to chronic infection. Infection dose versus parasite burden studies in C57BL/6J mice were conducted by injection with 10^3, 10^4, 10^5, 10^6 BFTs of the Brazil strain and 5, 50, and 500 BFTs of the Tulahuen strain of *T. cruzi*. Re-infection studies were conducted by injection of chronic

C3H/HeSnJ mice (previously infected with 10^6 Sylvio X10/4 strain of *T. cruzi*) with 10^6 Sylvio X10/4 strain, or 10^3 or 10^5 Brazil strain trypomastigotes.

DNA Preparation.

Heart and skeletal muscle tissues collected from mice at the indicated time points post-infection were minced using surgical blades (Fisher Scientific, Pittsburgh, PA). A 5X volume of sodium dodecyl sulfate (SDS)-proteinase K lysis buffer (116) was added to skeletal muscle and cardiac muscle samples from each of the mice. The lysis buffer consisted of 10mM Tris-HCl (pH 7.6) (BioRad Laboratories, Hercules, CA), 0.1 M NaCl (J.T. Baker, Phillipsburg, NJ), 10 mM EDTA (J.T. Baker), 0.5% SDS (BioRad) and 300 μg of proteinase K/ml (Roche, Indianapolis, IN). Samples were then heated for 2 hours at 55°C, and extracted twice with phenol:chloroform:isoamyl alcohol (25:24:1) (Sigma, St. Louis, MO). Cold ethanol (AAPER Alcohol and Chemical Co., Shellyville, KY), twice the volume of the extracted sample, was then added and samples were placed at -80°C for 30 minutes. Samples were centrifuged for 30 minutes at 13,000 rpm and washed with 70% ethanol, vacuum dried and resuspended in sterile water.

Generation of PCR Standards.

The standards for the PCR reactions were generated using 500 mg of minced normal tissue, either skeletal or cardiac muscle, to which 10^7 *T. cruzi* epimastigotes were added. The tissue was then treated, extracted and precipitated as described above. Once resuspended, the DNA was serially diluted with 25 mg/ml DNA from normal tissue. The standard 10-fold dilutions ranged from 0.01 to 1000 parasite equivalents per 50 ng of total DNA. A standard curve was generated from these dilutions to determine the parasite load of DNA from infected tissue samples.

Real-time Quantitative PCR.

Each PCR reaction contained 50 ng genomic DNA, 0.5 μM of *T. cruzi* 195-bp repeat DNA specific primers TCZ-F* 5'GCTCTTGCCCACAMGGGTGC-3', where M=A or C (TIB Molbiol; modified from (110), and TCZ-R 5'CCAAGCAGCGGATAGTTCAGG-3' ((110), modified), which amplify a 182-bp product, 10 μl Qiagen QuantiTect Sybr Green PCR Master Mix (Qiagen), and PCR-grade H_2O (Qiagen) to a final total volume of 20μl. Where indicated the following kDNA primers, which amplify a 330-bp product, were used; 0.075 μM of *T. cruzi* minicircle specific primers S36 5'GGGTTCGATTGGGGTTGGT-GT-3' ((108), modified) and S35 5'AAATAATGTACGGGKGAGATGCATGA-3' (K=G or T) (108). Separately, reactions containing 50 ng genomic DNA, 0.5 μM of murine-specific tumor necrosis factor-α (TNF-α) primers TNF-5241 5'TCCCTCTCATCAGTTCTATGGCCCA3' and TNF-5411 5'CAGCAAGCATCTATGCACTTAGACCCC3' (designed by Vector NTI), 10 μl Qiagen QuantiTect Sybr Green PCR Master Mix (Qiagen), and PCR-grade H_2O (Qiagen) to a final total volume of 20μl, were used as loading controls. Modification of original satellite and kDNA primers (108, 110) enhanced the sensitivity of the real-time PCR reactions.

The reaction mixes were loaded into Roche LightCycler™ Capillaries, capped, centrifuged for 10 seconds at 2000 rpm, and placed in the LightCycler™ (Roche). The cycling program for the LightCycler™ has four phases; denaturation, amplification, melting and cooling. In the denaturation phase the capillary is heated to 95°C at 20 °C/sec ramp and held for 15 minutes. During the 50 cycles of the amplification phase there are three steps; 95°C at 20°C/sec ramp for 10 seconds, then to 55°C at 20°C/sec ramp, for 15 sec, and 72°C at 2°C/sec ramp for a 5 sec hold. At the end of the 8 seconds at 72°C, the fluorescence intensity is acquired. The third phase is the melt which begins with 95°C at 20°C/sec ramp, 0 sec hold, then 60°C at 20°C/sec ramp, 30 sec hold, and finally 90°C

at 0.2°C/sec ramp, 0 sec hold. During the melting phase, the acquisition setting is set at "step". Finally, the cooling phase lasts one minute at 40°C at 20°C/sec. Data were acquired and analyzed with LightCycler™ Version 3.0 software.

Each LightCycler run contained two negative controls. Negative controls for PCR with *T. cruzi*-specific primers consisted of a reaction with no DNA added and a reaction with non-infected skeletal muscle DNA. Controls for PCR with murine-specific primers consisted of a reaction with no DNA added and a reaction with *T. cruzi* DNA. Each DNA sample was quantified in triplicate. Triplicate values for each *T. cruzi*-specific DNA sample were averaged and the *T. cruzi*-specific value was corrected by calculating the ratio of *T. cruzi*-specific product to averaged murine TNF-α product (loading control). Corrected values for each experimental group were averaged and the standard error of the mean was determined. Data in Table 1 include the average of triplicate values for each DNA sample (mean), standard deviation of triplicate values (S.D.), and the standard error of the mean (SEM) for the mean of the individual sample averages. The efficiency of amplification was determined using the following calculation: Efficiency (E) = $[10^{(-1/\text{slope})}]$ (117).

Results and Discussion

Primer selection

Two primer sets, both of which had been previously used for standard PCR-based detection of *T. cruzi*, were selected for evaluation in quantitative real-time PCR analysis. Primers S35 and S36 target a kinetoplast minicircle sequence (kDNA) present in approximately 120,000 copies (four minirepeats per ~30,000 minicircles in CL and Y strains) (108, 109). Primer set TCZ is capable of amplifying a 195-base, tandomly repeated genomic sequence present in approximately 120,000 copies in the Y strain of *T. cruzi* (110, 118). Optimal DNA extraction and amplification conditions were determined for parasite alone, for parasite addition to normal

mouse tissue, and for infected mouse tissue. Additionally, for each primer set the optimal PCR conditions were determined by adjusting primer concentration, annealing temperature, and extension time.

During each cycle of a real-time PCR reaction, the fluorescence of double-stranded DNA binding dyes incorporated into PCR products can be measured and recorded. In Figure 2.1A, *T. cruzi* DNA diluted with murine skeletal muscle DNA was amplified using primers for the 195-bp genomic sequence (satellite DNA). A typical amplification curve is shown, where two negative controls were used, a PCR reaction without DNA and a reaction with murine skeletal muscle DNA without *T. cruzi* DNA (0 parasites). From the dilution series a standard curve was generated (Figure 2.1B) with a nearly perfect negative relationship between cycle number and log concentration ($r = -0.999$).

Using a dilution series of *T. cruzi* DNA, the limits of detection for both the kDNA and satellite DNA primer sets were evaluated. The limit of detection of the satellite DNA primers was 0.01 parasite equivalents, while kDNA primers could detect only to the 0.1 parasite equivalents level (Figure 2.1C). Concentrations lower than 0.01 parasite equivalents were not detectable with either primer set. Attempts to increase detection sensitivity by digestion of DNA with topoisomerase (kDNA) or Nru 1, and sheering DNA by sonication or needle passage (satellite DNA) were not successful (data not shown). With a 0.01 parasite equivalents detection limit, satellite DNA primers were chosen to amplify *T. cruzi* DNA in subsequent experimental samples.

Normalization

The primary goal of this work is the development of a method to obtain accurate and sensitive quantification of *T. cruzi* in host tissues. Because we found that the recovery of DNA

from different tissue samples was significantly variable, it was considered important to have an internal control by which to normalize the amount of tissue being analyzed in each PCR reaction. For this purpose, we chose a single copy mouse gene, TNF-α, to correct for intra-sample variations in initial sample amount, DNA recovery, and sample loading.

Normalization with an external standard is possible only if amplification of both products, the *T. cruzi* 195-bp sequence and the murine TNF-α occurred with the same efficiency. A representative PCR run for each primer pair is shown in Figure 2.2, where the efficiency is nearly equal (TNF-α primers E=0.400, *T. cruzi* primers E=0.425). For normalization of each sample, the concentration of the target (*T. cruzi* DNA), as determined by real-time PCR, in each tissue sample was divided by the concentration of the murine TNF-α reference gene in the same tissue sample, as described in Materials and Methods.

Quantitative verification of tissue parasite load during *T. cruzi* infection

During the acute phase of infection, *T. cruzi* amastigote nests are found in abundance in a wide range of tissues (22, 111). In contrast, fewer parasites are apparent in the chronic phase of infection and these parasites are largely restricted to muscle tissue, with the specific tissue site being dependent on the host and parasite strain (19-21, 113-115). To evaluate the utility of real-time PCR for detecting *T. cruzi* in skeletal muscle samples, C57Bl/6J mice infected with the Brazil strain were assayed at different time points in the infection (Figure 2.3). Muscle samples from acutely infect mice (28 dpi) exhibit amplification products at early cycles, consistent with the expected higher parasite load, while similar tissues from mice later in the infection (150 dpi) required longer cycling times to reveal amplification products.

To verify the consistency of parasite load calculated by real-time PCR, and to further document the ability of the technique to detect the very low levels of parasites expected to be

present in tissues from chronically infected mice, the parasite load in cardiac muscle tissue from chronically infected C3H mice was determined in three separate real-time PCR runs (Table 1.). For each run, tissues from 5 mice were analyzed. The results confirm that real-time PCR can detect low levels of *T. cruzi* in tissues of chronically infected mice and that the data obtained can be compared between individual real-time PCR runs.

A number of studies have documented the restriction of *T. cruzi* to particular tissues during the chronic phase of the infection (19-21). Previously, we used in situ PCR to correlate parasite persistence with disease in two mouse:parasite strain combinations (21). This previous study showed that during the chronic stage of infection, parasites and disease are relatively restricted to the heart in the case of the C3H:Sylvio X10/4 combination and to the skeletal muscle in the case of C57Bl/6 mice infected with the Brazil strain. Additionally, this study indicates that the *T. cruzi* DNA detected in tissues is not due to long-term persistence of DNA but to parasite persistence in the tissues (21). To determine if real-time PCR analysis led to similar conclusions regarding parasite distribution in these chronic infections, we used quantitative real-time PCR to determine parasite tissue load in C3H/HeSnJ mice infected with the Sylvio X10/4 clone and C57Bl/6 mice infected with the Brazil strain of *T. cruzi*. As seen in Figure 2.4, at 300 days post-infection parasite load was not significantly greater in the cardiac muscle relative to skeletal muscle of C3H mice infected with the Sylvio X10/4 clone. In B6 mice infected with the Brazil strain of *T. cruzi*, 4 out of 5 mice were positive for *T. cruzi* in the skeletal muscle while none of the mice had detectable *T. cruzi* satellite DNA in the cardiac muscle. These data indicate that the Brazil strain of *T. cruzi* is not detectable in cardiac muscle in the chronic phase of infection in C57Bl/6J mice and localizes to the skeletal muscle. In C3H mice the observation of localization in cardiac muscle is not quantitatively verified in this set of

mice at this point in infection, the cardiac muscle and skeletal muscle have similar values. These data demonstrate the utility of real-time PCR in evaluating samples from experimental infections.

Issues relevant to endemic regions

In natural infections with *T. cruzi*, the infective dose of parasite received likely varies between individuals. However, the correlation, if any, between infective dose of *T. cruzi* and tissue parasite burden has not been quantitatively assessed. To evaluate this relationship, C57BL/6J mice were infected with varying numbers of the Brazil strain and the more virulent Tulahuen strain of *T. cruzi*. Skeletal and cardiac muscle from mice infected with the Tulahuen strain were collected at 20 dpi as C57BL/6J mice infected with this strain typically die within 25 days of infection. Tissues from mice infected with the Brazil stain were collected during the peak of the acute phase, 28 days post-infection. Increasing the infective dose of the Brazil strain yields increasing parasite burden in the skeletal muscle, the site of parasite persistence in this model, but no obvious pattern of parasite numbers in the cardiac muscle (Figure 2.5A). In contrast, infection with low and increasing numbers of Tulahuen strain parasites not only resulted in higher tissue parasite burdens than the higher numbers of Brazil strain parasites, but also resulted in a dose-dependent level of parasites in both the skeletal and cardiac muscle (Figure 2.5B).

In addition to variation in infective dose, infected hosts living in endemic regions also face the possibility of re-infection with *T. cruzi* (119). To determine if re-infection of chronically-infected mice altered the existing level of tissue parasite load in mice, the tissue parasite burden in chronically infected C3H mice was examined 14 days after re-infection with either 10^6 Sylvio X10/4, 10^3 Brazil, or 10^5 Brazil strain trypomastigotes. Although parasite load

was modestly higher in the skeletal muscle of re-infected mice, this difference was not statistically significant and no change was observed in tissue parasite load in the cardiac muscle (Figure 2.6). Thus, at least in this model, re-infection is not accompanied by a significant increase in the level of tissue-resident parasites.

These results demonstrate the utility of real-time PCR for quantitative measurement of tissue parasite load in experimental *T. cruzi* infection. Two *T. cruzi*-specific primers sets were optimized and the set amplifying the 195-base, tandomly repeated genomic sequence exhibited greater sensitivity than the primer set amplifying kinetoplast DNA. In addition to developing a highly quantitative and sensitive assay an internal reference, murine TNF-α, allows highly reproducible results. With this technique we demonstrated the ability to detect low levels of parasites in infected hosts, that tissue parasite load varies depending on parasite strain, tissue, time of infection, and dose of infection, but is not altered by re-infection. In addition, as *T. cruzi* DNA detected in tissues is not due to long-term persistence of DNA but to parasite persistence in the tissues (21), this technique should find utility in vaccination and drug studies in experimental animal models.

Table 2.1. Consistency of quantified product from three different real-time PCR runs

Individual mouse cardiac muscle sample	Parasite equivalents/50 ng of DNA			
	Run 1	Run 2	Run 3	Mean (S.D.)
1	2.754	2.718	2.341	2.604 (0.23)
2	2.236	2.228	2.566	2.343 (0.19)
3	1.798	1.588	1.893	1.760 (0.16)
4	2.560	2.808	2.682	2.683 (0.12)
5	0.444	0.386	0.535	0.455 (0.08)
Run Mean	1.958 (0.92)	1.945 (1.00)	2.003 (0.87)	1.969 (SEM = 0.41)

Figure 2.1. Standard curve generated from DNA of normal skeletal muscle and epimastigotes of *Trypanosoma cruzi*. Samples are of ten-fold dilutions of DNA (0.01 parasite equivalents to 1000 parasite equivalents). A. Representative amplification curves generated with primers specific to 195-base, tandomly repeated genomic sequence (satellite DNA). B. Standard curve generated from linear region of each amplification curve. C. Limit of detection of two *T. cruzi* DNA targets, satellite DNA and kDNA (ND=not detected).

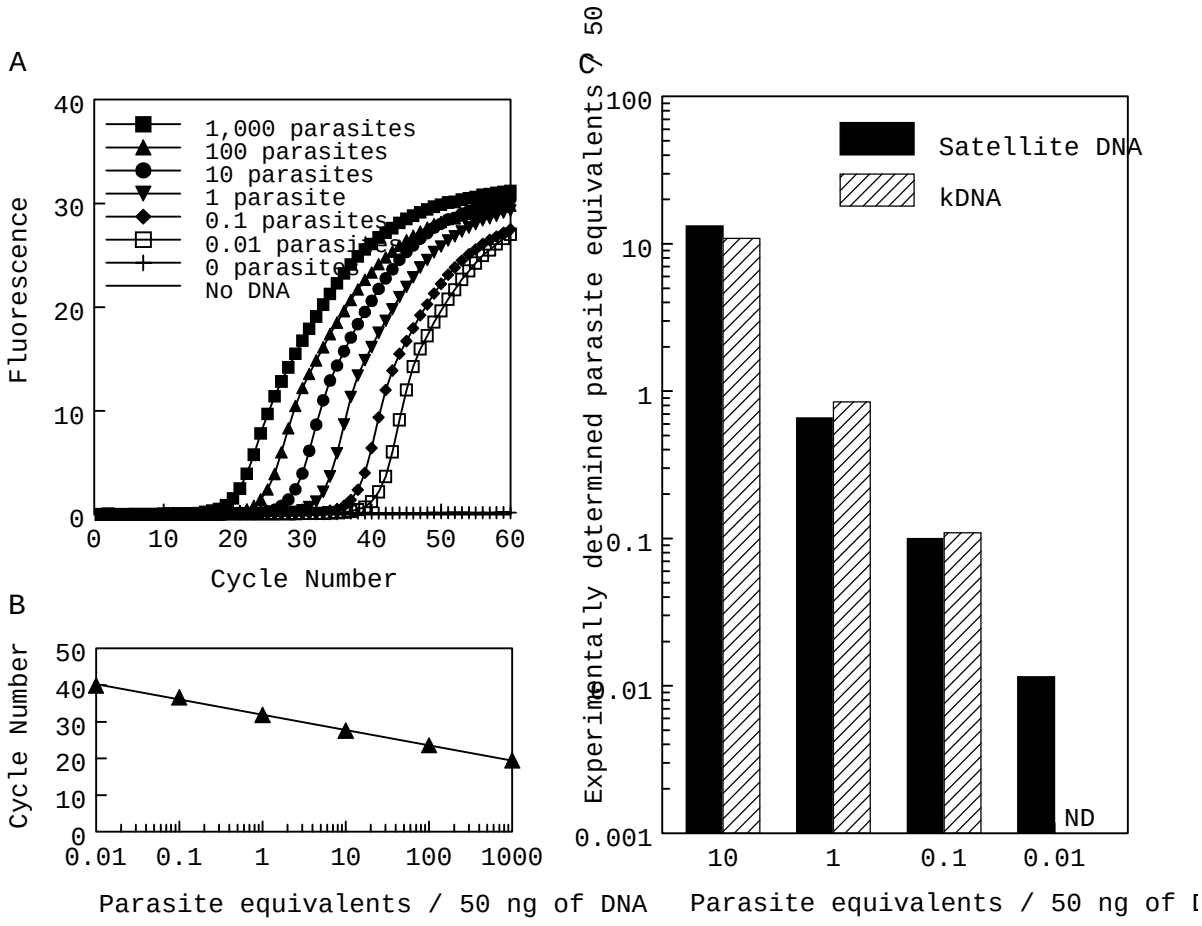
A
Fluorescence
Cycle Number
1,000 parasites
100 parasites
10 parasites
1 parasite
0.1 parasites
0.01 parasites
0 parasites
No DNA
B
Cycle Number
Parasite equivalents / 50 ng of DNA
C
Experimentally determined parasite equivalents / 50
Satellite DNA
kDNA
ND
Parasite equivalents / 50 ng of D

Figure 2.2. Efficiency of amplification. DNA extracted from the combination of normal skeletal muscle and *T. cruzi* was subsequently serially diluted with water. A ten-fold dilution series was amplified with primers specific to murine TNF-α (triangle) or primers specific to *T. cruzi* DNA (square). The cycle number of crossing point defines the log-linear portion of the amplification curve that starts at the cycle number where fluorescence rises above background. The cycle number of crossing point vs DNA dilutions were plotted to calculate the slope. Efficiency of amplification for each primer set was determined using the equation: Efficiency (E) = $[10^{(-1/slope)}]$.

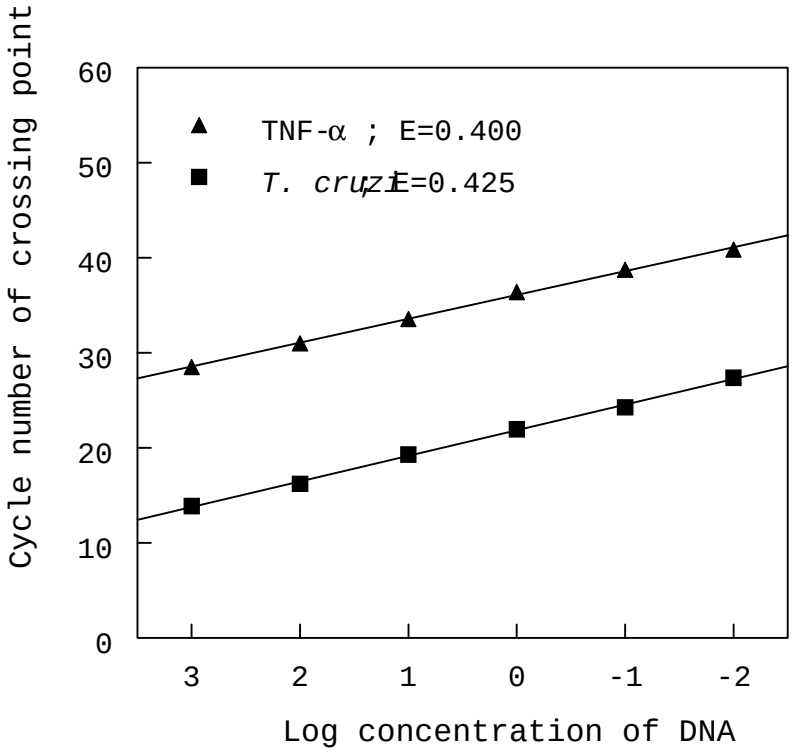
Cycle number of crossing point
60
50
40
30
20
10
0
TNF-α ; E=0.400
T. cruzi; E=0.425
3
2
1
0
-1
-2
Log concentration of DNA

Figure 2.3. Amplification of samples from B6 mice infected with 10^3 BFT of the Brazil strain of *T. cruzi*. Skeletal muscle was collected from mice at 28 (acute) and 150 (chronic) days post-infection.

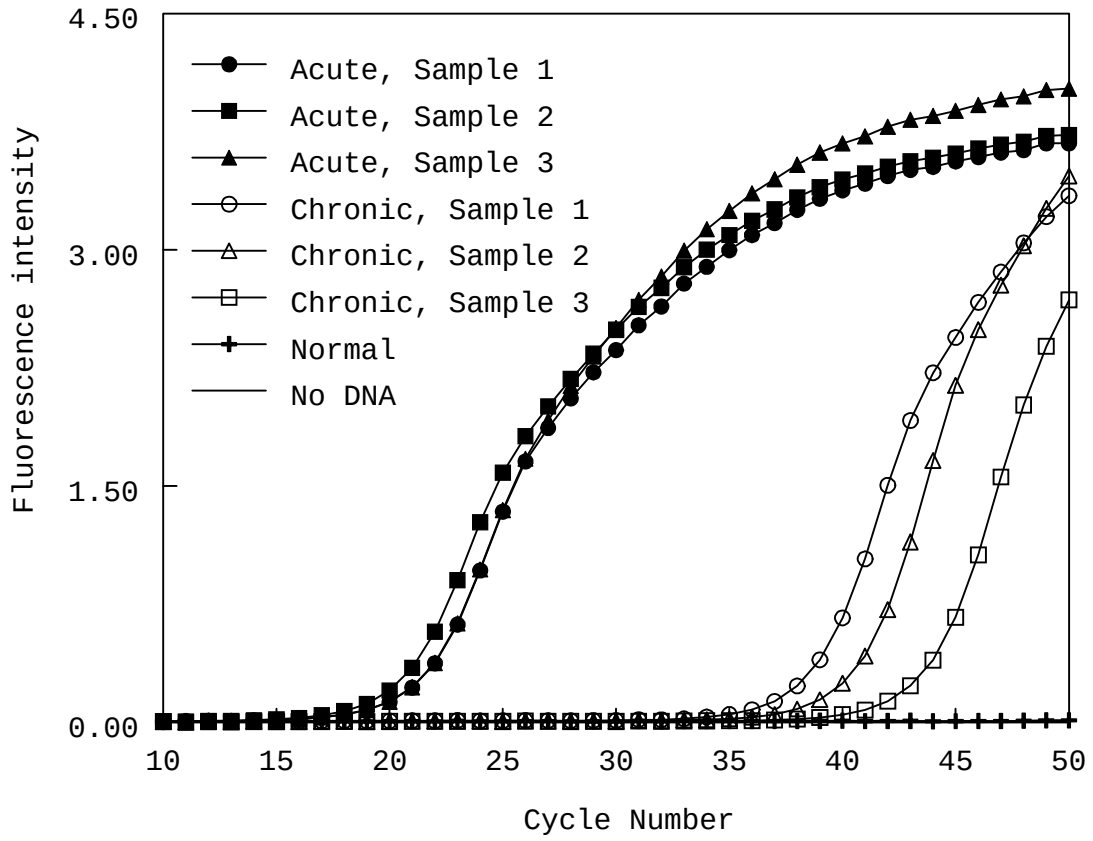
4.50
3.00
1.50
0.00
Fluorescence intensity
10
15
20
25
30
35
40
45
50
Cycle Number
Acute, Sample 1
Acute, Sample 2
Acute, Sample 3
Chronic, Sample 1
Chronic, Sample 2
Chronic, Sample 3
Normal
No DNA

Figure 2.4. Parasite burden in cardiac and skeletal muscle at 300 days post-infection in two parasite:mouse strain combinations. C3H/HeSnJ mice were infected with 10^6 fibroblast-derived trypomastigotes of the Sylvio X10/4 clone of *Trypanosoma cruzi* and C57BL/6 mice were infected with 10^3 BFT of the Brazil strain of *T. cruzi*. Data are a comparison of parasite burden in 50 ng of DNA isolated from infected muscle. ND = not detectable.

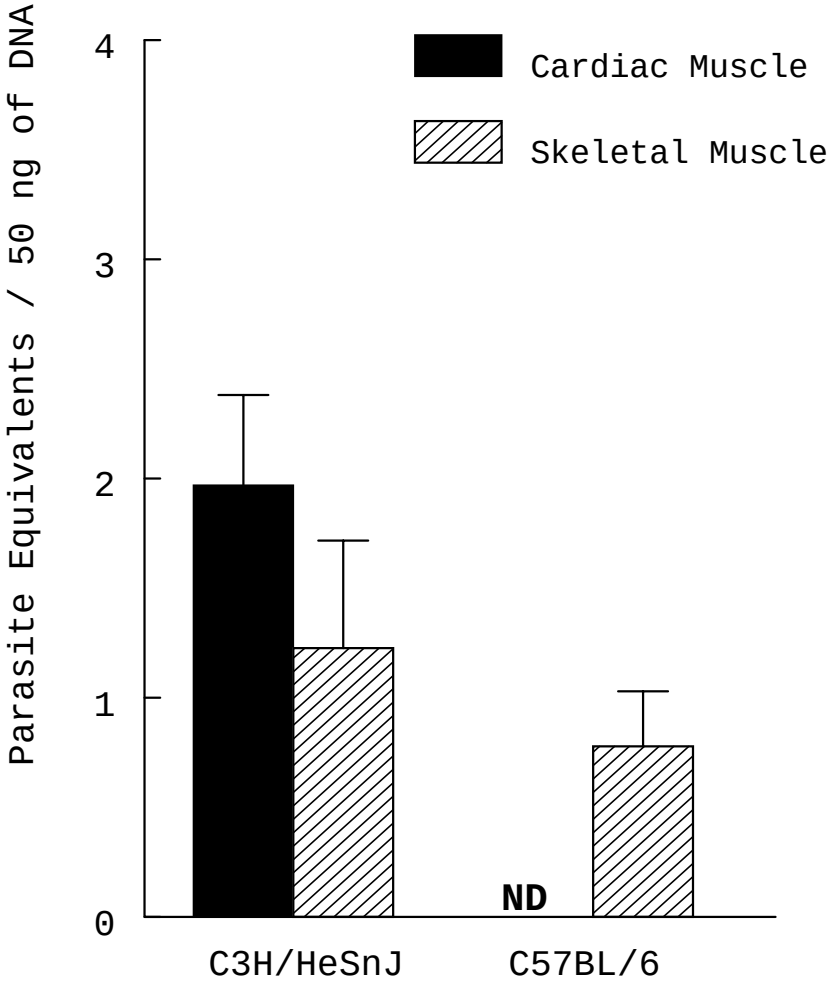
Parasite Equivalents / 50 ng of DNA
4
3
2
1
0
Cardiac Muscle
Skeletal Muscle
ND
C3H/HeSnJ
C57BL/6

Figure 2.5. Infective dose correlates with increased parasite burden in cardiac and skeletal muscle of C57BL/6 mice. C57BL/6 mice were infected with 10^3, 10^4, 10^5, or 10^6 BFT of the Brazil strain of *T. cruzi* and tissues were collected at 28 dpi (A). C57BL/6 mice were infected with 5, 50, or 500 BFT of the Tulahuen strain of *T. cruzi* (B) and tissues were collected at 20 dpi. Data are a comparison of parasite burden in 50 ng of DNA isolated from infected muscle.

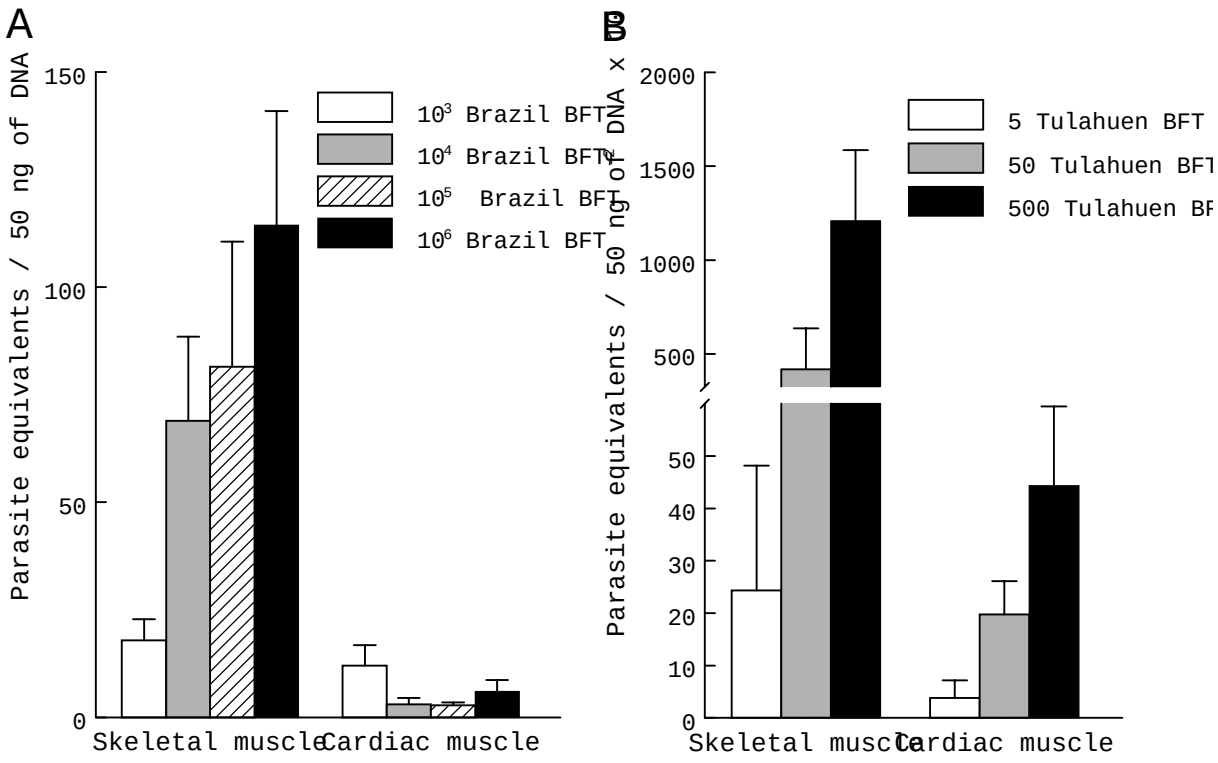
A
Parasite equivalents / 50 ng of DNA
150
100
50
0
10^3 Brazil BFT
10^4 Brazil BFT
10^5 Brazil BFT
10^6 Brazil BFT
Skeletal muscle
Cardiac muscle
B
Parasite equivalents / 50 ng of DNA x
2000
1500
1000
500
50
40
30
20
10
0
5 Tulahuen BFT
50 Tulahuen BFT
500 Tulahuen BF
Skeletal muscle
Cardiac muscle

Figure 2.6. Re-infection of chronically infected mice does not significantly increase tissue parasite burden. C3H/HeSnJ mice were infected with 10^6 fibroblast-derived trypomastigotes of the Sylvio X10/4 clone of *Trypanosoma cruzi*. At 250 dpi mice were re-infected with 10^6 fibroblast-derived trypomastigotes of the Sylvio X10/4 clone, 10^3 BFT of the Brazil strain of *T. cruzi* or10^5 BFT of the Brazil strain of *T. cruzi*. Cardiac and skeletal muscles were collected 14 days after re-infection. Data are a comparison of parasite burden in 50 ng of DNA isolated from infected muscle.

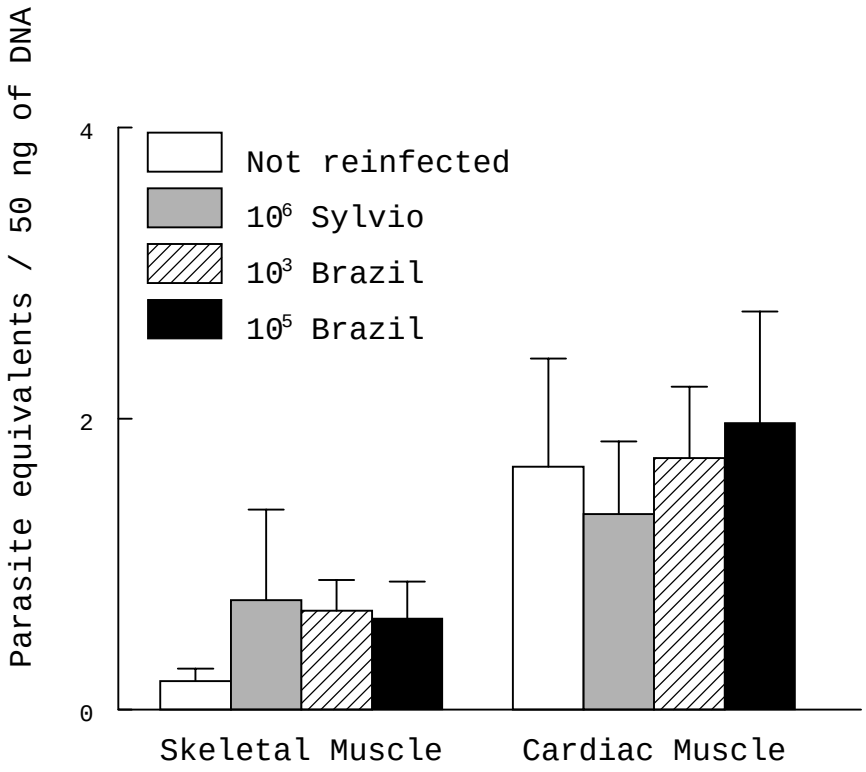
Parasite equivalents / 50 ng of DNA
4
2
0
Not reinfected
10^6 Sylvio
10^3 Brazil
10^5 Brazil
Skeletal Muscle
Cardiac Muscle

CHAPTER 3

NITRIC OXIDE IS NOT ESSENTIAL FOR CONTROL OF *TRYPANOSOMA CRUZI* INFECTION IN MICE[2]

[2] Cummings, K.L. and R.L. Tarleton. To be submitted to *Journal of Immunology*.

Abstract

Nitric oxide is important in the control of many intracellular pathogens. In this study, we used mice deficient in inducible nitric oxide synthase (iNOS, NOS2) to determine the role of nitric oxide (NO) in the *in vivo* control of *Trypanosoma cruzi* infection in mice. Two iNOS-deficient mouse strains, $Nos2^{tm1Lau}$ and Nos2 N5, infected with the Brazil strain of *T. cruzi* had comparable parasite loads and survival times as wild-type (WT) mice. The similarity in the outcome of infection between WT and iNOS deficient mice extended to infections with the more virulent Tulahuen strain of *T. cruzi*. In contrast to the ability of iNOS KO mice to survive Brazil strain infection, both WT and $Nos2^{tm1Lau}$ mice died within 32 days post-infection when treated with the NOS inhibitor aminoguanidine. Increased transcription of NOS1 or NOS3 is not found in iNOS knockout (KO) mice, indicating that absence of NO production through iNOS is not compensated for by increased production of other NOS isoforms. However, $Nos2^{tm1Lau}$ mice have enhanced expression of cytokines including TNF-α, IL-1, and MIP-1α when compared to WT and these alterations may in part compensate for the lack of iNOS. These results clearly show that NO production is not required for control to *T. cruzi* infection.

Introduction

Trypanosoma cruzi is the protozoan parasite that causes Chagas disease. Approximately18 million people in Latin America are infected with *T. cruzi* and an additional 40 million people are at risk of becoming infected. *T. cruzi* infection is estimated to result in 50,000 deaths annually (6). The infection is initiated by the entry of metacyclic trypomastigotes into the mammalian host and the subsequent invasion by these parasites of a wide variety of host cell types. Within host cells, *T. cruzi* converts into intracellular amastigote forms and replicates in

the host cell cytoplasm. As immune control of the infection is established and the infection progresses into the chronic phase, parasites are found predominantly in the muscle cells, which is also the site of disease. Control of *T. cruzi* infection requires the activation of multiple immune effector mechanisms. Mice lacking $CD4^+$ T cells, $CD8^+$ T cells, or antibody-producing B cells fail to control infection (25-31). $CD4^+$ T cells and $CD8^+$ T cells are an important source of cytokines, including the type 1 cytokine IFN-γ, and production of IFN-γ in the acute phase of infection is associated with resistance (78, 79, 120). Infection of IFN-γ-depleted (77) and IFN-γ knockout mice (72) results in death early in infection, demonstrating that IFN-γ is essential for control of *T. cruzi* infection.

Among the best studied functions of IFN-γ is the induction of the microbicidal product nitric oxide (NO). NO is an important cytotoxic and cytostatic factor in cell-mediated immune responses to many intracellular pathogens including *Leishmania* (121-124) and *Toxoplasma gondii* (125-127). NO production is catalyzed by the enzyme nitric oxide synthase (NOS) which exists in three isoforms, NOS1, NOS2 and NOS3 (82, 83, 128). Expression of NOS2, also known as iNOS, is regulated by a combination of cytokines and microbial products; bacterial LPS and the cytokine IFN-γ being among the most potent inducers (86, 129). *T. cruzi* itself (130), and glycoconjugates isolated from *T. cruzi* (131) can enhance levels of nitrite, a stable degradation product of NO, in macrophages. While primarily studied as a product of macrophages in the case of *T. cruzi* infection, iNOS production in response to pathogens and cytokines is induced in a wide variety of cell types, including NK cells, dendritic cells, neutrophils, endothelial cells, myocytes and fibroblasts (83, 86-90). Induction of iNOS expression in *T. cruzi*-infected macrophages, myocytes and fibroblasts results in a dramatic reduction in the ability of amastigotes to survive and replicate in these cells (91,132). This

regulation of parasite growth is reversed by the inclusion of inhibitors of iNOS in the culture, supporting the role of NO, rather than other cytokine-induced activities, in the control of *T. cruzi* infection *in vitro* (91, 92). *In vivo* studies have also suggested a critical role for NO production in the control of *T. cruzi* infection. Mice administered iNOS inhibitors N-monomethyl-L-arginine (L-NMMA), Nomega-nitro-L-arginine (NOARG), aminogunidine (AG) or NG L-arginine methyl ester (L-NAME) exhibit increased parasite levels and greater mortality as compared to untreated mice (89, 133-135). Although these *in vivo* and *in vitro* studies are strongly suggestive of a role for NO in immunity to *T. cruzi*, this conclusion rests primarily on the use of chemical inhibitors of iNOS, of which the absolute specificity for iNOS has not been proven.

In this study, we explored further the role of IFN-γ-inducible NOS in the control of *T. cruzi* infection. The two sets of iNOS-deficient mice used for this purpose, $Nos2^{tm1Lau}$ mice (93) and Nos2 N5 mice, were as resistant to *T. cruzi* as WT mice and the similarity in response of WT and iNOS KO mice was seen during infection with both the Brazil and Tulahuen strains of *T. cruzi*. This study clearly demonstrates that inducible nitric oxide synthase is not required for control of *T. cruzi* infection in mice but suggests that iNOS KO mice may compensate for the absence of NO production with the upregulation of cytokines important in immune control of *T. cruzi* infection.

Materials and methods

Mice and parasites.

Wild-type C57Bl/6J mice (WT), C57Bl/6-$Ifng^{tm1Ts}$ mice (GKO), and C57Bl/6-$Nos2^{tm1Lau}$ mice ($Nos2^{tm1Lau}$) (93) were obtained from The Jackson Laboratory (Bar Harbor, Maine) or were bred in our facilities. C57Bl/6Ai-Nos2 N5 (Nos2 N5), mice deficient in iNOS (94), were

obtained from Taconic (Hudson Valley, New York). Five female mice per strain were injected intraperitoneally with 10^3, 10^4, or 10^5 blood-form trypomastigotes (BFT) of the Brazil strain of *T. cruzi* or with 15 fibroblast-derived trypomastigotes of the Tulahuen strain of *T. cruzi* as indicated. Parasitemia was determined weekly and survival was monitored daily.

DNA Preparation.

Heart (50 mg) and skeletal muscle (300 mg) tissue were minced using surgical blades and added to 5X volume of sodium dodecyl sulfate (SDS)-proteinase K lysis buffer (136). The lysis buffer consisted of 10mM Tris-HCl [pH 7.6] (BioRad Laboratories, Hercules, CA), 0.1 M NaCl (J.T. Baker, Phillipsburg, NJ), 10 mM EDTA (J.T. Baker), 0.5% SDS (BioRad) and 300 μg of proteinase K/ml (Roche, Indianapolis, IN). The samples were then heated for 2 hours at 55°C and extracted twice with phenol:chloroform:isoamyl alcohol (25:24:1) (Sigma, St. Louis, MO). Cold ethanol (AAPER Alcohol and Chemical Co., Shellyville, KY), twice the volume of the extracted sample, was then added and samples were stored at -80°C for 30 minutes. Samples were centrifuged for 30 minutes at 14,000 rpm and washed with 70% ethanol, vacuum dried and resuspended in water.

Generation of PCR Standards for quantification of *T. cruzi*.

The standards for the PCR reactions were generated using 500 mg of minced normal tissue, either skeletal or cardiac muscle, to which 10^7 *T. cruzi* epimastigotes were added. The tissue was then treated, extracted and precipitated as described above. Once resuspended, the DNA was serially diluted with 25 mg/ml DNA from normal tissue. The standard 10-fold dilutions ranged from 0.01 to 1000 parasite equivalents per 50 ng of total DNA. A standard curve was generated from these dilutions to determine the parasite load of DNA from infected tissue samples.

Oligonucleotides

The following primer pairs amplified the *T. cruzi* 195-bp repeat DNA; TCZ-F* 5'GCT CTT GCC CAC AMG GGT GC-3', where M=A or C and TCZ-R 5'CCA AGC AGC GGA TAG TTC AGG-3' (modified from Moser, (110)). For amplification of the murine tumor necrosis alpha (TNF-α), the primer pair; TNF-5241 5'TCC CTC TCA TCA GTT CTA TGG CCC A3' and TNF-5411 5'CAG CAA GCA TCT ATG CAC TTA GAC CCC3' (designed by Vector NTI) was used. Murine cDNA was amplified with the following primers; iNOS F 5'-CAG CTG GGC TGT ACA AAC CTT-3' and R 5'-CAT TGG AAG TGA AGC GGT TCG-3'(137), nNOS F 5'-ACT GAC ACC CTG CAC CTG AAG A-3' and R 5'-GTG CGG ACA TCT TCT GAC TTC C-3', eNOS F 5'-CCT CGA GTA AAG AAC TGG GAA GTG-3' and R 5'-AAC TTC CTT GGA AAC ACC AGG G-3', IFNγ F 5'TTC TTC AGC AAC AGC AAG GCG A-3' and R 5'-TCC TTT TCC GCT TCC TGA GGC T-3' and GAPDH F 5'-TGT CGT GGA GTC TAC TGG TGT CTT C-3' and GAPDH R 5'-CGT GGT TCA CAC CCA TCA CAA-3'.

Real-time PCR of *T. cruzi* specific DNA.

Reactions contained 50 ng genomic DNA, 0.5 μM of *T. cruzi* specific primers TCZ-F and TCZ-R or murine-specific TNF-α primers TNF-5241and TNF-5411, 10 μl Qiagen QuantiTect Sybr Green PCR Master Mix (Qiagen), and PCR-grade H_2O (Qiagen) to a final total volume of 20μl. Reaction mixes were loaded into Roche LightCycler™ (Roche) and amplified using the following program: 95°C at 20 °C/sec ramp and held for 15 minutes, 50 cycles of 95°C at 20°C/sec ramp for 10 seconds, then to 55°C at 20°C/sec ramp, for 15 sec, and 72°C at 2°C/sec ramp for an 5 sec hold at the end of which fluorescence intensity was acquired. For melting curve generation, samples were heated to 95°C at 20°C/sec ramp, 0 sec hold, then 60°C at 20°C/sec ramp, 30 sec hold, and 90°C at 0.2°C/sec ramp, 0 sec hold. Finally, the samples were

cooled for one minute at 40°C at 20°C/sec. Data were acquired and analyzed with LightCycler™ Version 3.0 software.

Each LightCycler run contained two negative controls. Negative controls for PCR with *T. cruzi*-specific primers consisted of a reaction with no DNA added and a reaction with non-infected skeletal muscle DNA. Controls for PCR with murine-specific primers consisted of a reaction with no DNA added and a reaction with *T. cruzi* DNA. Each DNA sample was quantified in triplicate. Triplicate values for each *T. cruzi*-specific DNA sample were average and values were corrected by calculating the ratio of *T. cruzi*-specific product to averaged murine TNF-α product. Corrected values for each experimental group were then averaged and the standard error of the mean was determined. Statistical significance was determined by t-test where $P<0.05$ (*).

NO Assay

Normal and infected (10^3 Brazil strain BFT) C57BL/6J and C57BL/6-Nos2^{tm1Lau} mice were sacrificed 108 days after infection. Thioglycollate elicited peritoneal exudate cells (PEC) and spleen cells were plated in complete RPMI at 5 x 10^6 cells per well. Complete RPMI consisted of RPMI 1640 (Mediatech, Hendon, VA) supplemented with 10% FBS (Hyclone, Logan, UT), 2mM L-glutamine (Life Technologies, Rockville, MD), 1 mM sodium-pyruvate (Sigma), 50 μg/ml gentamicin (Sigma), β-Mercaptoethanol (Sigma). For splenocytes, 0.1 mM nonessential amino acids (Life Technologies) were added to complete RPMI. Adherent cells were obtained by culture in 24-well plates at 37°C, 5% CO_2 for 3-4 hours followed by 3 washes with RPMI. Complete medium plus or minus 100 U/ml IFN-γ (Genzyme, Cambridge, MA) and 10 ng/ml LPS (Calbiochem, San Diego, CA) was added and the cells were incubated at 37°C and 5% CO_2 for an additional 48 hours. Supernatants were collected and assayed for nitrite levels

using the Griess reaction (Promega, Madison, WI). Briefly, fifty µl of sample was dispensed in triplicate in 96-well flat bottomed plates and incubated at room temperature with 50 µl of 1% sulfanilamide (Sigma) for 10 minutes. Fifty µl of 0.1% N-1-naptheylethylenediamine dihydrochloride (Sigma) was added and allowed to incubate for 10 minutes. Absorbance at 540 nm was measured and compared to a sodium nitrite (Promega, Madison, WI) standard.

NOS inhibitor studies

C57Bl/6J, Nos2^{tm1Lau} and Nos2 N5 mice, five females per strain, were infected with 10^3 BFT of the Brazil strain of *T. cruzi*. Two days after infection, five mice per strain received drinking water containing 1% aminoguanidine (AG) (Sigma). Survival was monitored daily and parasitemia was monitored weekly.

Real-time PCR of NOS isoform mRNA

C57BL/6J, Nos2^{tm1Lau} and Nos2 N5 mice were infected with 10^3 Brazil BFT. At 21 dpi, skeletal and cardiac muscle and spleens were harvested and 1 ml TRI reagent (Sigma) per 100 mg of tissue was added. Tissues were homogenized and stored at -70°C prior to completion of the RNA extraction. Samples were centrifuged at 12,000 g for 10 minutes at 4°C and the supernatants transferred to fresh tubes with 0.2 ml chloroform per 1 ml of TRI Reagent. Samples were mixed and incubated on ice for 15 minutes and centrifuged at 13,000 rpm for 15 minutes at 4°C. The aqueous phase was transferred to a fresh tube and RNA was precipitated by adding 0.5 ml of isopropanol per 1 ml of TRI Reagent used for the initial homogenization. Samples were incubated at 4°C for 20 minutes and centrifuged at 13,000 rpm for 15 minutes at 4°C. The RNA pellet was washed twice with 75% ethanol, and centrifuged at 13,000 rpm for 5 minutes at 4°C before being resuspended in 200 µl RNase-free water.

DNA was removed by adding 30 µg RNA, 30 µl RQ1 RNase-Free DNase 10X Reaction Buffer, 30 U RQ1 RNase-Free DNase (Promega, Madison, WI), and nuclease-free water to 30 µg of RNA and incubating at 37°C for 30 minutes. RQ1 DNase Stop Solution (30 µl) was than added and tubes were incubated at 65°C for 10 minutes to inactivate the DNase. RNA was cleaned using RNeasy Mini kit (Qiagen, Valencia, CA). For first strand cDNA synthesis, 10 µg total RNA and 0.5 µg of oligo$(dT)_{12\text{-}18}$ primer (Invitrogen Life Technologies, Carlsbad, California) in a final volume of 20 µl was heated at 65°C for 10 minutes. A mixture of 5X first strand buffer (Invitrogen), 0.1 M DTT (Invitrogen) and 10 mM dNTP mix and RNasin was added to RNA and heated to 42°C. 200 U of SuperScript II RNase H^- Reverse Transcriptase (Invitrogen) was added to each reaction and incubated for 90 minutes at 42°C. 0.5 µl RNase H was added and incubated at 37°C for 30 minutes.

The obtained cDNA was diluted 1/10 with water and 2 µl were used for amplification. Reactions contained cDNA, 0.5 µM primer mix, 10 µl Qiagen QuantiTect Sybr Green PCR Master Mix (Qiagen), and PCR-grade H_2O (Qiagen) to a final total volume of 20µl. Reaction mixes were loaded into Roche LightCycler™ capillaries, centrifuged and placed in the LightCycler™ (Roche). The real-time PCR program is as follows; 95°C at 20 °C/sec ramp and held for 15 minutes, 70 cycles of 95°C at 20°C/sec ramp for 5 seconds, then to 55°C at 20°C/sec ramp, for 5 sec, and 72°C at 2°C/sec ramp for an 8 sec hold at the end of which fluorescence intensity was acquired. For melting curve generation, samples were heated to 95°C at 20°C/sec ramp, 0 sec hold, then 60°C at 20°C/sec ramp, 30 sec hold, and finally 90°C at 0.2°C/sec ramp, 0 sec hold. Finally, the samples were cooled for one minute at 40°C at 20°C/sec.

For quantification of mRNA expression levels, copy number was calculated from a standard curve, obtained by plotting known input concentrations of control plasmids at log dilutions to the PCR cycle number at which the fluorescence intensity is above background. PCR products for eNOS, nNOS, iNOS, IFN-γ, and GAPDH, amplified with the above primers and PCR program, were cloned into the pCR®2.1-TOPO vector (Invitrogen). cDNA from murine muscle tissue and splenocytes was amplified by real-time PCR with the eNOS, nNOS, iNOS, IFN-γ, and GAPDH primers listed above. Separately, reactions containing serially diluted control plasmids (10^7 to 10^1 copies), 0.5 μM of plasmid specific primers, 10 μl Qiagen QuantiTect Sybr Green PCR Master Mix (Qiagen), and PCR-grade H_2O (Qiagen) to a final total volume of 20μl, were used to generate standard curves. Individual sample values for NOS isoforms and IFN-γ were normalized by the housekeeping gene GAPDH and presented as number of transcripts per 10^7 copies of GAPDH. Samples were run in triplicate and corrected values for each sample were averaged. Individual sample averages were then averaged per mouse strain, standard deviation determined and standard error of the mean calculated. No amplification of non-specific products was observed. Statistical significance was determined by t-test where $P<0.05$ (*).

Bio-Plex mouse cytokine assay

Eight female C57Bl/6J and $Nos2^{tm1Lau}$ were infected with 10^3 BFT of the Brazil strain of *T. cruzi*. At 14 and 28 dpi splenocytes from four mice per group were harvested, pooled, plated (10^6 cells/well) in triplicate and stimulated with media alone, PMA (50 ng/ml) and calcium ionophore (500 ng/ml), a mixture of *T. cruzi*-specific peptides shown to be targets of CTL response (2.5μM) ((138) and Martin et. al. (unpublished)) or a *T. cruzi* lysate (25μg/ml). *T. cruzi* lysate generation was as follows; culture grown parasites were pelleted, washed, frozen at -70°C,

thawed, and sonicated. Freezing, thawing and sonication were repeated and debris was removed by centrifuging for 30 minutes at 4°C. Protein concentration was determined and the lysate was filter sterilized and stored at -20°C until use. Complete RPMI consisted of RPMI 1640 supplemented with 10% FBS, 2mM L-glutamine, 1 mM sodium-pyruvate, 50 μg/ml gentamicin, β-mercaptoethanol. Supernatants were collected after 24 hours of stimulation and stored at -70°C. Supernatants were assayed in triplicate. The Bio-Plex Mouse 18-Plex Cytokine Assay (Bio-Rad) was done according to the manufacturers protocol. Cytokine standards were diluted four-fold with media in final concentration from 32,000 pg/ml to 1.95 pg/ml. The mouse cytokines GM-CSF, INF-γ, TNF-α, IL-1α, IL-β, IL-2, IL-3, IL-4, IL-5, IL-6, IL-10, IL-12p40, IL-12p70, IL-17, G-CSF, KC, MIP-1α, RANTES, were analyzed. Calculated concentrations for each cytokine were averaged and the standard deviation determined. Statistical significance was determined by t-test where * ($P < 0.05$) designates significant difference in cytokine production between WT and $Nos2^{tm1Lau}$ cells.

Results

To address the requirement of IFN-γ-inducible nitric oxide synthase for control of *T. cruzi* infection, WT, $Nos2^{tm1Lau}$, and GKO mice were infected with 10^3 blood-form trypomastigotes (BFT) of the Brazil strain of *T. cruzi*. With this typically non-lethal infective dose, WT and $Nos2^{tm1Lau}$ mice survived acute *T. cruzi* infection with similar parasitemia and survival whereas the GKO mice exhibited a 50-fold higher parasitemia (Figure1A) and early mortality (Figure 3.1B). Approximately 60% of WT and 90% of $Nos2^{tm1Lau}$ mice survived beyond 120 days post infection (Figure 3.1B). Increasing the infective dose (10^5 BFT) resulted in similar survival in $Nos2^{tm1Lau}$ and WT mice to that of mice infected with 10^3 BFT (data not shown). To evaluate tissue parasite burden in both the acute and chronic phase of infection, real-

time PCR, which reliably detects 0.01 parasite equivalents/50 ng DNA, was utilized (139). At 28 dpi, Nos2^{tm1Lau} and WT mice parasite burden in the skeletal and cardiac muscle was not significantly different (Figure 3.2A). In contrast GKO mice had significantly greater tissue parasite burden in both tissues ($p<0.05$). The similarity in tissue parasite load in WT and Nos2^{tm1Lau} mice was also observed in the chronic phase of the infection (Day 150) (Figure 3.2B).

The observed resistance of the Nos2^{tm1Lau} mice to *T. cruzi* infection is at odds with the hypothesized importance of NO in control of *T. cruzi* infection and the demonstrated susceptibility of mice treated with iNOS inhibitors (89, 133, 134). In order to further establish that NO was not contributing to the control of *T. cruzi* in the iNOS KO mice we 1) confirmed that NO was not being produced at normal levels in these mice (Figure 3.3), 2) examined survival in a second iNOS KO strain and with a second parasite strain and 3) explored the contribution of other NOS isoforms to control of *T. cruzi* infection. Infection of an additional iNOS KO mouse strain, the Nos2 N5 strain, yielded comparable results to those obtained in the Nos2^{tm1Lau} strain (Figure 3.4). In this case, infection in the WT, Nos2^{tm1Lau}, Nos2 N5, and GKO mice was initiated with a 10-fold higher parasite dose, to assess whether NO production might be necessary under this condition. However, as in previous experiments, parasitemia, longevity and tissue parasite loads were not significantly different in the WT and two iNOS KO strains and clearly different from the GKO mice (Figure 3.4). Infection of mice with a more virulent parasite strain, the Tulahuen strain, also failed to reveal a differential susceptibility of iNOS KO mice relative to WT mice (Figure 3.5). In this case, infection with 15 fibroblast-derived trypomastigotes of the Tulahuen strain resulted in high parasitemia and 100% mortality during the acute phase of infection in WT, Nos2^{tm1Lau}, and Nos2 N5 mice (Figure 3.5A, 3.5B). Neither

the skeletal muscle nor cardiac muscle parasite load in the Nos2 N5 mice was significantly greater than WT or $Nos2^{tm1Lau}$ mice (Figure 3.5C).

These results solidly establish that mice lacking the ability to produce NO are nevertheless similar to WT mice in their ability to control (or not control) *T. cruzi* infection. However studies using iNOS inhibitors to treat mice infected with *T. cruzi* have arrived at the opposite conclusion i.e. that NO is a critical factor in the control of *T. cruzi* infection (89, 91, 92, 132-134). One explanation for this apparent contradiction is that the iNOS inhibitors used in these studies lacked specificity and therefore have activities that extend beyond inhibition of iNOS. To determine if a non-specific NOS inhibitor alters the response to *T. cruzi* in mice lacking iNOS, *T. cruzi* infected WT and iNOS KO mice were treated with aminoguanidine (AG). WT, $Nos2^{tm1Lau}$, and Nos2 N5 mice were infected with 10^3 Brazil BFT and treated with 1% AG after 2 days of infection. Treatment with AG resulted in increased parasitemia in WT and $Nos2^{tm1Lau}$ mice while the parasitemias of treated Nos2 N5 mice were similar to infected mice receiving normal drinking water (Figure 3.6A). 100% of WT mice and the majority of $Nos2^{tm1Lau}$ mice treated with AG died during the acute phase of the infection while the majority of Nos2 N5 mice treated with AG survived infection in two replicate experiments (Figure 3.6B and data not shown). These results demonstrate that the response of iNOS knockout mice to AG differs depending on the strains used.

We considered the possibility that iNOS KO mice may compensate for the lack of iNOS by increased expression of other NO producing enzymes, NOS1 and NOS3. Recent studies have shown that the expression of NOS1 and NOS3, which are found in cardiac and skeletal muscle (140-145), can be induced by infection as well as certain cytokines (146, 147). To investigate if NOS1 or NOS3 compensate for the lack of NOS2, WT, $Nos2^{tm1Lau}$, and Nos2 N5 mice were

infected with 10^3 Brazil BFT and at 21 dpi RNA was extracted from cardiac and skeletal muscle as well as splenocytes and the mRNA levels of NOS1 and NOS3 were determined by real-time PCR. Levels of transcription of NOS1 or NOS3 were not significantly different among WT, $Nos2^{tm1Lau}$, and Nos2 N5 mice in the cardiac muscle or spleen (Figure 3.7). In the skeletal muscle, transcription of IFN-γ by Nos2 N5 was significantly greater than that in WT mice, while transcription of NOS1 was significantly less than that of WT mice (Figure 3.7). Thus, the $Nos2^{tm1Lau}$ mice do not compensate for the lack of iNOS by increased expression of NOS1 or NOS3.

While iNOS KO mice do not compensate for the absence of iNOS by upregulation of other NOS isoforms, these animals may compensate in other ways such as through altered cytokine expression. To test this hypothesis, WT and $Nos2^{tm1Lau}$ mice were infected with 10^3 BFT of *T. cruzi* Brazil strain and at 14 and 28 dpi splenocytes from these mice were assayed for their *in vitro* cytokine response. Pooled splenocytes were cultured with media alone, PMA and calcium ionophore, a pool of *T. cruzi* peptides that are targets of *T. cruzi*-specific $CD8^+$ T cells, or a *T. cruzi* lysate and the levels of cytokines in culture supernatants were evaluated by an 18-plex cytokine assay. The cytokines measured included those involved in hematopoiesis (IL-3, GM-CSF, G-CSF), cellular trafficking (KC, MIP-1α, RANTES), and innate (TNF-α, IL-1α, IL-1β, IL-6, IL-10, IL-12p40, IL-12p70) and adaptive (IL-2, IL-4, IL-5, IL-17, INF-γ) immune responses. As a positive control, cells were stimulated with PMA and calcium ionophore, resulting in production of all 18 cytokines by cells from both WT and $Nos2^{tm1Lau}$ mice (data not shown). The levels of KC, RANTES, IL-2, IL-4, IL-10, IL-12p40, and IL-12p70 production by $Nos2^{tm1Lau}$ cells in response to *T. cruzi* peptides or lysate were not significantly different from that of WT cells (selected cytokines represented in Figure 3.8). However, upon stimulation with

either *T. cruzi* peptides or lysate, production of IFN-γ, TNF-α, IL-1α, IL-1β, IL-6, IL-17, GM-CSF, G-CSF, and MIP-1α was significantly increased in cells from iNOS KO mice as compared to WT cells (selected cytokines represented in Figure 3.9). These results show that cytokine production by $Nos2^{tm1Lau}$ mice is significantly upregulated compared to that of WT mice.

Discussion

This study sought to clarify the contribution of nitric oxide to the control of *T. cruzi* infection. NO has a number of important roles in immunity, including the induction and suppression of apoptosis, and microbicidal activity (reviewed in (148-152)). NO is critical to the control of numerous intracellular pathogens, including, influenza virus A, *Listeria monocytogenes*, *Leishmania major*, *Leishmaina donovani*, and *Toxoplasma gondii* (123, 124, 126, 153, 154). Substantial data have also been presented supporting NO as the mechanism by which IFN-γ controls *T. cruzi* infection (73, 89, 91, 92, 130, 132-134, 155-160). The enhanced susceptibility of *T. cruzi* infected IFN-γ and IFN-γ receptor-deficient mice has been attributed to significantly reduced NO production (161,73). Additionally, *T. cruzi* infection elevates iNOS levels in plasma (89) and a study of iNOS localization in *T. cruzi* infected mice revealed iNOS in cellular infiltrate and infected tissues (73). *T. cruzi*-infected mice administered iNOS inhibitors exhibit increased parasite levels and greater mortality as compared to untreated mice (89, 133, 134).

However, the specificity of iNOS inhibitors has recently come into question (reviewed in (162, 163). For example, the inhibitor aminoguanidine (AG), previously regarded as iNOS-specific, inhibits all NOS isoforms with selectivity for NOS1 and NOS2 being greater than for NOS3 (164, 165). Additionally, AG has various other activites, including the generation of hydrogen peroxide by inhibition of catalase (166, 167)(reviewed in (168)), the reduction of

advanced glycosylation end products in diabetes, the inhibition of oxidative modification of low density lipoproteins (169), inhibition of histamine metabolism (170), and the inhibition of polyamine catabolism (171). The lack of specificity of the iNOS inhibitors used in studies to assess the contribution of NO to control of *T. cruzi* infection brings into question the absolute necessity of iNOS for control of infection. In order to address this issue more directly, iNOS knockout mice were utilized in this study.

Two iNOS KO mouse lines were used to determine the necessity of iNOS for control of *T. cruzi* infection. The $Nos2^{tm1Lau}$ strain (C57Bl/6 background) lacks the calmodulin binding domain, which is required for iNOS activity (93) and the Nos2 N5 strain lacks the first four exons, including the translational start site and therefore produces no iNOS protein (94). In both KO mouse strains parasitemia, tissue parasite load, and mortality during infection with the Brazil strain or the Tulahuen strain of *T. cruzi* was similar to that of WT mice. These results clearly indicate that iNOS is not essential for control of *T. cruzi* infection in mice and contradict the previous assertion that NO induction by IFN-γ is the major mechanism of control of *T. cruzi* infection. The increased levels of NO production during *T. cruzi* infection appears to be only part of a larger network of activity stimulated by IFN-γ for control of *T. cruzi* infection.

One possible reason that iNOS KO mice are able to resist *T. cruzi* infection is that they compensate for the absence of iNOS by enhancement of other immune effector mechanisms. While resistance of iNOS KO mice to *T. cruzi* infection is not due to increased expression of the other NOS isoforms, compensation may occur through altered cytokine response during infection. Secretion of several cytokines including, IFN-γ, TNF-α, IL-1α, GM-CSF, and MIP-1α, was significantly increased by cells from infected iNOS KO mice upon *T. cruzi*-specific stimulation. IFN-γ is known to upregulate expression of several of the cyokines that are

increased in iNOS KO mice, including MIP-1α (59), IL-6 (172-174), GM-CSF (172), and TNF-α (175). A result of increased TNF-α and GM-CSF may be reduced infection of cells as was seen *in vitro* in the absence of nitric oxide (176). Additionally, MIP-1α is involved in cellular recruitment to tissues during acute *T. cruzi* infection and increased production by iNOS KO mice would be expected to enhance trafficking of effector cells to sites of infection (177). The altered cytokine response by iNOS KO mice may explain the survival of *T. cruzi* infection in the absence of iNOS.

The results of this study contradict the results from the *in vivo* studies using iNOS inhibitors (73, 89, 91, 92, 130, 132-134, 155-160) as well as recent studies using iNOS KO mice (74, 178, 179). In the later studies, iNOS KO mice on a 129sv x C57Bl/6 background succumbed to infection with the Tulahuen strain of *T. cruzi* (74, 178). The increased susceptibility of the iNOS KO mice in these studies may be explained by the inability of mice of the genetic background 129sv x C57Bl/6 to produce a compensatory response. The levels of IFN-γ, TNF-α, and IL-1α in the plasma of 129sv x C57Bl/6 infected iNOS mice did not increase upon infection (74) while in our study splenocytes from infected iNOS KO mice (C67Bl/6) had significantly increased levels of IFN-γ, TNF-α, and IL-1α upon stimulation with *T. cruzi* lysate. There have been other reports where the phenotypes of knockout mice are affected by genetic background (180-182).

In this study iNOS knockout mice were used to determine the necessity of iNOS in control of *T. cruzi* infection as previous studies used iNOS inhibitors that are now known to be non-specific. While there is strong evidence to support a role for NO in control of infection, our study demonstrates that NO is not an absolute requirement for control of *T. cruzi* infection and may instead be part of a network of IFN-γ inducible responses that together control *T. cruzi*

infection. The increased production of certain cytokines by infected Nos2^{tm1Lau} mice likely compensates for the lack of iNOS and contributes to the control of *T. cruzi* infection.

Figure 3.1. Parasitemia and survival of Nos2^{tm1Lau} mice infected with *T. cruzi*. C57BL/6J (WT) (triangle), Nos2^{tm1Lau} mice (circle), and GKO mice (diamond) were infected with 10^3 BFT of the Brazil strain of *T. cruzi* and parasitemia (A) and survival (B) were observed. Results were pooled from 3 experiments with a total of 15-20 mice.

A

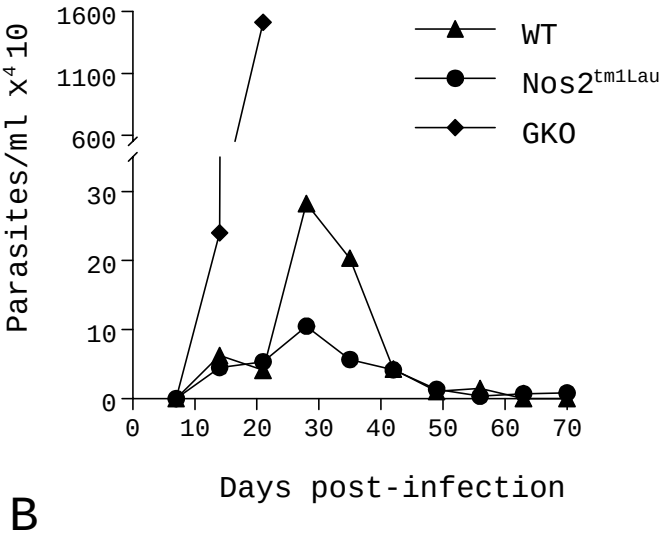
Parasites/ml x^{4}10
1600
1100
600
30
20
10
0
0 10 20 30 40 50 60 70
Days post-infection
WT
Nos2^{tm1Lau}
GKO

B

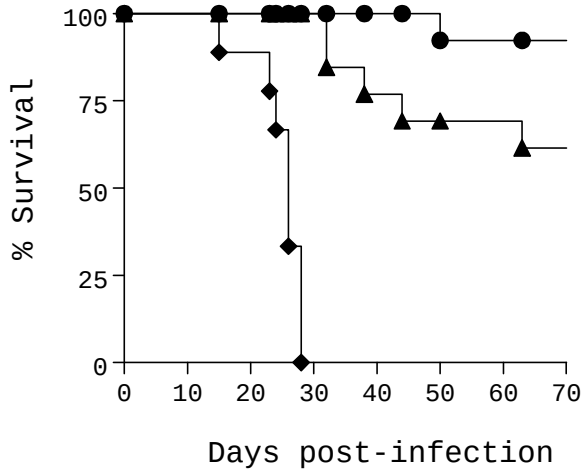
% Survival
100
75
50
25
0
0 10 20 30 40 50 60 70
Days post-infection

Figure 3.2. Tissue parasite burden of Nos2^{tm1Lau} mice infected with *T. cruzi*. C57BL/6J (WT), Nos2^{tm1Lau} mice, and GKO mice were infected with 10^3 BFT of the Brazil strain of *T. cruzi*. Tissue parasite burden was determined as stated in Materials and Methods at 28 (A) and 150 (B days post-infection. * $P < 0.05$.

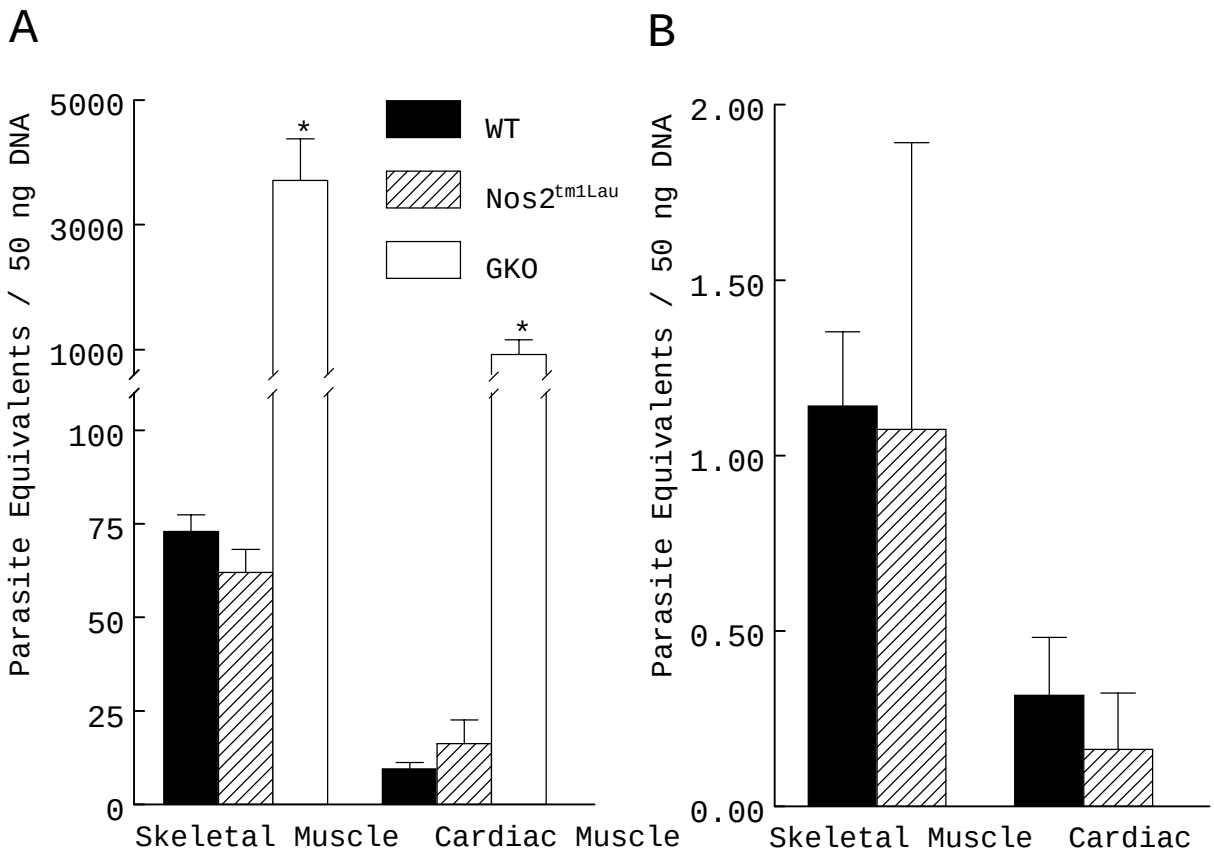
A
B
Parasite Equivalents / 50 ng DNA
5000
3000
1000
100
75
50
25
0
WT
Nos2tm1Lau
GKO
*
*
Skeletal Muscle
Cardiac Muscle
2.00
1.50
1.00
0.50
0.00
Skeletal Muscle
Cardiac

Figure 3.3. NO is not produced by stimulated cells from infected iNOS KO mice. PECs (A) and splenocytes (B) from WT and $Nos2^{tm1Lau}$ mice infected for 108 days were cultured in media alone of media containing 100 U/ml IFN-γ and 10 ng/ml LPS. After 48 hours supernatants were collected and assayed for nitrite levels using the Griess reaction.

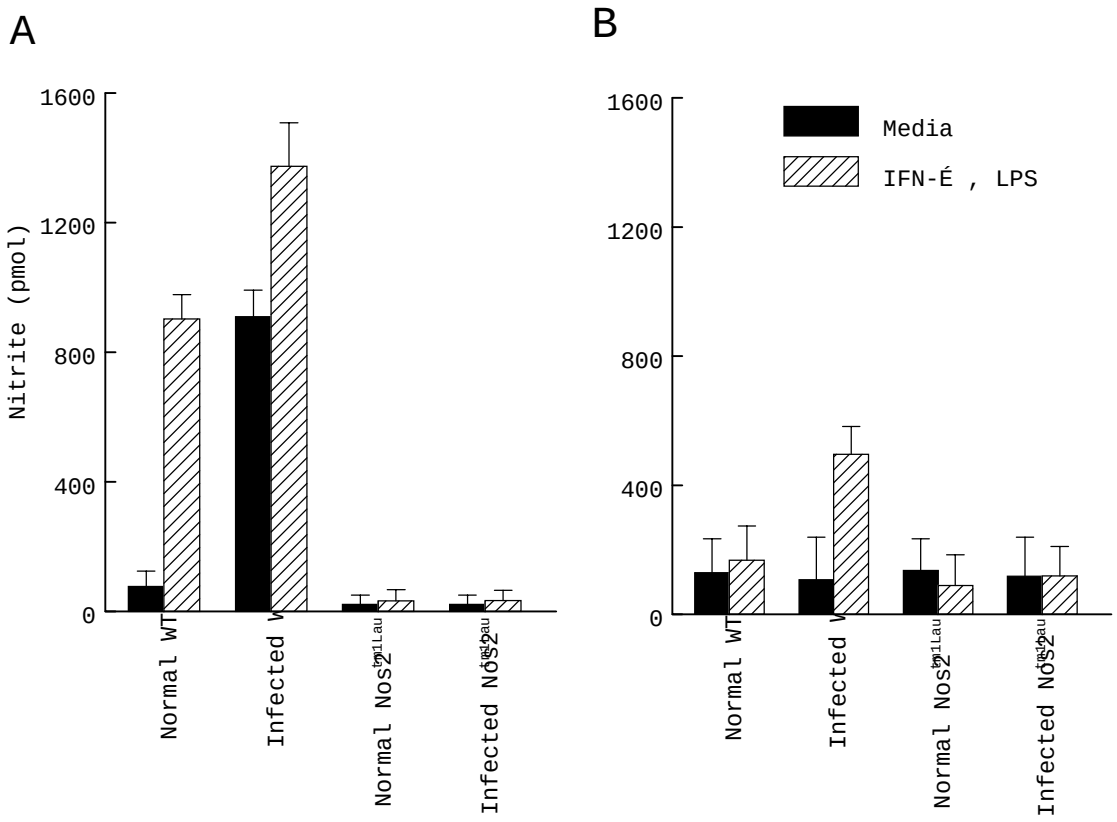
A
B
Nitrite (pmol)
1600
1200
800
400
0
Media
IFN-É , LPS
Normal WT
Infected WT
Normal Nos2 -/-
Infected Nos2 -/-

Figure 3.4. Response of second iNOS KO strain to *T. cruzi*. C57BL/6J (WT) (triangle), $Nos2^{tm1Lau}$ mice (circle), Nos2 N5 mice (square), and GKO mice (diamond) were infected with 10^4 BFT of the Brazil strain of *T. cruzi* and the parasitemia (A) and survival (B) were observed. Tissue parasite burden was determined as stated in Materials and Methods at 28 (C) and 150 (D) days post-infection. * $P < 0.05$.

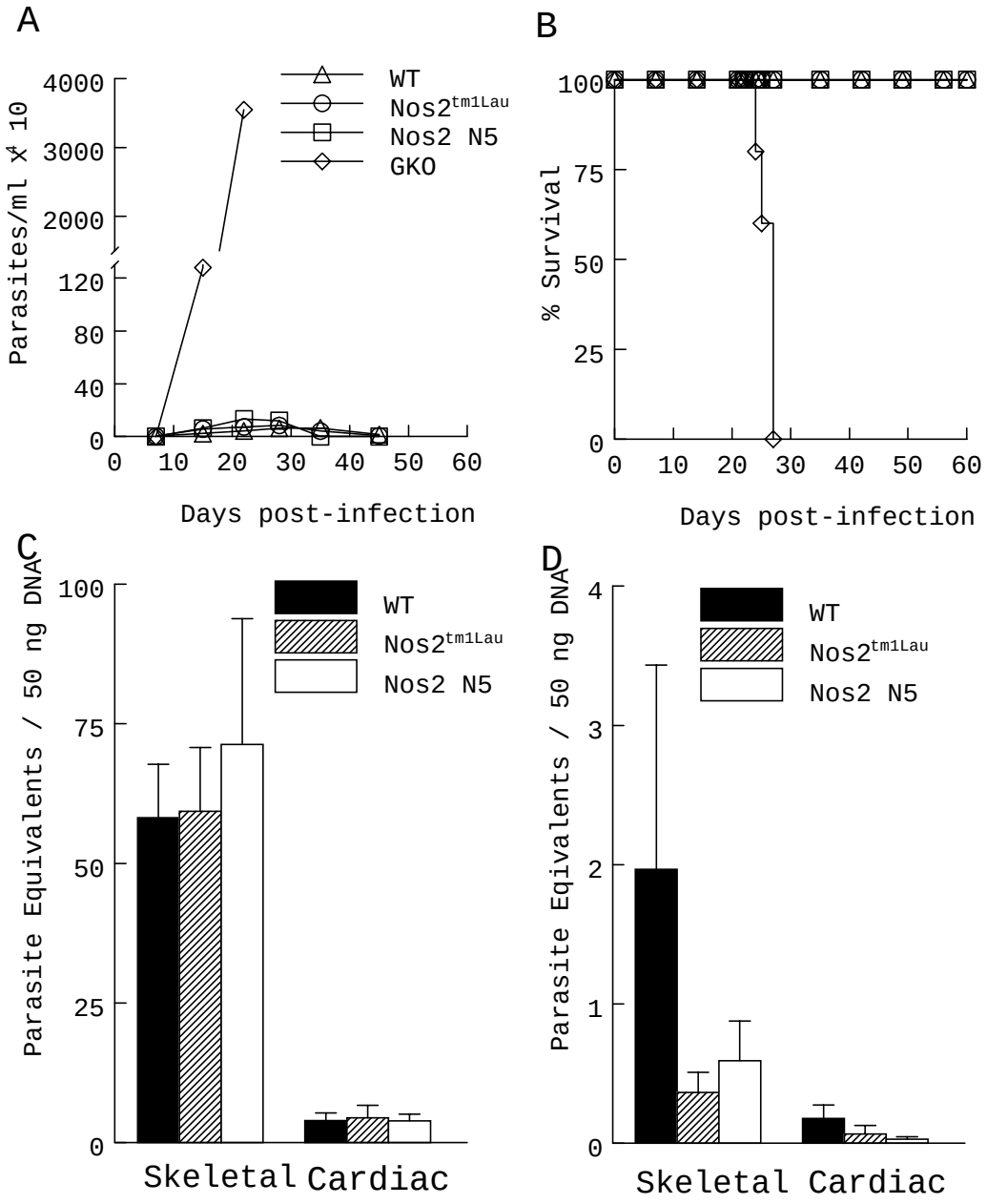
A
Parasites/ml x 10^4
4000
3000
2000
120
80
40
0
0 10 20 30 40 50 60
Days post-infection
WT
Nos2tm1Lau
Nos2 N5
GKO
B
% Survival
100
75
50
25
0
0 10 20 30 40 50 60
Days post-infection
C
Parasite Equivalents / 50 ng DNA
100
75
50
25
0
Skeletal Cardiac
WT
Nos2tm1Lau
Nos2 N5
D
Parasite Eqivalents / 50 ng DNA
4
3
2
1
0
Skeletal Cardiac
WT
Nos2tm1Lau
Nos2 N5

Figure 3.5. Response of iNOS KO mice to the Tulahuen strain of *T. cruzi*. C57BL/6J (WT), $Nos2^{tm1Lau}$ mice, and Nos2 N5 mice were infected with 15 BFT of the Tulahuen strain of *T. cruzi* and the parasitemia (A) and survival (B) were observed. Tissue parasite burden (C) was determined as stated in Materials and Methods at 21 days post-infection. * $P < 0.05$.

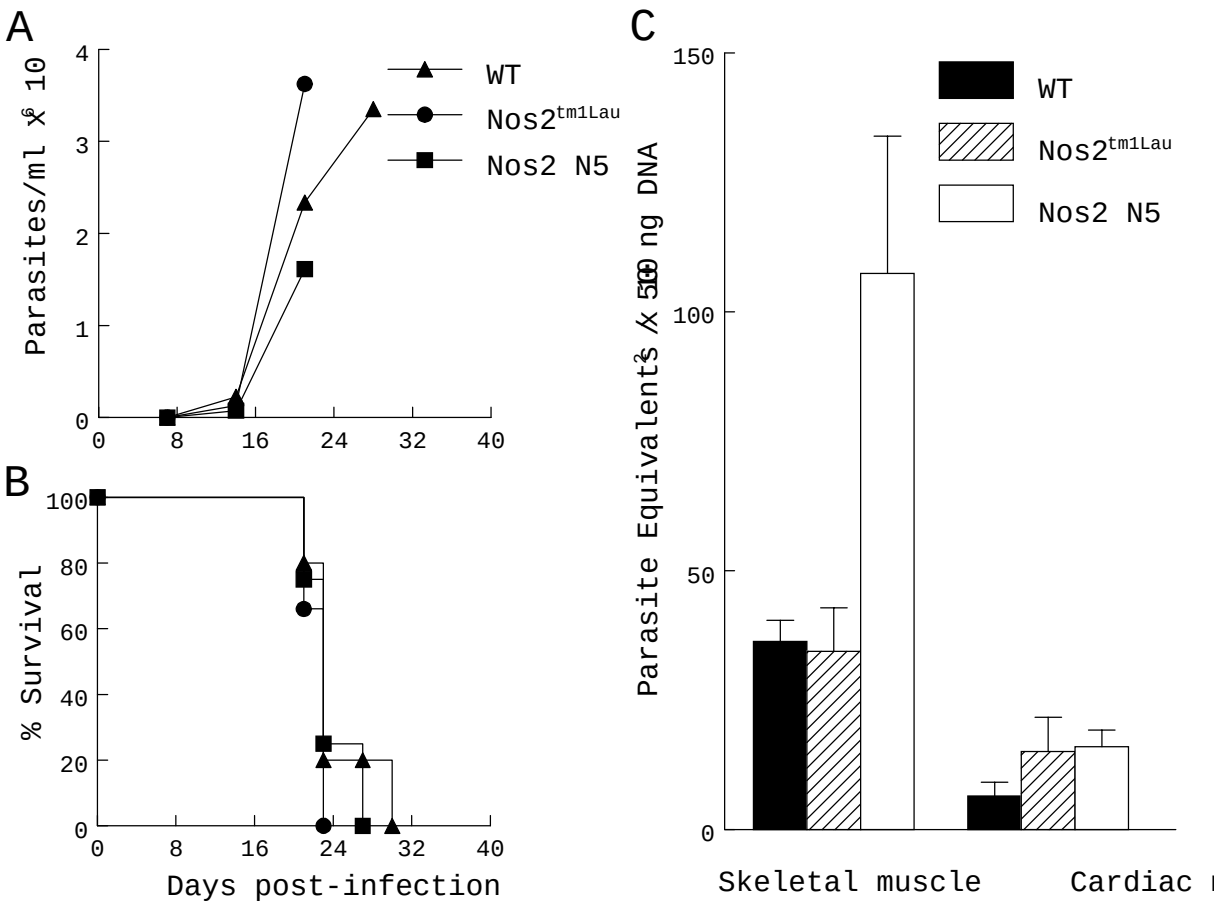
A
Parasites/ml X 10^6
4
3
2
1
0
0
8
16
24
32
40
WT
Nos2tm1Lau
Nos2 N5
B
% Survival
100
80
60
40
20
0
0
8
16
24
32
40
Days post-infection
C
Parasite Equivalents / X 500 ng DNA
150
100
50
0
WT
Nos2tm1Lau
Nos2 N5
Skeletal muscle
Cardiac

Figure 3.6. Treatment of infected iNOS KO mice with an NOS inhibitor. C57BL/6J (WT) (triangle), $Nos2^{tm1Lau}$ mice (circle), and Nos2 N5 mice (square) were infected with 10^3 BFT of the Brazil strain of *T. cruzi*. Two days after infection drinking water with 1% AG (filled) was administered. Parasitemia (A) and survival (B) were monitored.

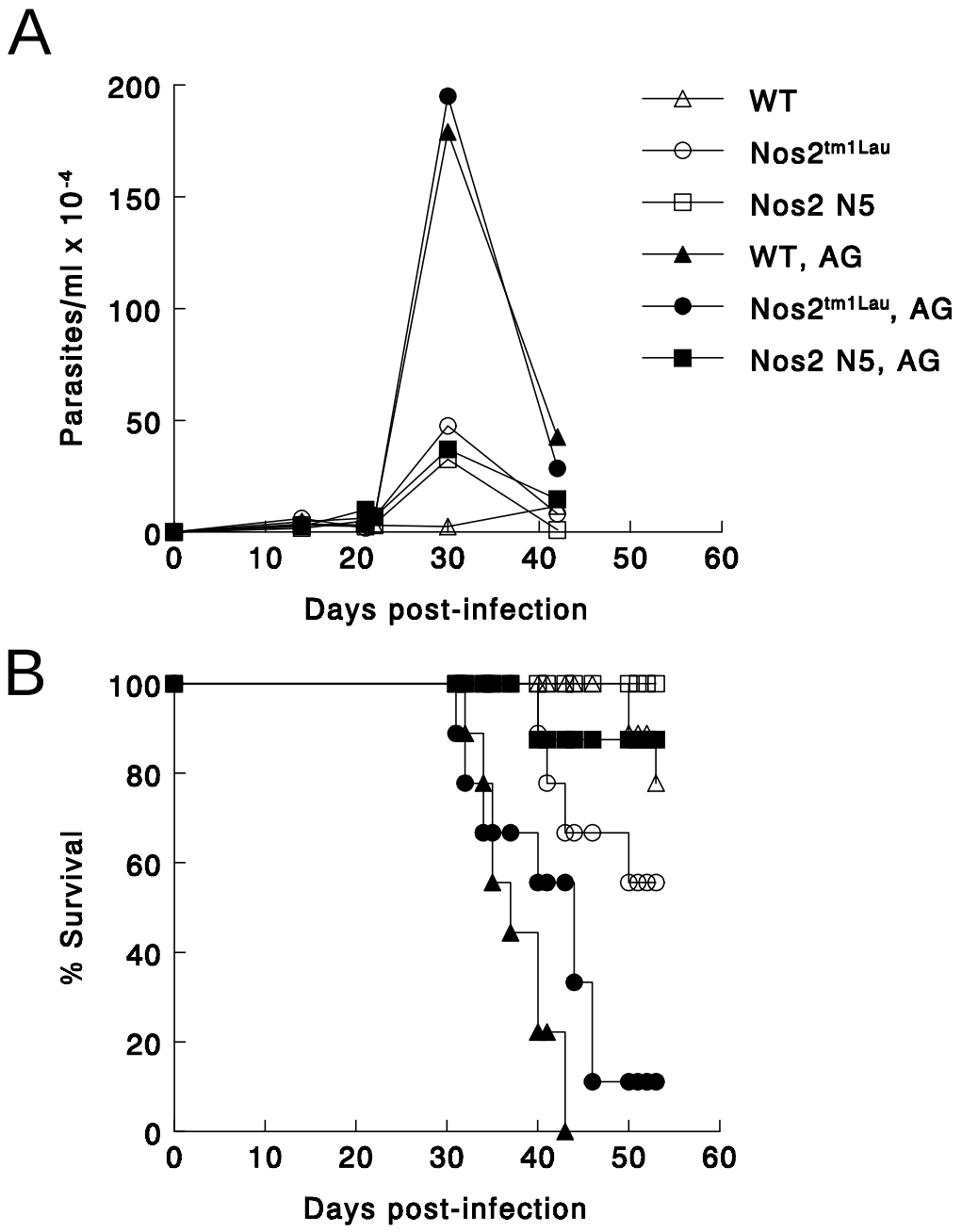
A
200
150
100
50
0
Parasites/ml x 10-4
0
10
20
30
40
50
60
Days post-infection
WT
Nos2tm1Lau
Nos2 N5
WT, AG
Nos2tm1Lau, AG
Nos2 N5, AG
B
100
80
60
40
20
0
% Survival
0
10
20
30
40
50
60
Days post-infection

Figure 3.7. iNOS KO mice do not compensate by increased NOS1 or NOS3 expression. C57BL/6J (WT), $Nos2^{tm1Lau}$ mice, and Nos2 N5 mice were infected with 10^3 BFT of the Brazil strain of *T. cruzi*. At 21 dpi, RNA from cardiac muscle (A), skeletal muscle (B) and spleen (C) was extracted and first-strand cDNA was synthesized. IFN-γ, nNOS, eNOS, and GAPDH transcript levels were quantified by real-time PCR. * $P < 0.05$.

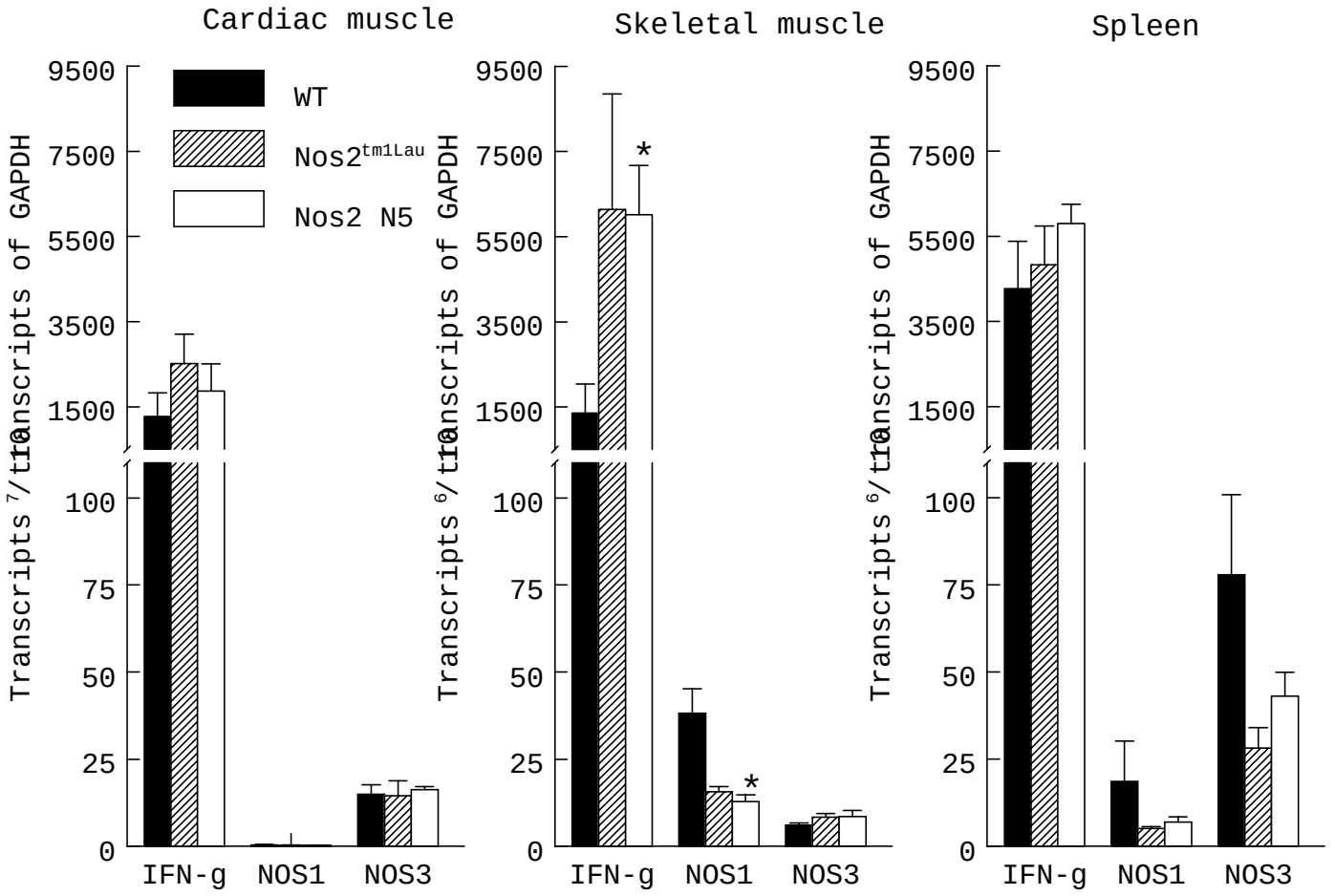
Cardiac muscle
Skeletal muscle
Spleen
WT
Nos2tm1Lau
Nos2 N5
Transcripts 7/10 transcripts of GAPDH
Transcripts 6/10 transcripts of GAPDH
9500
7500
5500
3500
1500
100
75
50
25
0
*
IFN-g
NOS1
NOS3

Figure 3.8. Cytokine production. C57BL/6J (WT) and Nos2^{tm1Lau} mice were infected with 10^3 BFT of the Brazil strain of *T. cruzi*. At 14 and 28 dpi splenocytes were harvested and stimulated with media, *T. cruzi*-specific peptides, or *T. cruzi* lysate. Culture supernatants were assayed in triplicate for cytokines using a Bio-Plex cytokine assay. * ($P < 0.05$) designates significant increase in cytokine production between by Nos2^{tm1Lau} cells.

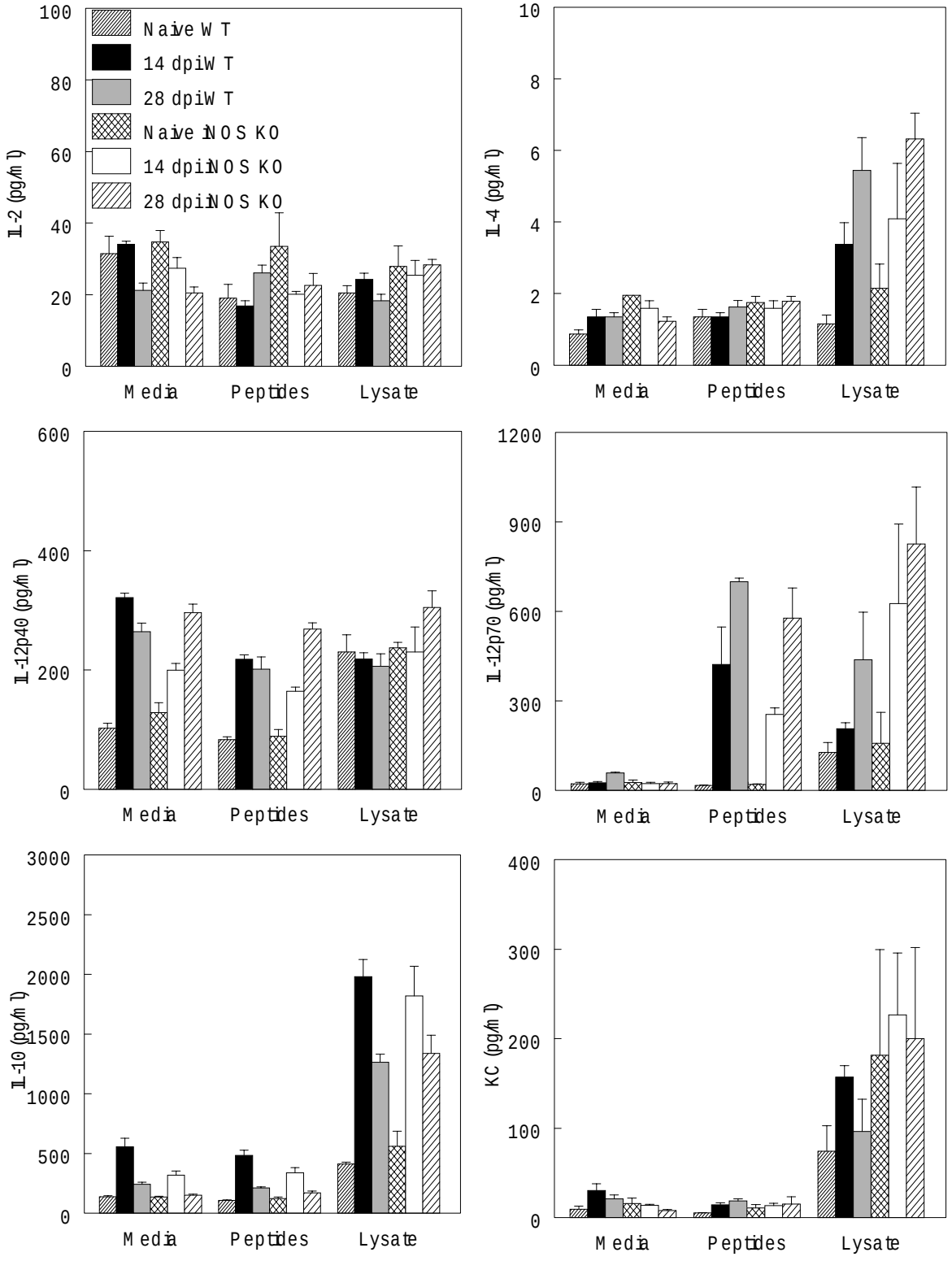
Naive WT
14 dpi WT
28 dpi WT
Naive iNOS KO
14 dpi iNOS KO
28 dpi iNOS KO
IL-2 (pg/ml)
IL-4 (pg/ml)
IL-12p40 (pg/ml)
IL-12p70 (pg/ml)
IL-10 (pg/ml)
KC (pg/ml)
Media
Peptides
Lysate

Figure 3.9. Increased cytokine production by cells from iNOS KO mice. C57BL/6J (WT) and Nos2^{tm1Lau} mice were infected with 10^3 BFT of the Brazil strain of *T. cruzi*. At 14 and 28 dpi splenocytes were harvested and stimulated with media, *T. cruzi*-specific peptides, or *T. cruzi* lysate. Culture supernatants were assayed in triplicate for cytokines using a Bio-Plex cytokine assay. * ($P < 0.05$) designates significant increase in cytokine production by Nos2^{tm1Lau} cells.

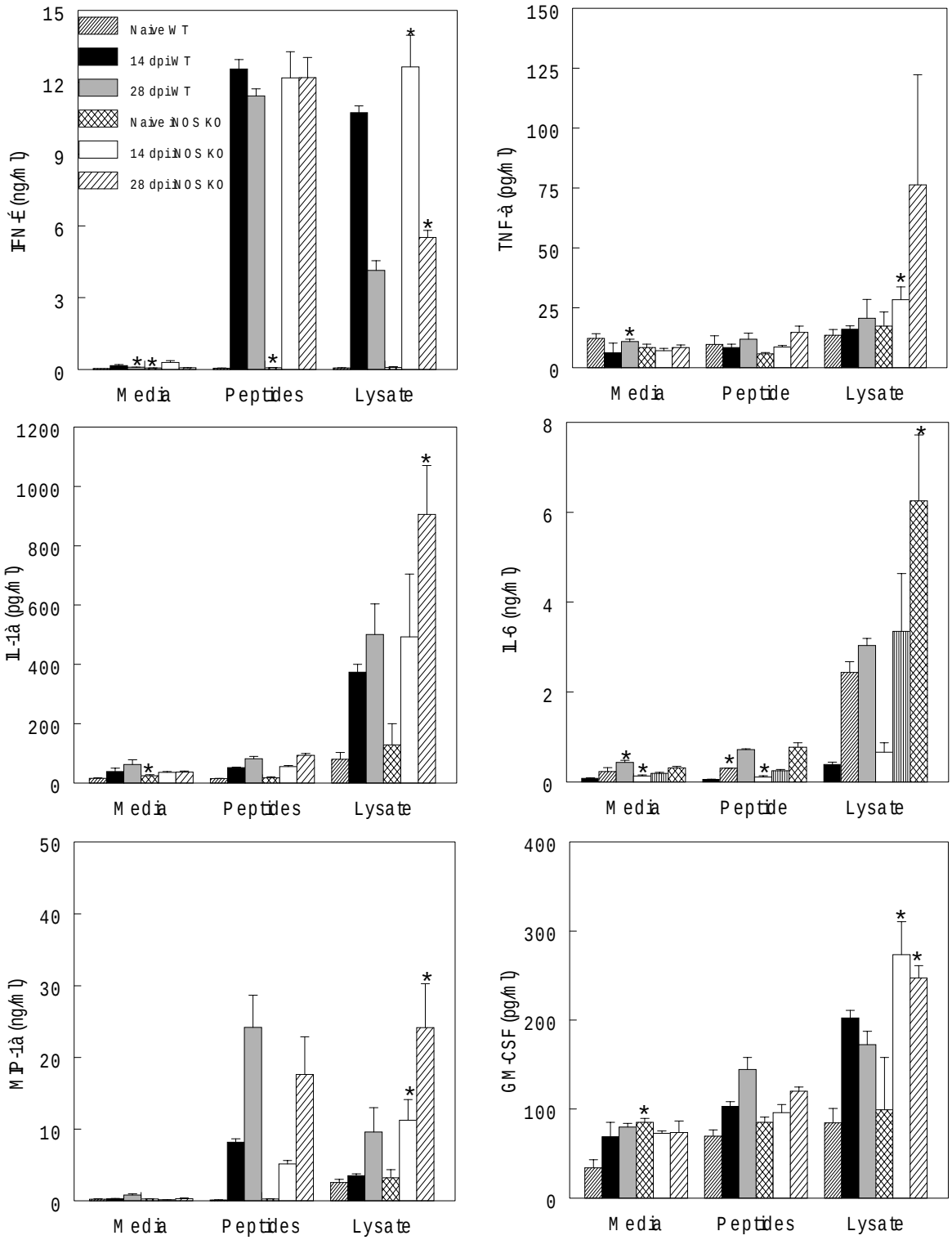
Naive WT
14 dpi WT
28 dpi WT
Naive iNOS KO
14 dpi iNOS KO
28 dpi iNOS KO
IFN-É (ng/ml)
TNF-à (pg/ml)
IL-1à (pg/ml)
IL-6 (ng/ml)
MIP-1à (ng/ml)
GM-CSF (pg/ml)
Media
Peptides
Peptide
Lysate

CHAPTER 4

ALTERED CHEMOKINE RECEPTOR EXPRESSION DURING *TRYPANOSOMA CRUZI* INFECTION IN INTERFERON-GAMMA DEFICIENT MICE[3]

[3] Cummings, K.L. and R.L. Tarleton. To be submitted to *Journal of Immunology*.

Abstract

Control of infection with *Trypanosoma cruzi* requires a competent cell-mediated immune response, and the trafficking of effector cells to sites of infection. While the pattern of chemokine expression during *T. cruzi* infection has been examined the expression of correlating chemokine receptors has not. Here we show that chemokine receptors are highly expressed in muscle during the acute infection and chemokine receptor expression was restricted to sites of parasite persistence during the chronic phase of infection. This implies that parasite persistence stimulates recruitment of effector T cells during the chronic phase of infection. Additionally, it is known that IFN-γ is essential for control of *T. cruzi* infection and so the chemokine receptor expression in infected mice in the absence of IFN-γ was examined. In infected IFN-γ-deficient mice, expression of the chemokine receptors CCR5, and CXCR3 in the cardiac muscle was significantly less than expression in infected WT mice while expression in skeletal muscle was delayed. The delay in chemokine receptor expression in the tissues implies a delay in recruitment of effector $CD4^+$ and $CD8^+$ cell populations necessary for control of *T. cruzi*. These results indicate that chemokine receptor expression occurs in sites of parasite persistence throughout the course of infection and that IFN-γ is important in modulating the chemokine receptor expression necessary for effector cell trafficking during *T. cruzi* infection.

Introduction

The causative agent of Chagas disease, *Trypanosoma cruzi*, is a protozoan parasite with both extracellular and intracellular life cycle stages. The extracellular trypomastigote stage infects hosts and invades various cell types where it converts to the intracellular amastigote form and replicates. Early in infection of mammals, *T. cruzi* can be found in the blood as

trypomastigotes and in tissues in amastigotes "nests". A protective immune response to *T. cruzi*, active against both life cycle stages, is generated and limits parasite numbers but is unable to clear *T. cruzi* from the majority of mammalian hosts. Approximately 30% of infected humans eventually develop morbidity associated with Chagas disease as a result of persistent *T. cruzi* infection, and currently there is no cure for *T. cruzi* infection.

In murine models of *T. cruzi* infection, survival beyond the acute phase of infection requires the generation of effective humoral and cell-mediated immune responses (25-31). Effective cell-mediated immune responses rely on the ability of antigen processing cells in the tissues to sample the environment, and to mature and traffic to secondary lymphoid organs where presentation of foreign antigen to naïve T cells occurs. From the spleen or lymph nodes, activated T cells migrate to sites of infection, following a chemokine gradient, and exhibit the effector functions required to control infection. One effector function of T cells that is essential for resistance to *T. cruzi* is the secretion of interferon-γ (IFN-γ) (72-76). IFN-γ was previously believed to mediate resistance to *T. cruzi* primarily by induction of nitric oxide by infected host cells. While this may be true in immunocompetent hosts, recent studies indicate that IFN-γ-inducible nitric oxide production is not essentail for control of *T. cruzi* infection (Cummigs et al unpublished), (183) and therefore the mechanism by which IFN-γ acts to control infection remains unclear.

Although IFN-γ is involved in many aspects of immune defense, its induction of chemokines which are involved in the recruitment of activated T cells maybe of particular importance (64, 102, 103). *T. cruzi* infection induces a variety of chemokines in murine tissues where disease develops (184-186). During the acute phase of infection, when parasites are dispersed widely in most host tissues (22), chemokines that recruit activated T cells (IFN-

gamma-inducible protein-10 (IP-10), monokine-induced by IFN-gamma (MIG)) and a mixture of leukocytes (macrophage inflammatory protein-1α (MIP-1α), macrophage inflammatory protein-1β (MIP-1β), monocyte chemoattractant protein-1 (MCP-1), and regulated upon activation in normal T cells (RANTES)) are expressed (184-186). Also, during the chronic phase of infection, expression of chemokines that recruit a mixture of leukocytes or activated T cells persists in tissues where disease develops (185, 186). Expression of IFN-γ-inducible MIG and IP-10 correlates with detection of T cells in *T. cruzi* infected tissue and neutralization of MIP-1α resulted in increased tissue parasite load (177, 187). Thus, it is clear that IFN-γ induced chemokine expression is involved in control of *T. cruzi* infection by directing T cells to sites of infection. However, what has not been determined and is thus the focus of this study is the pattern of chemokine receptor expression during the course of *T. cruzi* infection and how IFN-γ impacts this chemokine receptor expression.

This study examined chemokine receptor expression during *T. cruzi* infection in an attempt to correlate tissue chemokine receptor expression with chemokine expression and thus recruitment of cells to sites of parasite persistence. During the chronic phase of infection, expression of the chemokine receptors CCR5, and CXCR3, which are expressed on activated T cells, was increased in tissues where parasites persist and inflammation occurs. Additionally, this study asked whether chemokine and chemokine receptor expression is lost or reduced in mice deficient in IFN-γ. This study shows that in muscle where parasites persist and inflammation occurs there was expression of chemokine receptors that are expressed by activated T cells, and that in infected IFN-γ knockout mice (GKO) the lack of IFN-γ delays chemokine receptor expression in muscle and likely recruitment of T cells necessary for the control of *T. cruzi* infection.

Materials And Methods

Mice and Parasites

Wild-type C57Bl/6J mice (WT) and C57Bl/6-Ifng^{tm1Ts} mice (GKO) were obtained from The Jackson Laboratory (Bar Harbor, Maine) or were bred in our facility. Six to eight week old mice were injected intraperitoneally with 10^3 blood-form trypomastigotes (BFT) of the Brazil strain of *T. cruzi* which were maintained by biweekly passage through C3H/HeSnJ mice (bred in our facilities). C3H/HeSnJ mice were infected with 10^6 culture form trypomastigotes of the Sylvio X10/4 clone of *T. cruzi*. Survival was monitored daily.

RNase Protection Assay probe synthesis

Multi-probe

Pharmingen multi-probe template sets, mCR-6, mCR-5, mCK-5c, were transcribed *in vitro* using an Ambion MAXIscript kit following manufacturers instructions. Briefly, the transcription reaction contained 1 µl of each Pharmingen multiprobe template set, 2 µl 10X Transcription Buffer, 1 µl 10 mM ATP, 1 µl 10 mM CTP, 1 µl 10 mM GTP, 0.6 µl 10 mM UTP, and 0.4 µl of 10 mM biotin-11-UTP (Perkin Elmer Life Sciences, Massachusetts), 2 µl T7 RNA polymerase, and nuclease-free water to 20 µl. The transcription reaction was incubated for 1 hour at 37°C. DNase was added and samples were incubated for 30 minutes at 37°C. The volume was adjusted to 100 µl with nuclease-free water and probes were extracted with 100 µl phenol:choloroform: isoamyl alcohol. Probes were precipitated with 5 M NH_4OAc (1/10 volume) and 2.5 volumes ethanol. Reactions were stored for 30 minutes at -20°C. Probes were centrifuged at 4°C for 30 minutes, air dried and resuspended in 50µl RPA III Hybridization Solution.

Single probes

CXCR3 and MIG were cloned into the pT7T3[18] plasmid (Ambion, Texas). Murine CXCR3 and MIG were amplified by PCR in the following reaction: 0.2 mM dNTPs, 1.5 mM magnesium chloride, 1X Buffer (0.5 M potassium chloride, 0.1 M tris HCl pH 9), 0.5 mM forward primer and 0.5 mM reverse primer, cDNA template, and 2.5 units Taq polymerase. Primers for the amplification of murine MIG were MIG-F 5'-CCC AAG CTT ACC GTT GAT CAA ACC TGC CTA GAT CC-3' and MIG-R 5'-GGG GAA TTC TAT TAA AGG CTG CTC TGC-3'. Primers for the amplification of murine CXCR3 were CXCR3-F 5'-CCC AAG CTT ACC GTT GTA CGT GTA GCC CTC ACC TGC ATA GTT G and CXCR3-R 5'-GGG GAA TTC CAG CAG AAC AGC TAG GAT ATG GGC ATA G-3'. The PCR program to amplify CXCR3 and MIG included an initial denaturation at 95°C for 5 minutes, 45 cycles of amplification with 1 minute at 95°C, 1 minute at 55°C and 1 minute at 72°C, followed by 7 minutes of extension at 72°C. PCR products and pT7/T3[18] were digested with *Hin*d III and *Eco*R I and gel purified. Plasmid and insert were ligated overnight at 16°C, transformed into DH5α cells and plated on ampicillin agar. Colonies were screened for inserts by restriction digest with *Hin*d III and *Eco*R I.

Plasmids were linearized with *Hin*d III (2 hours at 37°C) and the enzyme was heat inactivated. The linearized fragments were gel purified and cleaned using Qiagen RNeasy Mini kit RNA clean-up protocol. Linearized template (1 μg), 2 μl T7 polymerase, 10 mM ATP, 10 mM GTP, 10 mM CTP, 0.6 μl of 10 mM UTP, 0.4 μl 10 mM biotin-11-UTP, 2 μl 10X transcription buffer and nuclease-free water were combined in 20 ul volume and incubated at 37°C for 1 hour. DNase was added to each reaction and incubated for 30 minutes at 37°C. Probes were cleaned by Qiagen RNeasy Mini kit (Qiagen, California) and were purified by adding an equal volume of Gel Loading Buffer II (Ambion), heating 3 minutes at 95°C, loading

pre-rinsed wells of 5% TBE-urea pre-cast gel (Bio-Rad, California) and run at 200 V for 30 minutes. The gel was soaked in ethidium bromide for probe visualization with a UV light source. Bands were added to Probe Elution Buffer (Ambion), incubated at 37°C overnight, and probes were eluted with 3 volumes of ethanol (30 minutes on ice) and centrifuged for 10 minutes at 4°C. Ethanol was removed, probes were air dried and dissolved in 50 µl RPA Hybridization Buffer. Pharmingen mGAPDH and mL32 probes were also transcribed using the above protocol.

RNase Protection Assay (RPA)

RNA was extracted from spleen, lymph nodes, and skeletal and cardiac muscle using UltraSpec (Bio-Tex Laboratories Inc., Texas). Tissue was added to UltraSpec (1 ml/100 mg tissue) and homogenized. Chloroform (0.2 ml/1 ml UltraSpec) was added to homogenized tissue, vortexed and the mixture was centrifuged for 15 minutes at 4°C after 5 minutes on ice. The aqueous phase was transferred and an equal volume of isopropanol was added. Samples were incubated on ice for at least 20 minutes then centrifuged at 4°C for 15 minutes. Samples were washed twice with 75% ethanol, air dried, resuspended in RNase-free water, DNase treated and cleaned.

Ten µg of individual RNA samples and yeast RNA controls were vacuum dried without heat and resuspended in 8 µl RPA III Hybridization Solution (Ambion/Pierce SuperSignal RPA III kit). Probes were added to RNA, heated 2-3 minutes at 95°C and hybridized overnight at 56°C. RNase A/T1 in RNase Digestion III Buffer was added to RNA samples and digested yeast RNA control. RNase Digestion III Buffer alone was added to yeast RNA for full-length probe controls. Samples were incubated at 30°C for 45 minutes and 150 µl Inactivation/Precipitation III Solution was added and incubated 30 minutes at -20°C. Samples were microcentrifuged at

4°C for 30 minutes, supernatant removed, and air dried 5 minutes. Samples were resuspended in 4 µl Gel Loading Buffer II (Ambion). Full-length probe/yeast controls were resuspended in 40 µl Gel Loading Buffer II. Samples were heated at 95°C for 3-5 minutes and quenched on ice. Wells of 5% TBE-Urea gel (Bio-Rad) were pre-rinsed and 4 µl of sample were loaded to wells. Gels were run at 200 V until the xylene cyanol band migrated ¾ of the length of the gel. The RNA was transferred to positively charged membrane (Ambion) using Trans-Blot Semi-dry transfer cell (Bio-Rad); run at 20 V for 30 min and the membrane was UV cross-linked.

Protected RNA was detected by blocking membranes in SuperSignal RPA III Blocking Buffer for 15 minutes on an orbital shaker. 100 µl SuperSignal RPA III stabilized streptavidin-horseradish peroxidase conjugate was added to SuperSignal RPA III Blocking Buffer and the membranes were incubated for 15 minutes. The membranes were rinsed in 2X wash buffer and washed 4 times in 2X wash buffer for 7 minutes per wash. Membranes were incubated in SuperSignal RPA III Substrate Equilibration Buffer for 5 minutes, then incubated 5 minutes in SuperSignal RPA III Luminol/Enhancer Solution mixed with SuperSignall RPA III Stable Peroxide Solution. Membranes were exposed to BioMax Light-1 imaging film (Kodak) and developed.

Quantitation of RNase Protection assay results was determined by densitometry readings. For each band representing a chemokine or chemokine receptor the density was determined using AlphaImager 2000 spot-denso software (Alpha Innotech Corp., San Leandro, California.). The resulting density for the L32 control from each RNA sample was divided by the highest L32 density value and this value was then used to normalize the chemokine and chemokine receptor density values for each RNA sample. Per mouse group, the normalized value for each

chemokine and chemokine receptor was averaged and the standard deviation calculated. A t-test was used to determine statistical significance of $P<0.05$.

cDNA synthesis

DNase treated and cleaned RNA from C57BL/6J and GKO mice infected with 10^3 Brazil BFT was used as template for cDNA synthesis. For first strand cDNA synthesis, 10 μg total RNA and 0.5 μg of oligo$(dT)_{12-18}$ primer (Invitrogen Life Technologies, Carlsbad, California) in a final volume of 20 μl was heated at 65°C for 10 minutes. A mixture of 5X first strand buffer (Invitrogen), 0.1 M DTT (Invitrogen) and 10 mM dNTP mix and RNasin was added to RNA and heated to 42°C. 200 U of SuperScript II RNase H^- reverse transcriptase (Invitrogen) was added to each reaction and incubated for 90 minutes at 42°C. 0.5 μl RNase H was added and incubated at 37°C for 30 minutes.

Real-time PCR of IFN-γ mRNA

Reactions contained 1:10 dilution of cDNA, 0.5 μM primer mix, 10 μl Qiagen QuantiTect Sybr Green PCR Master Mix (Qiagen), and PCR-grade H_2O (Qiagen) to a final total volume of 20μl. Primers for amplification of IFN-γ were MuIFNgdbF 5'-TCA AGT GGC ATA GAT GTG GAA GAA-3' and MuIFNgdbR 5'-TGG CTC TGC AGG ATT TTC ATG-3' (188). Primers for amplification of murine GAPDH: forward 5'-TGT CGT GGA GTC TAC TGG TGT CTT C-3' and reverse 5'-CGT GGT TCA CAC CCA TCA CAA-3'. The real-time PCR program is as follows; 95°C at 20 °C/sec ramp and held for 15 minutes, 70 cycles of 95°C at 20°C/sec ramp for 5 seconds, then to 55°C at 20°C/sec ramp, for 5 sec, and 72°C at 2°C/sec ramp for an 8 sec hold at the end of which fluorescence intensity was acquired. For melting curve generation, samples were heated to 95°C at 20°C/sec ramp, 0 sec hold, then 60°C at

20°C/sec ramp, 30 sec hold, and finally 90°C at 0.2°C/sec ramp, 0 sec hold. Finally, the samples were cooled for one minute at 40°C at 20°C/sec.

For quantification of mRNA expression levels, copy number was calculated from a standard curve, obtained by plotting known input concentrations of control plasmids at log dilutions to the PCR cycle number at which the fluorescence intensity is above background. PCR products for murine IFN-γ and GAPDH were amplified and cloned into the pCR®2.1-TOPO vector (Invitrogen). cDNA from murine muscle tissue and splenocytes was amplified by real-time PCR with IFN-γ and GAPDH primers. Separately, reactions containing serially diluted control plasmids (10^7 to 10^1 copies), 0.5 μM of plasmid specific primers, 10 μl Qiagen QuantiTect Sybr Green PCR Master Mix (Qiagen), and PCR-grade H_2O (Qiagen) to a final total volume of 20μl, were used to generate standard curves. Individual sample values for IFN-γ were normalized to the housekeeping gene GAPDH and presented as number of transcripts per 10^7 copies of GAPDH. Samples were run in triplicate and corrected values for each sample were averaged. Individual sample averages were then averaged per mouse strain, standard deviations determined and standard errors of the mean calculated. Amplification of non-specific products was not observed.

Results

Chemokine and chemokine receptor expression in tissue during *T. cruzi* infection

To examine chemokine receptor expression in *T. cruzi* infection, two mouse:parasite strain combinations were used. C57Bl/6 mice infected with the Brazil strain of *T. cruzi* control the acute infection and exhibit parasite persistence and inflammatory foci in the skeletal muscle (21, 136) while C3H/HeSnJ mice chronically infected with the Sylvio X10/4 clone of *T. cruzi* show inflammation in the cardiac muscle but not in the skeletal muscle (20-21). RNA from

skeletal and cardiac muscle was collected at 28 and 150 days post infection (dpi) from C57Bl/6J mice (B6) infected with 10^3 blood form trypomastigotes (BFT) of the Brazil strain of *T. cruzi* and from cardiac muscle of C3H/HeSnJ (C3H) mice at 170 dpi with the *T. cruzi* Sylvio X10/4 clone. During the acute phase of infection mRNA for chemokine receptors CCR1,CCR2, CCR5 and CXCR3 was observed in both skeletal and cardiac muscle (Figure 4.1A and 4.2A), in agreement with the fact that a prominent T cell population is present (31, 185, 189, 190). CXCR2, expressed on neutrophils, was not significantly induced by *T. cruzi* infection while CXCR4, which is constitutively expressed, was seen in naïve and infected tissues. As previously reported, chemokines were elevated in concert with the increase in IFN-γ mRNA levels and also correlated with the increase in mRNA for chemokine receptors (Figure 4.1B, 4.1C and 4.2B). RANTES and MIP-1α, the ligands for CCR5, MCP-1 a ligand of CCR2, and IP-10 and MIG, ligands for CXCR3 were all upregulated in concert with their respective receptors. These data indicate that IFN-γ inducible chemokines and receptors correlate well with the strong recruitment of effector T cells to both cardiac and skeletal muscle during the acute phase of *T. cruzi* infection.

During the chronic phase of infection, expression of chemokine receptors was expected in tissues where parasite persistence occurs as $CD4^+$ and $CD8^+$ T cells are found in these tissues (31, 185). In the B6/Brazil infection model, *T. cruzi* persistence and inflammation occurs almost exclusively in the skeletal muscle in the chronic phase of infection (21, 136). In comparison to the acute phase, the expression of CCR1, CCR2, CCR5, and CXCR3 was significantly reduced in skeletal and cardiac muscle during the chronic stage of infection in this model (Figure 4.1A and 4.2A). Though a trend toward increased levels of several chemokine receptor/ligand mRNA sets in skeletal muscle was observed, including expression of CCR5, RANTES and MIP-1α and

CXCR3, IP-10 and MIG, only the expression of CXCR3 and its ligand IP-10 were significantly greater in the skeletal muscle than in the cardiac muscle. Unexpectedly, the chemokine receptor and ligand expression at sites of parasite persistence was different in the two models of chronic infection. In the B6/Brazil model, CXCR3 and its ligand IP-10 was expressed at sites of parasite persistence, while in the C3H/Sylvio model, CCR1, CCR5 and RANTES were significantly higher than in naïve mice (Figure 4.1A, 4.1B). Previous studies have shown that IFN-γ is crucial for the control of *T. cruzi* infection and these data demonstrate that IFN-γ-inducible chemokines and chemokine receptors are upregulated at sites of parasite persistence and inflammation during the acute and chronic stages of the infection.

The effect of an absence in IFN-γ production on chemokine receptor expression in muscle was next addressed using IFN-γ deficient mice. IFN-γ-deficient (GKO) mice are highly susceptible to *T. cruzi* infection, dying before 30 dpi (72), and thus examination of chemokine receptor expression was restricted to the early acute phase of infection. Cardiac and skeletal muscle RNA from B6 and GKO mice infected with 10^3 BFTs was collected at 14 and 21 dpi. As expected, the expression of the IFN-γ inducible chemokines and chemokine receptors CCR1, CCR5, CXCR3, MIP-1α, IP-10 and MIG was reduced at 14 dpi. Surprisingly, however, the expression of RANTES, MIP-1α, MIG, CCR1, CCR5, and CXCR3 reached WT expression levels by 21 dpi in the skeletal muscle. In the cardiac muscle, neither IP-10 nor MIG reached WT expression levels and CXCR3 expression was significantly reduced compared to expression in WT mice at 21 dpi (Figure 4.4B, 4.4E, and 4.4F). Also, while RANTES and CCR5 expression in infected GKO skeletal muscle was delayed, the expression of CCR1 and MIP-1α was similar to that of WT mice (4.3A, 4.3C, 4.3D, and 4.3F). In the cardiac muscle, expression of CCR5 was significantly reduced while expression of RANTES, MIP-1α, and CCR1 were all

delayed (4.3A, 4.3C, 4.3D, and 4.3F). Thus, the absence of IFN-γ during *T. cruzi* infection did not result in a complete loss of chemokine expression nor chemokine receptor expression, though expression of specific chemokines and chemokine receptors was significantly delayed or reduced.

Discussion

This study examined the chemokine receptors that are expressed on activated T cells in muscle tissue as well as the effect of IFN-γ on expression of these receptors during *T. cruzi* infection. IFN-γ is critical for the control of *T. cruzi* in mammals; mice treated with anti-IFN-γ antibodies and mice lacking IFN-γ are highly susceptible to early death from *T. cruzi* infection (72-78). Additionally, *T. cruzi* infected mice respond to IFN-γ administration with enhanced parasite clearance and increased survival as compared to non-treated infected mice (79, 80). Among the many properties of IFN-γ is the induction of T cell attracting chemokines (64, 102, 103), including IP-10 an essential chemokine for the recruitment of both $CD4^+$ and $CD8^+$ T cells in *Toxoplasma gondii* infection and likely plays a similar role in *T. cruzi* infected tissues (101). In addition MIP-1α, MIG, and RANTES well characterized recruiters of activated T lymphocytes (64, 102, 103, 191, 192). Additionally, the T cell expressed chemokine receptors CXCR3 (193) and CCR5 (194) are reported to be induced by IFN-γ.

Recently, chemokine production at sites of *T. cruzi* infection in mice was examined (177, 185-187). In the acute and chronic phases of *T. cruzi* infection, intense tissue inflammation and parasite infection induces the production of proinflammatory and regulatory cytokines (75, 158, 195-197). At the site of infection, the inflammatory reaction is dominated by $CD4^+$ and $CD8^+$ lymphocytes (104). In this study we show that the expression of chemokine receptors CCR1, CCR5, and CXCR3 is detected by 14 dpi in infected WT mice, which is consistent with receptor

expression on type 1 $CD4^+$ effector cells and $CD8^+$ effector cells. Additionally, this chemokine receptor expression correlated with ligand expression, as the receptor/ligand sets CCR5/RANTES/MIP-1α, CCR2/MCP-1, CXCR3/IP-10/MIG were increased upon infection. At the same time, expression of CCR3 and CCR4, indicative of a type 2 $CD4^+$ effector T cell infiltrate, was not detected (data not shown). Previous studies showed that infiltration of $CD8^+$ T cells during *T. cruzi* infection was associated with expression of RANTES, MIG, IP-10, MCP-1 and MIP-1a (185, 187). Taken together, these data correlate chemokine receptor expression with chemokine expression and presence of $CD4^+$ and $CD8^+$ lymphocytes seen in previous studies (104, 185, 187).

Immune control of tissue parasitism in *T. cruzi* infection is accompanied by decreased inflammation and few detectable parasites (104). The continued presence of parasites in chronically infected tissues may be sufficient to stimulate the expression of IP-10 and MIG and resultant migration of leukocytes. (186). In this study expression of chemokine receptors and their ligands was detected at higher levels in tissues where parasites persist. Interestingly, the two models of chronic *T. cruzi* infection had disparate chemokine receptor/ligand expression, though both were likely sufficient for migration of leukocytes as was seen by Talvani et. al. (186).

T cell migration into *T. cruzi*-infected tissues is largely attributed to IFN-γ-inducible chemokines. In this study we also addressed the effect of the absence of IFN-γ on chemokine receptor and ligand expression. In the absence of IFN-γ both the chemokine and the chemokine receptor expression in muscle was delayed. Although the expression of IP-10 and MIG were significantly decreased in infected mice deficient in IFN-γ the expression was not completely lost. In addition to induction by IFN-γ, IP-10 can also be induced by IFNα/β, IL-1, TNF and

LPS (62, 199-201). Induction of IP-10 and MIG in GKO mice has also been observed in mice infected with vaccinia virus and expression was accounted for by IFN-α and IFN-α/β, respectively (202-203). Induction of IP-10 and MIG in *T. cruzi* infected IFN-γ-deficient mice, was not seen in a study by Aliberti et. al. which found very low lymphocyte migration to sites of infection (187). Our study found a trend toward the delay in chemokine expression and a correlated delay in levels of chemokine receptor expression in infected GKO mice. This delay in expression of chemokine receptors also likely correlates with a delayed effector T cell migration to sites of infection, resulting in the reduced control of infection and increased susceptibility observed in mice deficient in IFN-γ.

This study examined the expression of chemokine receptors that are expressed on activated T cells as well as the effect of IFN-γ on expression of these receptors during *T. cruzi* infection. The expression of both chemokine receptors and ligands was greater during the acute phase when parasites are prevalent and a subsequent decrease in expression during the chronic phase. Significant expression of chemokine receptors known to be expressed on activated T cells was found in tissues where parasites persist in the chronic phase of infection. The loss of IFN-γ production in the acute phase of infection significantly altered expression of the chemokine receptors CCR5 and CXCR3 in the cardiac muscle as well as the expression of their ligands. The delay in recruitment of effector T cells, as implied by the delay in receptor expression in infected IFN-γ-deficient mice early in acute phase, could explain the extreme susceptibility of mice deficient in IFN-γ.

Figure 4.1. Expression levels of CC-chemokine family members during course of *T. cruzi* infection. A. Skeletal and cardiac muscle RNA from C57Bl/6J collected at 26 dpi and 150 dpi and C3H/HeSnJ mice infected for ~170 dpi was hybridized to multi-probe set of CC-chemokine receptor family members as described in Material and Methods. B. Skeletal and cardiac muscle RNA from C57Bl/6J collected at 26 dpi and 150 dpi and C3H/HeSnJ mice infected for ~170 dpi was hybridized to multi-probe set of CC-chemokine family members as described in Material and Methods. C. IFN-γ mRNA levels were calculated by real-time PCR and normalized with transcripts of GAPDH. * indicates significant difference between naïve and chronic C3H samples ($P<0.05$).

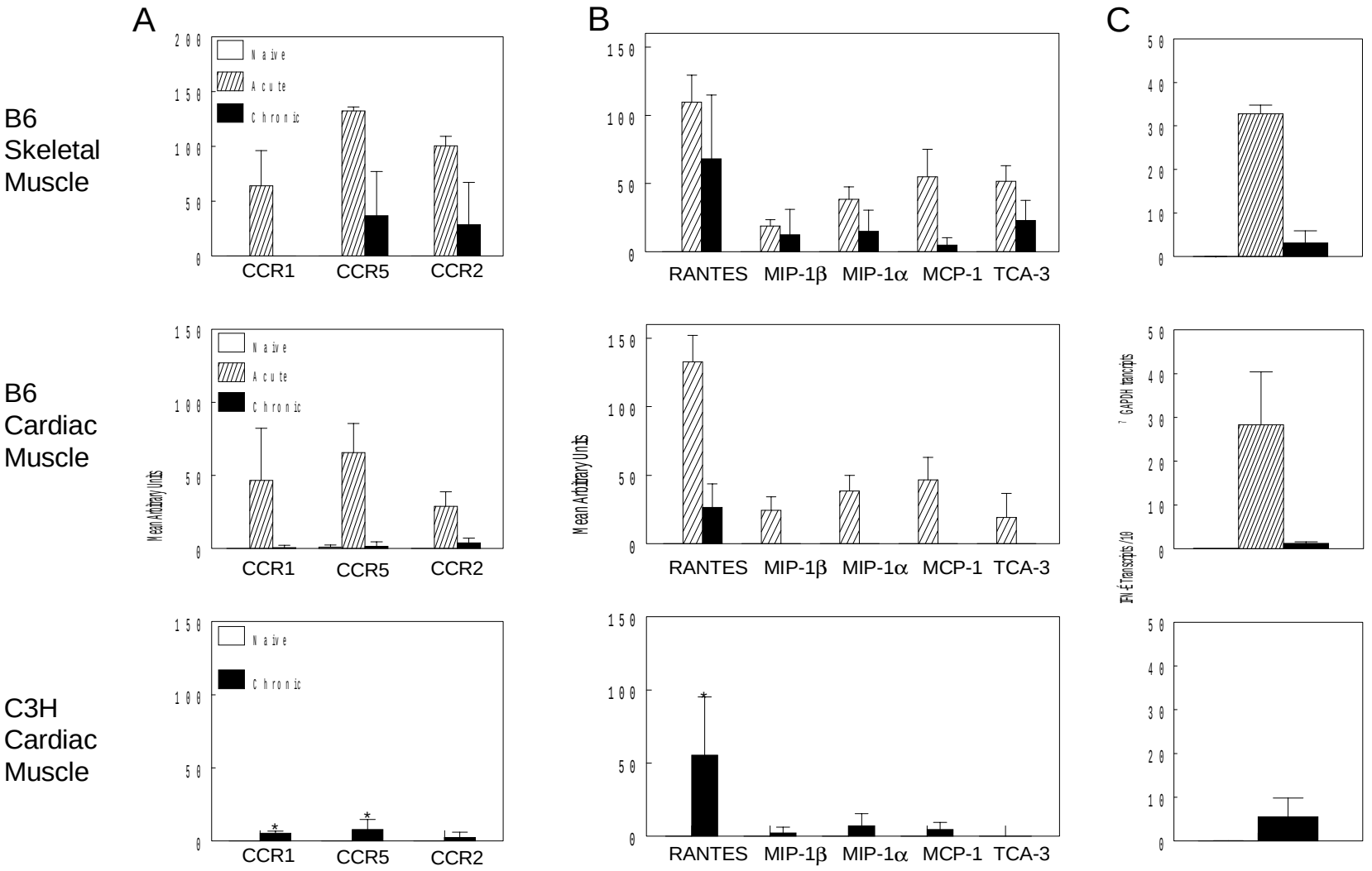
A
B
C
B6 Skeletal Muscle
B6 Cardiac Muscle
C3H Cardiac Muscle
Naive
Acute
Chronic
CCR1
CCR5
CCR2
RANTES
MIP-1β
MIP-1α
MCP-1
TCA-3
Mean Arbitrary Units
IFN-ε Transcripts /10
GAPDH transcripts

Figure 4.2. Expression levels of CXC-chemokine family members during course of *T. cruzi* infection. A. Skeletal and cardiac muscle RNA from C57Bl/6J collected at 26 dpi and 150 dpi and C3H/HeSnJ mice infected for ~170 dpi was hybridized to multi-probe set of CXC-chemokine receptor family members as described in Material and Methods. B. Skeletal and cardiac muscle RNA from C57Bl/6J collected at 26 dpi and 150 dpi and C3H/HeSnJ mice infected for ~170 dpi was hybridized to multi-probe set of CXC-chemokine family members as described in Material and Methods. * indicates significant difference between skeletal muscle and cardiac muscle ($P<0.05$).

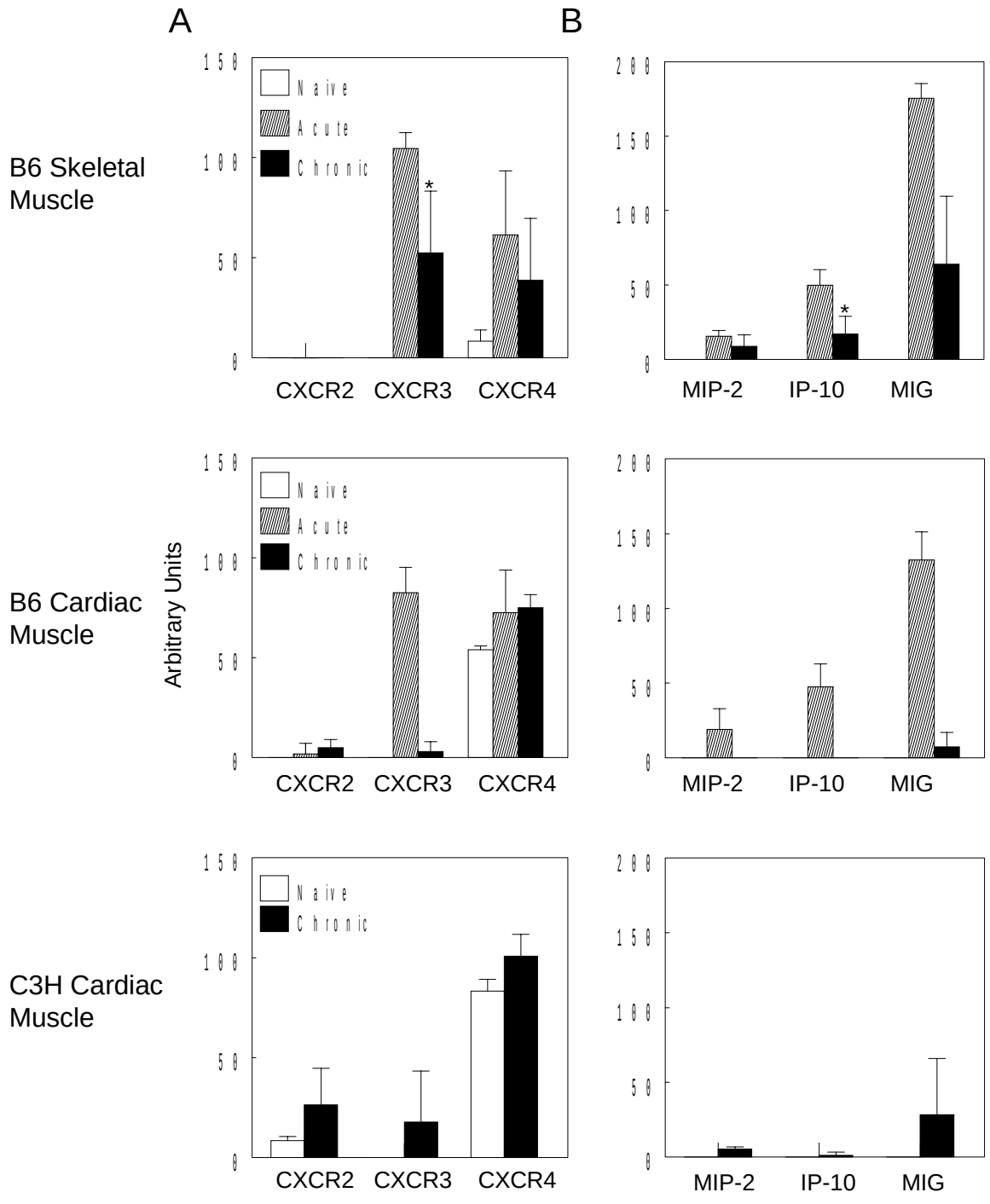
A
B
B6 Skeletal Muscle
B6 Cardiac Muscle
C3H Cardiac Muscle
Arbitrary Units
Naive
Acute
Chronic
CXCR2
CXCR3
CXCR4
MIP-2
IP-10
MIG
*
*
0
50
100
150
200

Figure 4.3. Expression levels of CC-chemokine family members in mice deficient in IFN-γ. A. Skeletal and cardiac muscle RNA from C57Bl/6J collected at 14 dpi and 21dpi was hybridized to multi-probe set of CC-chemokine receptor family members as described in Material and Methods. B. Skeletal and cardiac muscle RNA from C57Bl/6J collected at 14 dpi and 21 dpi was hybridized to multi-probe set of CC-chemokine family members as described in Material and Methods. C. IFN-γ mRNA levels were calculated by real-time PCR and normalized with transcripts of GAPDH. * indicates significant difference between WT and GKO samples ($P<0.05$).

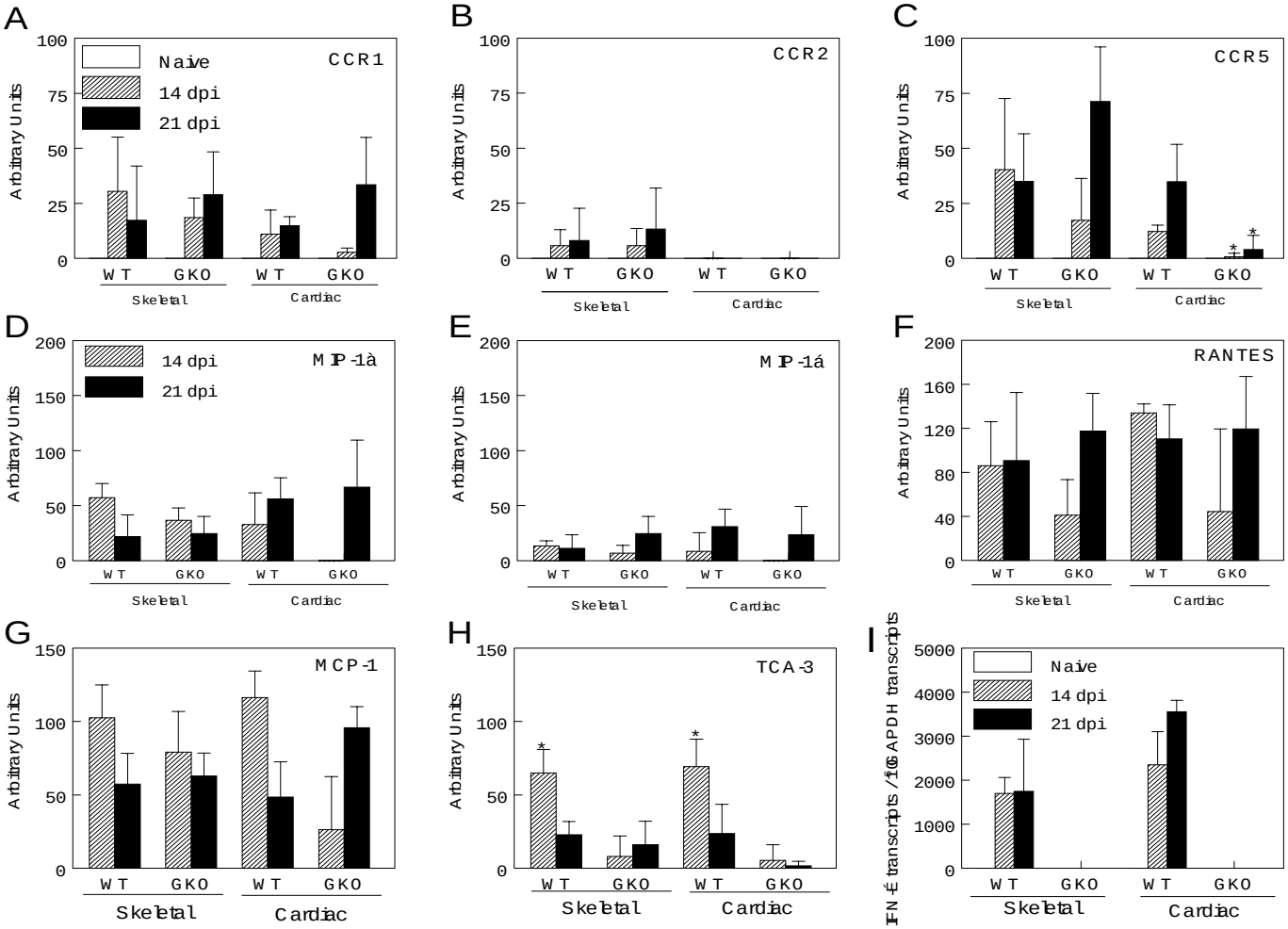
A
CCR1
Naive
14 dpi
21 dpi
Arbitrary Units
WT
GKO
Skeletal
Cardiac
B
CCR2
C
CCR5
D
MIP-1à
E
MIP-1á
F
RANTES
G
MCP-1
H
TCA-3
I
IFN-É transcripts /10^6 GAPDH transcripts

Figure 4.4. Expression levels of CXC-chemokine family members in mice deficient in IFN-γ. A. Skeletal and cardiac muscle RNA from C57Bl/6J collected at 14 dpi and 21dpi was hybridized to multi-probe set of CXC-chemokine receptor family members as described in Material and Methods. B. Skeletal and cardiac muscle RNA from C57Bl/6J collected at 14 dpi and 21 dpi was hybridized to multi-probe set of CXC-chemokine family members as described in Material and Methods. * indicates significant difference between WT and GKO samples.

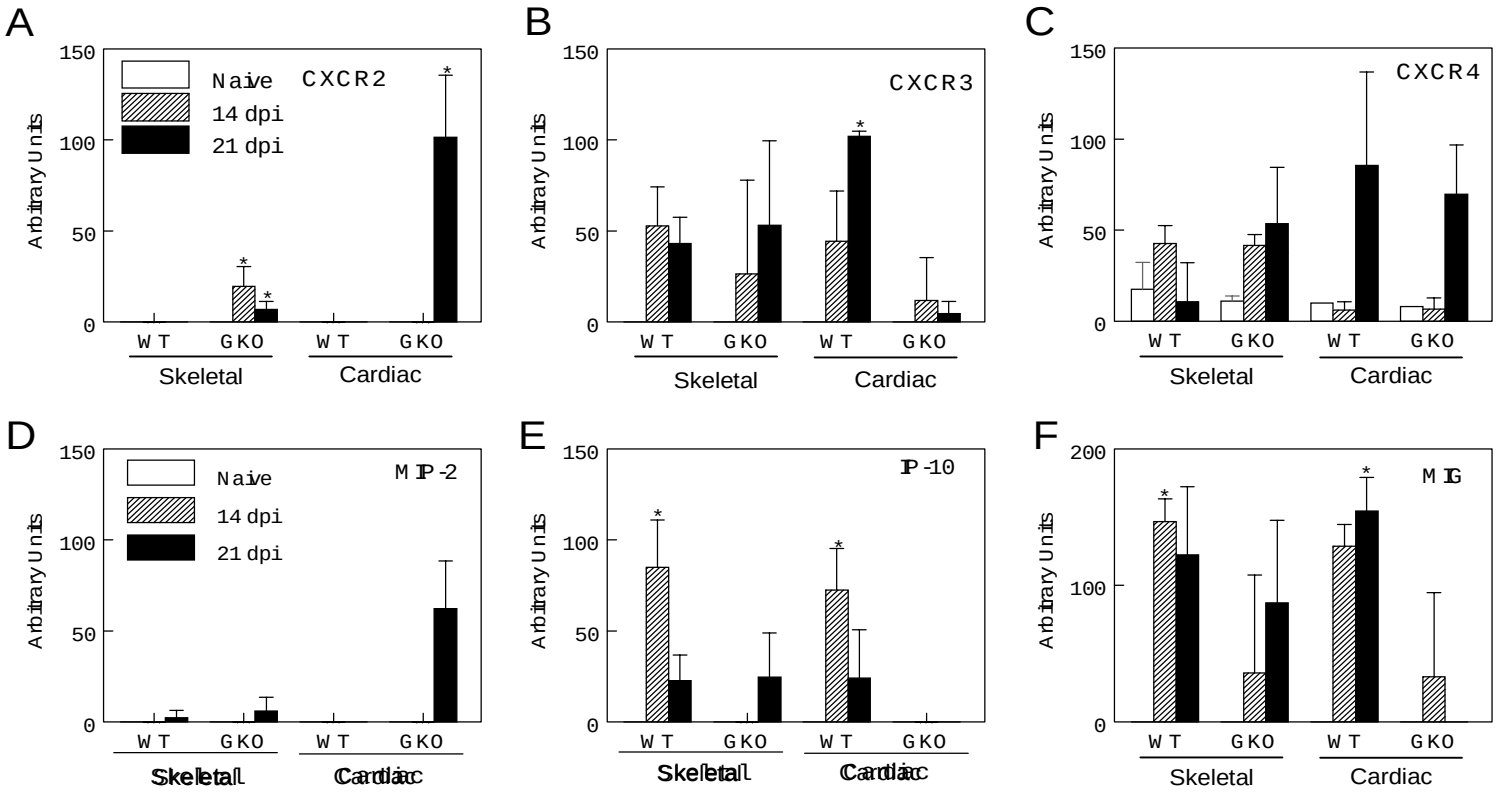
A
B
C
D
E
F
Naive
14 dpi
21 dpi
CXCR2
CXCR3
CXCR4
MIP-2
IP-10
MIG
Arbitrary Units
150
100
50
0
200
WT
GKO
Skeletal
Cardiac

CONCLUSIONS

This study sought to determine the mechanism(s) of interferon-γ mediated control of *Trypanosoma cruzi* infection in mice. Interferon-γ induces the anti-microbicidal agent nitric oxide (NO) as well as the chemokine and chemokine receptors that are involved in the recruitment of effector cells to sites of infection. Although previous studies have suggested that NO is the major IFN-γ induced mechanism of control of *T. cruzi* infection, this study demonstrates that mice with targeted mutations in the iNOS gene are nevertheless able to control *T. cruzi* infection. Control of infection in iNOS KO mice is not the result of increased expression of NO from other NOS isoforms but is accompanied by enhanced production of selected cytokines. Additionally, IFN-γ induction of chemokines and chemokine receptors mediates recruitment of effector cells to sites of infection. Chemokine and chemokine receptor expression is delayed in the absence of IFN-γ, likely delaying recruitment of effector cells necessary for control of *T. cruzi* infection. Nitric oxide production as well as chemokine and chemokine receptor expression are part of a network of IFN-γ inducible responses that contribute to the control *T. cruzi* infection.

REFERENCES

1. Division of Parasitic Disease CDC. Chagas Disease Fact Sheet.

2. World Health Organization. Chagas disease (American trypanosomiasis); prevention and control, burdens and trends.

3. World Health Organization. Chagas disease. Thirteenth Programme Report UNDP/TDR. Geneve., 1997.

4. Moncayo A. Chagas disease: current epidemiological trends after the interruption of vectorial and transfusional transmission in the Southern Cone countries. Mem Inst Oswaldo Cruz 2003;98:577-91.

5. Schofield CJ, Maudlin I. Trypanosomiasis control. Int J Parasitol 2001;31:614-9.

6. World Health Organization. Tropical Disease Research Fifteenth Programme Report Progress 1999-2000, 2000.

7. Leiby DA, Read EJ, Lenes BA, et al. Seroepidemiology of *Trypanosoma cruzi*, etiologic agent of Chagas' disease, in US blood donors. J Infect Dis 1997;176:1047-52.

8. Blood Safety: Surveillance of Emerging Infectious Diseases: A.R.C.-W.H.D., 2000.

9. Grant IH, Gold JW, Wittner M, et al. Transfusion-associated acute Chagas disease acquired in the United States. Ann Intern Med 1989;111:849-51.

10. Shulman IA. Intervention strategies to reduce the risk of transfusion-transmitted *Trypanosoma cruzi* infection in the United States. Transfus Med Rev 1999;13:227-34.

11. Zayas CF, et al.,. Chagas Disease After Organ Transplantation --- United States: CDC Morbidity and Mortality Weekly Report, 2001:210.

12. Herwaldt BL, Grijalva MJ, Newsome AL, et al. Use of polymerase chain reaction to diagnose the fifth reported US case of autochthonous transmission of *Trypanosoma cruzi*, in Tennessee, 1998. J Infect Dis 2000;181:395-9.

13. Rodriques Coura J, de Castro SL. A critical review on Chagas disease chemotherapy. Mem Inst Oswaldo Cruz 2002;97:3-24.

14. Urbina JA. Specific treatment of Chagas disease: current status and new developments. Curr Opin Infect Dis 2001;14:733-41.

15. Fralish BH, Tarleton RL. Genetic immunization with LYT1 or a pool of trans-sialidase genes protects mice from lethal *Trypanosoma cruzi* infection. Vaccine 2003;21:3070-80.

16. Garcia F, Sepulveda P, Liegeard P, et al. Identification of HLA-A*0201-restricted cytotoxic T-cell epitopes of *Trypanosoma cruzi* TcP2beta protein in HLA-transgenic mice and patients. Microbes Infect 2003;5:351-9.

17. Boscardin SB, Kinoshita SS, Fujimura AE, Rodrigues MM. Immunization with cDNA expressed by amastigotes of *Trypanosoma cruzi* elicits protective immune response against experimental infection. Infect Immun 2003;71:2744-57.

18. Garg N, Tarleton RL. Genetic immunization elicits antigen-specific protective immune responses and decreases disease severity in *Trypanosoma cruzi* infection. Infect Immun 2002;70:5547-55.

19. Postan M, McDaniel JP, Dvorak JA. Studies of *Trypanosoma cruzi* clones in inbred mice. II. Course of infection of C57BL/6 mice with single-cell-isolated stocks. Am J Trop Med Hyg 1984;33:236-8.

20. Postan M, Dvorak JA, McDaniel JP. Studies of *Trypanosoma cruzi* clones in inbred mice. I. A comparison of the course of infection of C3H/HEN- mice with two clones isolated from a common source. Am J Trop Med Hyg 1983;32:497-506.

21. Zhang L, Tarleton RL. Parasite persistence correlates with disease severity and localization in chronic Chagas' disease. J Infect Dis 1999;180:480-6.

22. Lenzi HL, Oliveira DN, Lima MT, Gattass CR. *Trypanosoma cruzi*: paninfectivity of CL strain during murine acute infection. Exp Parasitol 1996;84:16-27.

23. Brodskyn CI, da Silva AM, Takehara HA, Mota I. Characterization of antibody isotype responsible for immune clearance in mice infected with *Trypanosoma cruzi*. Immunol Lett 1988;18:255-8.

24. Scott MT, Moyes L. 75Se-methionine labelled *Trypanosoma cruzi* blood trypomastigotes: opsonization by chronic infection serum facilitates killing in spleen and liver. Clin Exp Immunol 1982;48:754-7.

25. Kumar S, Tarleton RL. The relative contribution of antibody production and CD8+ T cell function to immune control of *Trypanosoma cruzi*. Parasite Immunol 1998;20:207-16.

26. Rottenberg ME, Riarte A, Sporrong L, et al. Outcome of infection with different strains of *Trypanosoma cruzi* in mice lacking CD4 and/or CD8. Immunol Lett 1995;45:53-60.

27. Rottenberg ME, Bakhiet M, Olsson T, et al. Differential susceptibilities of mice genomically deleted of CD4 and CD8 to infections with *Trypanosoma cruzi* or Trypanosoma brucei. Infect Immun 1993;61:5129-33.

28. Tarleton RL, Grusby MJ, Postan M, Glimcher LH. *Trypanosoma cruzi* infection in MHC-deficient mice: further evidence for the role of both class I- and class II-restricted T cells in immune resistance and disease. Int Immunol 1996;8:13-22.

29. Tarleton RL. Depletion of CD8+ T cells increases susceptibility and reverses vaccine-induced immunity in mice infected with *Trypanosoma cruzi*. J Immunol 1990;144:717-24.

30. Tarleton RL, Sun J, Zhang L, Postan M. Depletion of T-cell subpopulations results in exacerbation of myocarditis and parasitism in experimental Chagas' disease. Infect Immun 1994;62:1820-9.

31. Sun J, Tarleton RL. Predominance of CD8+ T lymphocytes in the inflammatory lesions of mice with acute *Trypanosoma cruzi* infection. Am J Trop Med Hyg 1993;48:161-9.

32. Tarleton RL, Grusby MJ, Zhang L. Increased susceptibility of Stat4-deficient and enhanced resistance in Stat6-deficient mice to infection with *Trypanosoma cruzi*. J Immunol 2000;165:1520-5.

33. Low HP, Santos MA, Wizel B, Tarleton RL. Amastigote surface proteins of *Trypanosoma cruzi* are targets for CD8+ CTL. J Immunol 1998;160:1817-23.

34. Wizel B, Nunes M, Tarleton RL. Identification of *Trypanosoma cruzi* trans-sialidase family members as targets of protective CD8+ TC1 responses. J Immunol 1997;159:6120-30.

35. Wizel B, Palmieri M, Mendoza C, et al. Human infection with *Trypanosoma cruzi* induces parasite antigen-specific cytotoxic T lymphocyte responses. J Clin Invest 1998;102:1062-71.

36. Wizel B, Garg N, Tarleton RL. Vaccination with trypomastigote surface antigen 1-encoding plasmid DNA confers protection against lethal *Trypanosoma cruzi* infection. Infect Immun 1998;66:5073-81.

37. Boehm U, Klamp T, Groot M, Howard JC. Cellular responses to interferon-gamma. Annu Rev Immunol 1997;15:749-95.

38. Mosmann TR, Coffman RL. TH1 and TH2 cells: different patterns of lymphokine secretion lead to different functional properties. Annu Rev Immunol 1989;7:145-73.

39. Shtrichman R, Samuel CE. The role of gamma interferon in antimicrobial immunity. Curr Opin Microbiol 2001;4:251-9.

40. Yoshida A, Koide Y, Uchijima M, Yoshida TO. IFN-gamma induces IL-12 mRNA expression by a murine macrophage cell line, J774. Biochem Biophys Res Commun 1994;198:857-61.

41. Trinchieri G, Scott P. Interleukin-12: a proinflammatory cytokine with immunoregulatory functions. Res Immunol 1995;146:423-31.

42. Thierfelder WE, van Deursen JM, Yamamoto K, et al. Requirement for Stat4 in interleukin-12-mediated responses of natural killer and T cells. Nature 1996;382:171-4.

43. Kaplan MH, Sun YL, Hoey T, Grusby MJ. Impaired IL-12 responses and enhanced development of Th2 cells in Stat4-deficient mice. Nature 1996;382:174-7.

44. Lighvani AA, Frucht DM, Jankovic D, et al. T-bet is rapidly induced by interferon-gamma in lymphoid and myeloid cells. Proc Natl Acad Sci U S A 2001;98:15137-42.

45. Chang CH, Flavell RA. Class II transactivator regulates the expression of multiple genes involved in antigen presentation. J Exp Med 1995;181:765-7.

46. Kern I, Steimle V, Siegrist CA, Mach B. The two novel MHC class II transactivators RFX5 and CIITA both control expression of HLA-DM genes. Int Immunol 1995;7:1295-9.

47. Mach B, Steimle V, Martinez-Soria E, Reith W. Regulation of MHC class II genes: lessons from a disease. Annu Rev Immunol 1996;14:301-31.

48. Epperson DE, Arnold D, Spies T, Cresswell P, Pober JS, Johnson DR. Cytokines increase transporter in antigen processing-1 expression more rapidly than HLA class I expression in endothelial cells. J Immunol 1992;149:3297-301.

49. Min W, Pober JS, Johnson DR. Kinetically coordinated induction of TAP1 and HLA class I by IFN-gamma: the rapid induction of TAP1 by IFN-gamma is mediated by Stat1 alpha. J Immunol 1996;156:3174-83.

50. Johnson DR, Pober JS. Tumor necrosis factor and immune interferon synergistically increase transcription of HLA class I heavy- and light-chain genes in vascular endothelium. Proc Natl Acad Sci U S A 1990;87:5183-7.

51. Kimura A, Israel A, Le Bail O, Kourilsky P. Detailed analysis of the mouse H-2Kb promoter: enhancer-like sequences and their role in the regulation of class I gene expression. Cell 1986;44:261-72.

52. Kelly A, Powis SH, Glynne R, Radley E, Beck S, Trowsdale J. Second proteasome-related gene in the human MHC class II region. Nature 1991;353:667-8.

53. Belich MP, Glynne RJ, Senger G, Sheer D, Trowsdale J. Proteasome components with reciprocal expression to that of the MHC-encoded LMP proteins. Curr Biol 1994;4:769-76.

54. Dustin ML, Rothlein R, Bhan AK, Dinarello CA, Springer TA. Induction by IL 1 and interferon-gamma: tissue distribution, biochemistry, and function of a natural adherence molecule (ICAM-1). J Immunol 1986;137:245-54.

55. Rosenman SJ, Shrikant P, Dubb L, Benveniste EN, Ransohoff RM. Cytokine-induced expression of vascular cell adhesion molecule-1 (VCAM-1) by astrocytes and astrocytoma cell lines. J Immunol 1995;154:1888-99.

56. Mortarini R, Belli F, Parmiani G, Anichini A. Cytokine-mediated modulation of HLA-class II, ICAM-1, LFA-3 and tumor-associated antigen profile of melanoma cells. Comparison with anti-proliferative activity by rIL1-beta, rTNF-alpha, rIFN-gamma, rIL4 and their combinations. Int J Cancer 1990;45:334-41.

57. Chang HC, Hsu F, Freeman GJ, Griffin JD, Reinherz EL. Cloning and expression of a gamma-interferon-inducible gene in monocytes: a new member of a cytokine gene family. Int Immunol 1989;1:388-97.

58. Brown Z, Gerritsen ME, Carley WW, Strieter RM, Kunkel SL, Westwick J. Chemokine gene expression and secretion by cytokine-activated human microvascular endothelial cells. Differential regulation of monocyte chemoattractant protein-1 and interleukin-8 in response to interferon-gamma. Am J Pathol 1994;145:913-21.

59. Kasama T, Strieter RM, Lukacs NW, Lincoln PM, Burdick MD, Kunkel SL. Interferon gamma modulates the expression of neutrophil-derived chemokines. J Investig Med 1995;43:58-67.

60. Marfaing-Koka A, Devergne O, Gorgone G, et al. Regulation of the production of the RANTES chemokine by endothelial cells. Synergistic induction by IFN-gamma plus TNF-alpha and inhibition by IL-4 and IL-13. J Immunol 1995;154:1870-8.

61. Luster AD, Ravetch JV. Genomic characterization of a gamma-interferon-inducible gene (IP-10) and identification of an interferon-inducible hypersensitive site. Mol Cell Biol 1987;7:3723-31.

62. Vanguri P, Farber JM. Identification of CRG-2. An interferon-inducible mRNA predicted to encode a murine monokine. J Biol Chem 1990;265:15049-57.

63. Farber JM. A macrophage mRNA selectively induced by gamma-interferon encodes a member of the platelet factor 4 family of cytokines. Proc Natl Acad Sci U S A 1990;87:5238-42.

64. Taub DD, Conlon K, Lloyd AR, Oppenheim JJ, Kelvin DJ. Preferential migration of activated CD4+ and CD8+ T cells in response to MIP-1 alpha and MIP-1 beta. Science 1993;260:355-8.

65. Snapper CM, Paul WE. Interferon-gamma and B cell stimulatory factor-1 reciprocally regulate Ig isotype production. Science 1987;236:944-7.

66. Collins JT, Dunnick WA. Germline transcripts of the murine immunoglobulin gamma 2a gene: structure and induction by IFN-gamma. Int Immunol 1993;5:885-91.

67. Kamijo R, Harada H, Matsuyama T, et al. Requirement for transcription factor IRF-1 in NO synthase induction in macrophages. Science 1994;263:1612-5.

68. Xie QW, Whisnant R, Nathan C. Promoter of the mouse gene encoding calcium-independent nitric oxide synthase confers inducibility by interferon gamma and bacterial lipopolysaccharide. J Exp Med 1993;177:1779-84.

69. Morris SM, Jr., Billiar TR. New insights into the regulation of inducible nitric oxide synthesis. Am J Physiol 1994;266:E829-39.

70. Cassatella MA, Bazzoni F, Flynn RM, Dusi S, Trinchieri G, Rossi F. Molecular basis of interferon-gamma and lipopolysaccharide enhancement of phagocyte respiratory burst capability. Studies on the gene expression of several NADPH oxidase components. J Biol Chem 1990;265:20241-6.

71. Eklund EA, Skalnik DG. Characterization of a gp91-phox promoter element that is required for interferon gamma-induced transcription. J Biol Chem 1995;270:8267-73.

72. Torrico F, Heremans H, Rivera MT, Van Marck E, Billiau A, Carlier Y. Endogenous IFN-gamma is required for resistance to acute Trypanosoma cruzi infection in mice. J Immunol 1991;146:3626-32.

73. Rottenberg ME, Castanos-Velez E, de Mesquita R, Laguardia OG, Biberfeld P, Orn A. Intracellular co-localization of *Trypanosoma cruzi* and inducible nitric oxide synthase (iNOS): evidence for dual pathway of iNOS induction. Eur J Immunol 1996;26:3203-13.

74. Holscher C, Kohler G, Muller U, Mossmann H, Schaub GA, Brombacher F. Defective nitric oxide effector functions lead to extreme susceptibility of *Trypanosoma cruzi*-infected mice deficient in gamma interferon receptor or inducible nitric oxide synthase. Infect Immun 1998;66:1208-15.

75. Silva JS, Morrissey PJ, Grabstein KH, Mohler KM, Anderson D, Reed SG. Interleukin 10 and interferon gamma regulation of experimental *Trypanosoma cruzi* infection. J Exp Med 1992;175:169-74.

76. McCabe RE, Meagher SG, Mullins BT. Endogenous interferon-gamma, macrophage activation, and murine host defense against acute infection with *Trypanosoma cruzi*. J Infect Dis 1991;163:912-5.

77. Petray PB, Rottenberg ME, Bertot G, et al. Effect of anti-gamma-interferon and anti-interleukin-4 administration on the resistance of mice against infection with reticulotropic and myotropic strains of *Trypanosoma cruzi*. Immunol Lett 1993;35:77-80.

78. Minoprio P, el Cheikh MC, Murphy E, et al. Xid-associated resistance to experimental Chagas' disease is IFN-gamma dependent. J Immunol 1993;151:4200-8.

79. Reed SG. In vivo administration of recombinant IFN-gamma induces macrophage activation, and prevents acute disease, immune suppression, and death in experimental *Trypanosoma cruzi* infections. J Immunol 1988;140:4342-7.

80. McCabe R, Meagher S, Mullins B. Gamma interferon suppresses acute and chronic *Trypanosoma cruzi* infection in cyclosporin-treated mice. Infect Immun 1991;59:1633-8.

81. Zhang L, Tarleton RL. Characterization of cytokine production in murine *Trypanosoma cruzi* infection by in situ immunocytochemistry: lack of association between susceptibility and type 2 cytokine production. Eur J Immunol 1996;26:102-9.

82. Drapier JC, Wietzerbin J, Hibbs JB, Jr. Interferon-gamma and tumor necrosis factor induce the L-arginine-dependent cytotoxic effector mechanism in murine macrophages. Eur J Immunol 1988;18:1587-92.

83. Ding AH, Nathan CF, Stuehr DJ. Release of reactive nitrogen intermediates and reactive oxygen intermediates from mouse peritoneal macrophages. Comparison of activating cytokines and evidence for independent production. J Immunol 1988;141:2407-12.

84. Gao J, Morrison DC, Parmely TJ, Russell SW, Murphy WJ. An interferon-gamma-activated site (GAS) is necessary for full expression of the mouse iNOS gene in response to interferon-gamma and lipopolysaccharide. J Biol Chem 1997;272:1226-30.

85. Baek KJ, Thiel BA, Lucas S, Stuehr DJ. Macrophage nitric oxide synthase subunits. Purification, characterization, and role of prosthetic groups and substrate in regulating their association into a dimeric enzyme. J Biol Chem 1993;268:21120-9.

86. Hibbs JB, Jr., Vavrin Z, Taintor RR. L-arginine is required for expression of the activated macrophage effector mechanism causing selective metabolic inhibition in target cells. J Immunol 1987;138:550-65.

87. Kilbourn RG, Belloni P. Endothelial cell production of nitrogen oxides in response to interferon gamma in combination with tumor necrosis factor, interleukin-1, or endotoxin. J Natl Cancer Inst 1990;82:772-6.

88. Kilbourn RG, Gross SS, Lodato RF, et al. Inhibition of interleukin-1-alpha-induced nitric oxide synthase in vascular smooth muscle and full reversal of interleukin-1-alpha-induced hypotension by N omega-amino-L-arginine. J Natl Cancer Inst 1992;84:1008-16.

89. Vespa GN, Cunha FQ, Silva JS. Nitric oxide is involved in control of *Trypanosoma cruzi*-induced parasitemia and directly kills the parasite in vitro. Infect Immun 1994;62:5177-82.

90. Werner-Felmayer G, Werner ER, Fuchs D, Hausen A, Reibnegger G, Wachter H. Tetrahydrobiopterin-dependent formation of nitrite and nitrate in murine fibroblasts. J Exp Med 1990;172:1599-607.

91. Munoz-Fernandez MA, Fernandez MA, Fresno M. Synergism between tumor necrosis factor-alpha and interferon-gamma on macrophage activation for the killing of intracellular *Trypanosoma cruzi* through a nitric oxide-dependent mechanism. Eur J Immunol 1992;22:301-7.

92. Gazzinelli RT, Oswald IP, Hieny S, James SL, Sher A. The microbicidal activity of interferon-gamma-treated macrophages against *Trypanosoma cruzi* involves an L-arginine-dependent, nitrogen oxide-mediated mechanism inhibitable by interleukin-10 and transforming growth factor-beta. Eur J Immunol 1992;22:2501-6.

93. Laubach VE, Shesely EG, Smithies O, Sherman PA. Mice lacking inducible nitric oxide synthase are not resistant to lipopolysaccharide-induced death. Proc Natl Acad Sci U S A 1995;92:10688-92.

94. MacMicking JD, Nathan C, Hom G, et al. Altered responses to bacterial infection and endotoxic shock in mice lacking inducible nitric oxide synthase [published erratum appears in Cell 1995 Jun 30;81(7):following 1170]. Cell 1995;81:641-50.

95. Wei XQ, Charles IG, Smith A, et al. Altered immune responses in mice lacking inducible nitric oxide synthase. Nature 1995;375:408-11.

96. Tarleton RL, Zhang L, Downs MO. "Autoimmune rejection" of neonatal heart transplants in experimental Chagas disease is a parasite-specific response to infected host tissue. Proc Natl Acad Sci U S A 1997;94:3932-7.

97. Tarleton RL, Koller BH, Latour A, Postan M. Susceptibility of beta 2-microglobulin-deficient mice to *Trypanosoma cruzi* infection [see comments]. Nature 1992;356:338-40.

98. Garg N, Nunes MP, Tarleton RL. Delivery by *Trypanosoma cruzi* of proteins into the MHC class I antigen processing and presentation pathway. J Immunol 1997;158:3293-302.

99. Cyster JG. Chemokines and cell migration in secondary lymphoid organs. Science 1999;286:2098-102.

100. Banchereau J, Steinman RM. Dendritic cells and the control of immunity. Nature 1998;392:245-52.

101. Khan IA, MacLean JA, Lee FS, et al. IP-10 is critical for effector T cell trafficking and host survival in Toxoplasma gondii infection. Immunity 2000;12:483-94.

102. Baggiolini M, Dewald B, Moser B. Human chemokines: an update. Annu Rev Immunol 1997;15:675-705.

103. Baggiolini M. Chemokines and leukocyte traffic. Nature 1998;392:565-8.

104. Talvani A, Ribeiro CS, Aliberti JC, et al. Kinetics of cytokine gene expression in experimental chagasic cardiomyopathy: tissue parasitism and endogenous IFN-gamma as important determinants of chemokine mRNA expression during infection with *Trypanosoma cruzi* [In Process Citation]. Microbes Infect 2000;2:851-66.

105. Heid CA, Stevens J, Livak KJ, Williams PM. Real time quantitative PCR. Genome Res 1996;6:986-94.

106. Najioullah F, Thouvenot D, Lina B. Development of a real-time PCR procedure including an internal control for the measurement of HCMV viral load. J Virol Methods 2001;92:55-64.

107. Lin MH, Chen TC, Kuo T, Tseng CC, Tseng CP. Real-time PCR for quantitative detection of *Toxoplasma gondii.* J Clin Microbiol 2000;38:4121-5.

108. Sturm NR, Degrave W, Morel C, Simpson L. Sensitive detection and schizodeme classification of *Trypanosoma cruzi* cells by amplification of kinetoplast minicircle DNA sequences: use in diagnosis of Chagas' disease. Mol Biochem Parasitol 1989;33:205-14.

109. Degrave W, Fragoso SP, Britto C, et al. Peculiar sequence organization of kinetoplast DNA minicircles from *Trypanosoma cruzi*. Mol Biochem Parasitol 1988;27:63-70.

110. Moser DR, Kirchhoff LV, Donelson JE. Detection of *Trypanosoma cruzi* by DNA amplification using the polymerase chain reaction. J Clin Microbiol 1989;27:1477-82.

111. Monteon VM, Furuzawa-Carballeda J, Alejandre-Aguilar R, Aranda-Fraustro A, Rosales-Encina JL, Reyes PA. American trypanosomosis: in situ and generalized features of parasitism and inflammation kinetics in a murine model. Exp Parasitol 1996;83:267-74.

112. Postan M, Cheever AW, Dvorak JA, McDaniel JP. A histopathological analysis of the course of myocarditis in C3H/He mice infected with Trypanosoma cruzi clone Sylvio-X10/4. Trans R Soc Trop Med Hyg 1986;80:50-5.

113. Reis MM, Higuchi MdL, Benvenuti LA, et al. An in situ quantitative immunohistochemical study of cytokines and IL-2R+ in chronic human chagasic myocarditis: correlation with the presence of myocardial *Trypanosoma cruzi* antigens. Clin Immunol Immunopathol 1997;83:165-72.

114. Lane JE, Olivares-Villagomez D, Vnencak-Jones CL, McCurley TL, Carter CE. Detection of *Trypanosoma cruzi* with the polymerase chain reaction and in situ hybridization in infected murine cardiac tissue. Am J Trop Med Hyg 1997;56:588-95.

115. Vago AR, Macedo AM, Adad SJ, Reis DD, Correa-Oliveira R. PCR detection of *Trypanosoma cruzi* DNA in oesophageal tissues of patients with chronic digestive Chagas' disease [letter]. Lancet 1996;348:891-2.

116. Kirchhoff LV, Votava JR, Ochs DE, Moser DR. Comparison of PCR and microscopic methods for detecting *Trypanosoma cruzi*. J Clin Microbiol 1996;34:1171-5.

117. Stordeur P, Poulin LF, Craciun L, et al. Cytokine mRNA quantification by real-time PCR. J Immunol Methods 2002;259:55-64.

118. Gonzalez A, Prediger E, Huecas ME, Nogueira N, Lizardi PM. Minichromosomal repetitive DNA in *Trypanosoma cruzi*: its use in a high-sensitivity parasite detection assay. Proc Natl Acad Sci U S A 1984;81:3356-60.

119. de Andrade AL, Zicker F, de Oliveira RM, et al. Randomised trial of efficacy of benznidazole in treatment of early *Trypanosoma cruzi* infection. Lancet 1996;348:1407-13.

120. Nabors GS, Tarleton RL. Differential control of IFN-gamma and IL-2 production during *Trypanosoma cruzi* infection. J Immunol 1991;146:3591-8.

121. Green SJ, Meltzer MS, Hibbs JB, Jr., Nacy CA. Activated macrophages destroy intracellular *Leishmania major* amastigotes by an L-arginine-dependent killing mechanism. J Immunol 1990;144:278-83.

122. Liew FY, Millott S, Parkinson C, Palmer RM, Moncada S. Macrophage killing of *Leishmania* parasite in vivo is mediated by nitric oxide from L-arginine. J Immunol 1990;144:4794-7.

123. Diefenbach A, Schindler H, Donhauser N, et al. Type 1 interferon (IFNalpha/beta) and type 2 nitric oxide synthase regulate the innate immune response to a protozoan parasite. Immunity 1998;8:77-87.

124. Murray HW, Nathan CF. Macrophage microbicidal mechanisms in vivo: reactive nitrogen versus oxygen intermediates in the killing of intracellular visceral *Leishmania donovani*. J Exp Med 1999;189:741-6.

125. Adams LB, Hibbs JB, Jr., Taintor RR, Krahenbuhl JL. Microbiostatic effect of murine-activated macrophages for *Toxoplasma gondii*. Role for synthesis of inorganic nitrogen oxides from L-arginine. J Immunol 1990;144:2725-9.

126. Scharton-Kersten TM, Yap G, Magram J, Sher A. Inducible nitric oxide is essential for host control of persistent but not acute infection with the intracellular pathogen *Toxoplasma gondii*. J Exp Med 1997;185:1261-73.

127. Khan IA, Schwartzman JD, Matsuura T, Kasper LH. A dichotomous role for nitric oxide during acute *Toxoplasma gondii* infection in mice. Proc Natl Acad Sci U S A 1997;94:13955-60.

128. Stuehr DJ, Marletta MA. Induction of nitrite/nitrate synthesis in murine macrophages by BCG infection, lymphokines, or interferon-gamma. J Immunol 1987;139:518-25.

129. Martin E, Nathan C, Xie QW. Role of interferon regulatory factor 1 in induction of nitric oxide synthase. J Exp Med 1994;180:977-84.

130. Metz G, Carlier Y, Vray B. *Trypanosoma cruzi* upregulates nitric oxide release by IFN-gamma-preactivated macrophages, limiting cell infection independently of the respiratory burst. Parasite Immunol 1993;15:693-9.

131. Camargo MM, Andrade AC, Almeida IC, Travassos LR, Gazzinelli RT. Glycoconjugates isolated from *Trypanosoma cruzi* but not from *Leishmania* species membranes trigger nitric oxide synthesis as well as microbicidal activity in IFN-gamma-primed macrophages. J Immunol 1997;159:6131-9.

132. Bourguignon SC, Alves CR, Giovanni-De-Simone S. Detrimental effect of nitric oxide on *Trypanosoma cruzi* and *Leishmania major* like cells. Acta Trop 1997;66:109-18.

133. Petray P, Rottenberg ME, Grinstein S, Orn A. Release of nitric oxide during the experimental infection with *Trypanosoma cruzi*. Parasite Immunol 1994;16:193-9.

134. Petray P, Castanos-Velez E, Grinstein S, Orn A, Rottenberg ME. Role of nitric oxide in resistance and histopathology during experimental infection with *Trypanosoma cruzi*. Immunol Lett 1995;47:121-6.

135. Saeftel M, Fleischer B, Hoerauf A. Stage-dependent role of nitric oxide in control of *Trypanosoma cruzi* infection. Infect Immun 2001;69:2252-9.

136. Kirchhoff LV, Votava JR, Ochs DE, Moser DR. Comparison of PCR and microscopic methods for detecting *Trypanosoma cruzi*. J Clin Microbiol 1996;34:1171-5.

137. Overbergh L, Valckx D, Waer M, Mathieu C. Quantification of murine cytokine mRNAs using real time quantitative reverse transcriptase PCR. Cytokine 1999;11:305-12.

138. Low HP, Santos MA, Wizel B, Tarleton RL. Amastigote surface proteins of *Trypanosoma cruzi* are targets for CD8+ CTL. J Immunol 1998;160:1817-23.

139. Cummings KL, Tarleton RL. Rapid quantitation of *Trypanosoma cruzi* in host tissue by real-time PCR. Mol Biochem Parasitol 2003;129:53-9.

140. Feron O, Belhassen L, Kobzik L, Smith TW, Kelly RA, Michel T. Endothelial nitric oxide synthase targeting to caveolae. Specific interactions with caveolin isoforms in cardiac myocytes and endothelial cells. J Biol Chem 1996;271:22810-4.

141. Vodovotz Y, Russell D, Xie QW, Bogdan C, Nathan C. Vesicle membrane association of nitric oxide synthase in primary mouse macrophages. J Immunol 1995;154:2914-25.

142. Kobzik L, Stringer B, Balligand JL, Reid MB, Stamler JS. Endothelial type nitric oxide synthase in skeletal muscle fibers: mitochondrial relationships. Biochem Biophys Res Commun 1995;211:375-81.

143. Feron O, Dessy C, Opel DJ, Arstall MA, Kelly RA, Michel T. Modulation of the endothelial nitric-oxide synthase-caveolin interaction in cardiac myocytes. Implications for the autonomic regulation of heart rate. J Biol Chem 1998;273:30249-54.

144. Chang WJ, Iannaccone ST, Lau KS, et al. Neuronal nitric oxide synthase and dystrophin-deficient muscular dystrophy. Proc Natl Acad Sci U S A 1996;93:9142-7.

145. Xu KY, Huso DL, Dawson TM, Bredt DS, Becker LC. Nitric oxide synthase in cardiac sarcoplasmic reticulum. Proc Natl Acad Sci U S A 1999;96:657-62.

146. Komatsu T, Bi Z, Reiss CS. Interferon-gamma induced type I nitric oxide synthase activity inhibits viral replication in neurons. J Neuroimmunol 1996;68:101-8.

147. Barna M, Komatsu T, Reiss CS. Activation of type III nitric oxide synthase in astrocytes following a neurotropic viral infection. Virology 1996;223:331-43.

148. Brunet LR. Nitric oxide in parasitic infections. Int Immunopharmacol 2001;1:1457-67.

149. Liew FY, Li Y, Moss D, Parkinson C, Rogers MV, Moncada S. Resistance to *Leishmania major* infection correlates with the induction of nitric oxide synthase in murine macrophages. Eur J Immunol 1991;21:3009-14.

150. Hibbs JB, Jr., Taintor RR, Vavrin Z. Macrophage cytotoxicity: role for L-arginine deiminase and imino nitrogen oxidation to nitrite. Science 1987;235:473-6.

151. Abrahamsohn IA, Coffman RL. Cytokine and nitric oxide regulation of the immunosuppression in *Trypanosoma cruzi* infection. J Immunol 1995;155:3955-63.

152. Kroncke KD, Fehsel K, Suschek C, Kolb-Bachofen V. Inducible nitric oxide synthase-derived nitric oxide in gene regulation, cell death and cell survival. Int Immunopharmacol 2001;1:1407-20.

153. Karupiah G, Chen JH, Mahalingam S, Nathan CF, MacMicking JD. Rapid interferon gamma-dependent clearance of influenza A virus and protection from consolidating pneumonitis in nitric oxide synthase 2-deficient mice. J Exp Med 1998;188:1541-6.

154. MacMicking JD, Nathan C, Hom G, et al. Altered responses to bacterial infection and endotoxic shock in mice lacking inducible nitric oxide synthase. Cell 1995;81:641-50.

155. Munoz-Fernandez MA, Fernandez MA, Fresno M. Activation of human macrophages for the killing of intracellular Trypanosoma cruzi by TNF-alpha and IFN-gamma through a nitric oxide-dependent mechanism. Immunol Lett 1992;33:35-40.

156. Olivares Fontt E, Vray B. Relationship between granulocyte macrophage-colony stimulating factor, tumour necrosis factor-alpha and *Trypanosoma cruzi* infection of murine macrophages. Parasite Immunol 1995;17:135-41.

157. Rottenberg ME, Sporrong L, Persson I, Wigzell H, Orn A. Cytokine gene expression during infection of mice lacking CD4 and/or CD8 with Trypanosoma cruzi. Scand J Immunol 1995;41:164-70.

158. Silva JS, Vespa GN, Cardoso MA, Aliberti JC, Cunha FQ. Tumor necrosis factor alpha mediates resistance to *Trypanosoma cruzi* infection in mice by inducing nitric oxide production in infected gamma interferon-activated macrophages. Infect Immun 1995;63:4862-7.

159. Norris KA, Schrimpf JE, Flynn JL, Morris SM, Jr. Enhancement of macrophage microbicidal activity: supplemental arginine and citrulline augment nitric oxide production in murine peritoneal macrophages and promote intracellular killing of *Trypanosoma cruzi*. Infect Immun 1995;63:2793-6.

160. Castanos-Velez E, Maerlan S, Osorio LM, et al. Trypanosoma cruzi infection in tumor necrosis factor receptor p55-deficient mice. Infect Immun 1998;66:2960-8.

161. Martins GA, Vieira LQ, Cunha FQ, Silva JS. Gamma interferon modulates CD95 (Fas) and CD95 ligand (Fas-L) expression and nitric oxide-induced apoptosis during the acute phase of Trypanosoma cruzi infection: a possible role in immune response control. Infect Immun 1999;67:3864-71.

162. Boer R, Ulrich WR, Klein T, Mirau B, Haas S, Baur I. The inhibitory potency and selectivity of arginine substrate site nitric-oxide synthase inhibitors is solely determined by their affinity toward the different isoenzymes. Mol Pharmacol 2000;58:1026-34.

163. Alderton WK, Cooper CE, Knowles RG. Nitric oxide synthases: structure, function and inhibition. Biochem J 2001;357:593-615.

164. Wolff DJ, Lubeskie A. Aminoguanidine is an isoform-selective, mechanism-based inactivator of nitric oxide synthase. Arch Biochem Biophys 1995;316:290-301.

165. Wolff DJ, Gauld DS, Neulander MJ, Southan G. Inactivation of nitric oxide synthase by substituted aminoguanidines and aminoisothioureas. J Pharmacol Exp Ther 1997;283:265-73.

166. Ou P, Wolff SP. Aminoguanidine: a drug proposed for prophylaxis in diabetes inhibits catalase and generates hydrogen peroxide in vitro. Biochem Pharmacol 1993;46:1139-44.

167. Lopez-Belmonte J, Whittle BJ. Aminoguanidine-provoked leukocyte adherence to rat mesenteric venules: role of constitutive nitric oxide synthase inhibition. Br J Pharmacol 1995;116:2710-4.

168. Thiemermann C. Nitric oxide and septic shock. Gen Pharmacol 1997;29:159-66.

169. Picard S, Parthasarathy S, Fruebis J, Witztum JL. Aminoguanidine inhibits oxidative modification of low density lipoprotein protein and the subsequent increase in uptake by macrophage scavenger receptors. Proc Natl Acad Sci U S A 1992;89:6876-80.

170. Bieganski T, Kusche J, Lorenz W, Hesterberg R, Stahlknecht CD, Feussner KD. Distribution and properties of human intestinal diamine oxidase and its relevance for the histamine catabolism. Biochim Biophys Acta 1983;756:196-203.

171. Seiler N, Bolkenius FN, Knodgen B. The influence of catabolic reactions on polyamine excretion. Biochem J 1985;225:219-26.

172. Galy AH, Spits H. IL-1, IL-4, and IFN-gamma differentially regulate cytokine production and cell surface molecule expression in cultured human thymic epithelial cells. J Immunol 1991;147:3823-30.

173. Yi AK, Chace JH, Cowdery JS, Krieg AM. IFN-gamma promotes IL-6 and IgM secretion in response to CpG motifs in bacterial DNA and oligodeoxynucleotides. J Immunol 1996;156:558-64.

174. Sanceau J, Wijdenes J, Revel M, Wietzerbin J. IL-6 and IL-6 receptor modulation by IFN-gamma and tumor necrosis factor-alpha in human monocytic cell line (THP-1). Priming effect of IFN-gamma. J Immunol 1991;147:2630-7.

175. Koerner TJ, Adams DO, Hamilton TA. Regulation of tumor necrosis factor (TNF) expression: interferon-gamma enhances the accumulation of mRNA for TNF induced by lipopolysaccharide in murine peritoneal macrophages. Cell Immunol 1987;109:437-43.

176. Olivares Fontt EO, De Baetselier P, Heirman C, Thielemans K, Lucas R, Vray B. Effects of granulocyte-macrophage colony-stimulating factor and tumor necrosis factor alpha on *Trypanosoma cruzi* trypomastigotes. Infect Immun 1998;66:2722-7.

177. Petray P, Corral R, Meckert P, Laguens R. Role of macrophage inflammatory protein-1alpha (MIP-1alpha) in macrophage homing in the spleen and heart pathology during experimental infection with *Trypanosoma cruzi.* Acta Trop 2002;83:205-11.

178. Chandra M, Tanowitz HB, Petkova SB, et al. Significance of inducible nitric oxide synthase in acute myocarditis caused by *Trypanosoma cruzi* (Tulahuen strain). Int J Parasitol 2002;32:897-905.

179. Michailowsky V, Silva NM, Rocha CD, Vieira LQ, Lannes-Vieira J, Gazzinelli RT. Pivotal role of interleukin-12 and interferon-gamma axis in controlling tissue parasitism and inflammation in the heart and central nervous system during Trypanosoma cruzi infection. Am J Pathol 2001;159:1723-33.

180. Sadlack B, Lohler J, Schorle H, et al. Generalized autoimmune disease in interleukin-2-deficient mice is triggered by an uncontrolled activation and proliferation of CD4+ T cells. Eur J Immunol 1995;25:3053-9.

181. Sadlack B, Merz H, Schorle H, Schimpl A, Feller AC, Horak I. Ulcerative colitis-like disease in mice with a disrupted interleukin-2 gene. Cell 1993;75:253-61.

182. Schorle H, Holtschke T, Hunig T, Schimpl A, Horak I. Development and function of T cells in mice rendered interleukin-2 deficient by gene targeting. Nature 1991;352:621-4.

183. Huang H, Chan J, Wittner M, et al. Expression of cardiac cytokines and inducible form of nitric oxide synthase (NOS2) in *Trypanosoma cruzi*-infected mice. J Mol Cell Cardiol 1999;31:75-88.

184. Aliberti JC, Machado FS, Souto JT, et al. beta-Chemokines enhance parasite uptake and promote nitric oxide-dependent microbiostatic activity in murine inflammatory macrophages infected with *Trypanosoma cruzi*. Infect Immun 1999;67:4819-26.

185. dos Santos PV, Roffe E, Santiago HC, et al. Prevalence of CD8(+)alpha beta T cells in Trypanosoma cruzi-elicited myocarditis is associated with acquisition of CD62L(Low)LFA-1(High)VLA-4(High) activation phenotype and expression of IFN-gamma-inducible adhesion and chemoattractant molecules. Microbes Infect 2001;3:971-84.

186. Talvani A, Ribeiro CS, Aliberti JC, et al. Kinetics of cytokine gene expression in experimental chagasic cardiomyopathy: tissue parasitism and endogenous IFN-gamma as important determinants of chemokine mRNA expression during infection with *Trypanosoma cruzi*. Microbes Infect 2000;2:851-66.

187. Aliberti JC, Souto JT, Marino AP, et al. Modulation of chemokine production and inflammatory responses in interferon-gamma- and tumor necrosis factor-R1-deficient mice during *Trypanosoma cruzi* infection. Am J Pathol 2001;158:1433-40.

188. Giulietti A, Overbergh L, Valckx D, Decallonne B, Bouillon R, Mathieu C. An overview of real-time quantitative PCR: applications to quantify cytokine gene expression. Methods 2001;25:386-401.

189. Sato MN, Yamashiro-Kanashiro EH, Tanji MM, Kaneno R, Higuchi ML, Duarte AJ. CD8+ cells and natural cytotoxic activity among spleen, blood, and heart lymphocytes during the acute phase of *Trypanosoma cruzi* infection in rats. Infect Immun 1992;60:1024-30.

190. Mirkin GA, Jones M, Sanz OP, Rey R, Sica RE, Gonzalez Cappa SM. Experimental Chagas' disease: electrophysiology and cell composition of the neuromyopathic inflammatory lesions in mice infected with a myotropic and a pantropic strain of *Trypanosoma cruzi*. Clin Immunol Immunopathol 1994;73:69-79.

191. Lee AH, Hong JH, Seo YS. Tumour necrosis factor-alpha and interferon-gamma synergistically activate the RANTES promoter through nuclear factor kappaB and interferon regulatory factor 1 (IRF-1) transcription factors. Biochem J 2000;350 Pt 1:131-8.

192. Tran EH, Prince EN, Owens T. IFN-gamma shapes immune invasion of the central nervous system via regulation of chemokines. J Immunol 2000;164:2759-68.

193. Nakajima C, Mukai T, Yamaguchi N, et al. Induction of the chemokine receptor CXCR3 on TCR-stimulated T cells: dependence on the release from persistent TCR-triggering and requirement for IFN-gamma stimulation. Eur J Immunol 2002;32:1792-801.

194. Iwasaki M, Mukai T, Nakajima C, et al. A mandatory role for STAT4 in IL-12 induction of mouse T cell CCR5. J Immunol 2001;167:6877-83.

195. Aliberti JC, Cardoso MA, Martins GA, Gazzinelli RT, Vieira LQ, Silva JS. Interleukin-12 mediates resistance to *Trypanosoma cruzi* in mice and is produced by murine macrophages in response to live trypomastigotes. Infect Immun 1996;64:1961-7.

196. Chandrasekar B, Melby PC, Troyer DA, Colston JT, Freeman GL. Temporal expression of pro-inflammatory cytokines and inducible nitric oxide synthase in experimental acute Chagasic cardiomyopathy. Am J Pathol 1998;152:925-34.

197. Zhang L, Tarleton RL. Persistent production of inflammatory and anti-inflammatory cytokines and associated MHC and adhesion molecule expression at the site of infection and disease in experimental *Trypanosoma cruzi* infections. Exp Parasitol 1996;84:203-13.

198. Machado FS, Martins GA, Aliberti JC, Mestriner FL, Cunha FQ, Silva JS. *Trypanosoma cruzi*-infected cardiomyocytes produce chemokines and cytokines that trigger potent nitric oxide-dependent trypanocidal activity. Circulation 2000;102:3003-8.

199. Luster AD, Unkeless JC, Ravetch JV. Gamma-interferon transcriptionally regulates an early-response gene containing homology to platelet proteins. Nature 1985;315:672-6.

200. Ohmori Y, Wyner L, Narumi S, Armstrong D, Stoler M, Hamilton TA. Tumor necrosis factor-alpha induces cell type and tissue-specific expression of chemoattractant cytokines in vivo. Am J Pathol 1993;142:861-70.

201. Ohmori Y, Hamilton TA. A macrophage LPS-inducible early gene encodes the murine homologue of IP-10. Biochem Biophys Res Commun 1990;168:1261-7.

202. Mahalingam S, Karupiah G. Expression of the interferon-inducible chemokines MuMig and Crg-2 following vaccinia virus infection in vivo. Immunol Cell Biol 2000;78:156-60.

203. Mahalingam S, Chaudhri G, Tan CL, John A, Foster PS, Karupiah G. Transcription of the interferon gamma (IFN-gamma)-inducible chemokine Mig in IFN-gamma-deficient mice. J Biol Chem 2001;276:7568-74.